PETROGENESIS OF ULTRAMAFIC XENOLITHS FROM THE CANADIAN CORDILLERA AND ALASKA

John Whitman Prescott

McGill University, Montreal

15 November 1983

A thesis submitted

to the Faculty of Graduate Studies and Research

in partial fulfillment of the

requirements for the M.Sc. degree in Geology

Plate 1: MOUNT MCKINLEY, ALASKA

As the highest point in North America, it symbolizes the power of geological processes in the Cordillera.

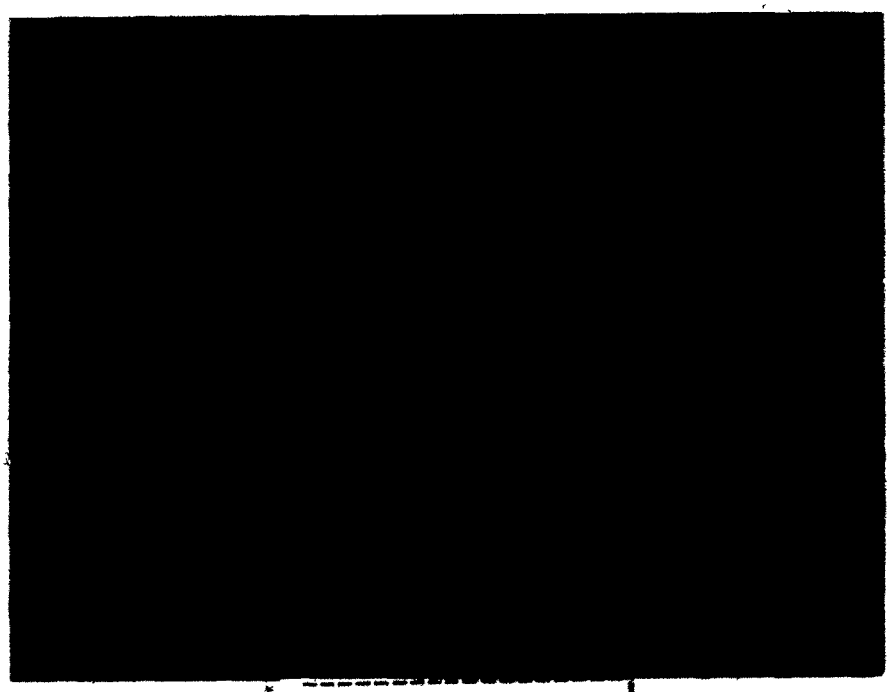

COLOURED PICTURES
Images en couleur

ABSTRACT

Four ultramafic xenolith localities along the northern Rocky Mountain Cordillera are compared to a fifth suite that occurs along an extension of this trend at Nunivak Island, in western Alaska. Whereas all five suites contain harzburgite (group 1) xenoliths with coarse equant textures and Cr-diopside-rich spinel lherzolite (group 3) xenoliths with granoblastic textures, rocks directly equivalent to the dominant porphyroclastic-textured spinel lherzolite (group 2) xenoliths from the Cordillera are absent at Nunivak. Instead, Nunivak samples with modes similar to the Cordilleran lherzolite-2 xenoliths have coarse textures, contain either amphibole, mica or more commonly, hydrous fine-grained melt zones. Chemical analyses show that both the compositionally barren harzburgite-1 and depleted lherzolite-2 (or equivalent) xenoliths can be derived by increasing degrees of pseudo-invariant partial melting from parent compositions equivalent to those of fertile pyroxene-rich lherzolite-3 xenoliths. The continental lithosphere beneath the Cordillera appears to be significantly more fertile than that with oceanic affinities, as beneath Nunivak Island.

SOMMAIRE

On compare les xénolithes ultramafiques récoltés à quatre endroits dans le Nord de la cordillère des Rocheuses à une suite qui provient d'une continuation de cet axe, sur l'île Nunivak, dans la partie occidentale de l'Alaska. Quoique les cinq suites contiennent des xénolithes de harzburgite à texture grenue-équante (groupe-1) et de lherzolite à spinelle + diopside chromifère et à texture granoblastique (groupe-3), les roches qui équivalent le groupe prédominant dans les localités de la cordillère (groupe-2: lherzolite à spinelle et à texture porphyroclastique) manquent à Nunivak. A leur place, on trouve une suite à composition modale semblable mais à grain grossier; de plus, ces roches contiennent soit de l'amphibole, du mica ou, le plus souvent, des zones hydratées à grain fin qui ont passé à l'état de fusion. Selon les résultats d'analyses chimiques, les compositions harzburgitiques, à composition stérile (groupe-1), et lherzolitiques, géochimiquement appauvries (groupe-2), résulteraient d'une fusion partielle pseudo-invariante progressive d'une roche-mère semblable en composition à une lherzolite fertile riche en pyroxène. La lithosphère continentale sous les Rocheuses semble décidément plus fertile que la lithosphère a affinité océanique, comme celle qui se trouve sous l'île de Nunivak.

TABLE OF CONTENTS

LIST OF FIGURES

LIST OF PLATES

LIST OF TABLES

LIST OF APPENDICES

STATEMENT OF ORIGINALITY

Regional comparisons of basalt-hosted ultramafic xenolith localities include global surveys (Forbes & Kuno 1965) or surveys of geographically limited areas in France (Brown et al. 1980), Japan (Takahashi 1978) and British Columbia (Littlejohn & Greenwood 1974, Fiesinger & Nicholls 1977). In this study, xenolith localities have been compared over a much larger area, effectively including the length of the Canadian Cordillera and Alaska. The data base available for the Jacques Lake, Castle Rock, Fort Selkirk and Prindle Volcano localities has been significantly augmented by the author's statistically-based field work during the summer of 1980. This study is also significant in that it includes the Nunivak Island xenolith suite collected by D. M. Francis during the summers of 1972 and 1973. All of the analytical data presented, including modes, mineral and calculated bulk compositions, were obtained by the author with one exception: mineral compositions for the Nunivak Island xenolith suite were supplied by D. M. Francis. Consequently, the description of the Nunivak Island samples is considered separately in Chapter 6, with frequent reference to the petrological observations and inferences of Francis (1974, 1978).

ACKNOWLEDGEMENTS

This study arose from conversations with Professor D. M. Francis during the winter of 1980. It has benefitted at every stage from Don's interest and the unique environment he generated in which to learn. Don bore the costs of an extensive field season, sample preparation and computer time on N.S.E.R.C. grants to him. His continued financial support in the form of research assistantships is gratefully acknowledged. I would like to thank Professor R. F. Martin for his continuing friendship and interest in this project, and for his willingness to accept the responsibilities of co-advisor in the spring of 1981. I am grateful to Dr. F. R. Boyd and the staff of the Geophysical Laboratory, Carnegie Institute of Washington for their hospitality in allowing free use of their microprobe facilities during the fall of 1981. I also thank Ms. Laura Sue Gould for being a capable and conscientous assistant during the Summer 1980 field season, in spite of errant bears, approaching forest fires and a very long walk from Prindle Volcano. At various stages in this study, I have benefitted from discussions with Dr. J. G. Souther (Geological Society of Canada), Prof. J. T. Gutmann (Wesleyan University) and Ms. Eva Schandl (the Royal Ontario Museum) and the staff and students of the Department of Geological Sciences at McGill University. Lastly, I would like to thank my parents, William and Barbara Prescott, to whom this project is dedicated.

1. INTRODUCTION

Ultramafic rocks found in alpine type plutonic complexes, in ophiolites and in xenolith suites of alkalic basalts, kimberlites and carbonatites (Carswell 1980) are the only known samples of the upper mantle and deepest layers of the Earth's crust. Petrological studies of ultramafic xenoliths have provided important constraints on the composition of the upper mantle (Carter 1970, Ringwood 1975) and evidence of deformational (Basu 1975, Carter & Ave 'Lallement 1970, Mercier & Nicholas 1976) and metasomatic processes (Boettcher & O'Neill 1980, Francis 1976a, Wass 1979, 1980) that occur there. Numerous experimental studies on such xenoliths and compositionally simplified analogues have established the stability fields of upper mantle mineral assemblages in terms of temperature and pressure. Many xenolith studies have relied on the trace element and isotopic chemistry composition of samples to reconstruct the petrogenetic history of the upper mantle (Frey & Green 1974, 1978, Menzies & Murthy 1980). More recently, complementary isotopic studies have focused on the relationship between crustal and upper mantle xenoliths and their host basalts (Roden 1982). In addition, several regional studies (Brown et al. 1980, Takahashi 1978) have correlated the distribution of rock types and the compositional and deformational characteristics of specific xenolith populations with tectonic environment.

Recent studies of basalt-hosted ultramafic xenoliths from

the northern Rocky Mountain Cordillera (Fig. 1) have described both individual xenolith localities (Brearley et al. 1982, Fujii & Scarfe 1981, 1981b, Hamilton & Scarfe 1982) and groups of comparable localities in western Canada (Fiesinger & Nicholls 1977, Littlejohn & Greenwood 1974, Scarfe et al. 1982). Nicholls et al. (1982) examined the composition of a variety of xenolith-bearing and related basalts in western Canada, and compared the compositions of the entrained ultramafic xenoliths with those calculated for the partial melting of a pyrolite model mantle: they relied predominantly on limited, previously published, data for the xenoliths.

This paper presents the results of a study of xenolith suites found in late Tertiary to Quaternary alkali basalt cinder cones and maars, which extend along the Rocky Mountain Cordillera in western Canada and Alaska (Fig. 1). In this study, peridotite xenoliths from the Jacques Lake, Castle Rock, Fort Selkirk, and Prindle Volcano cinder cones are compared with those from Nunivak Island, the latter lying off the western coast of Alaska (Francis 1974, 1976a, b). Although the four Cordilleran localities have been previously described (Foster et al. 1966, Littlejohn & Greenwood 1974, Sinclair et al. 1978), the volcanic stratigraphy and xenolith population at each has been carefully restudied by the author in the field. The distribution of lithologies was statistically determined and used to select representative groups of ultramafic xenoliths samples from each suite for further study. Special attention was given to the variations in

Figure 1: REGIONAL MAP

Geology compiled from Tipper et al. (1981), Churkin et al. (1980), Beikman et al. (1981) and Sinclair et al. (1978)

Stars: Xenolith localities included in this study: JL Jacques Lake, CR Castle Rock, FS Fort Selkirk, PV Prindle Volcano, NI Nunivak Island.

Squares: Other known xenolith localities: 1) Littlejohn & Greenwood (1978), 2) Fiesinger & Nicholls (1977), 3) Nicholls et al. (1982), 4) Scarfe et al. (1982), 5) Fujii et al. (1981), 6) R. Forbes, pers. comm. 1981, 7) J. Hoare, pers. comm. 1981, 8) C. Bacon, pers. comm. 1982.

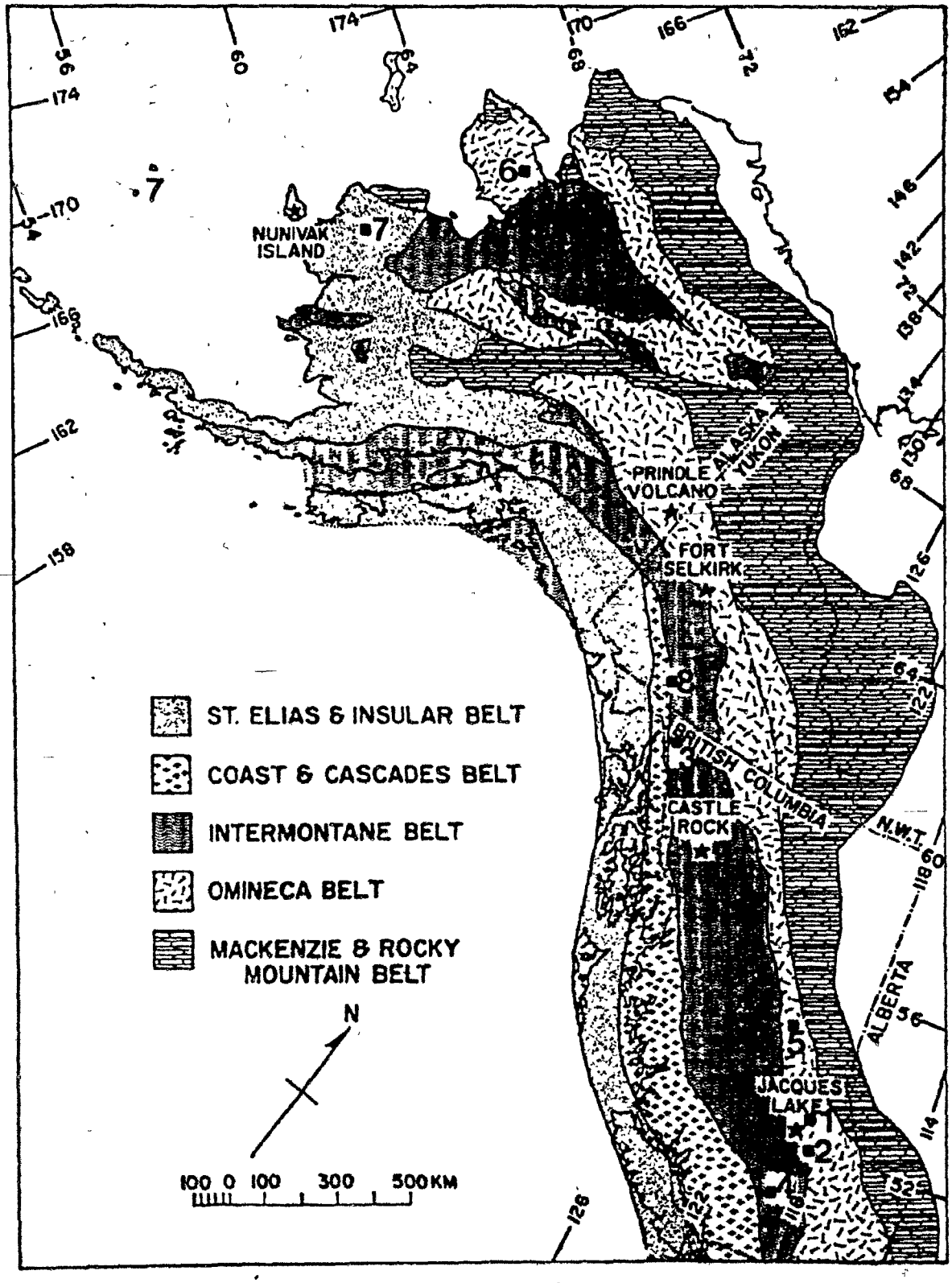
NUNIVAK ISLAND
PRINDLE VOLCANO
FORT SELKIRK
CASTLE ROCK
JACQUES LAKE
ALASKA
YUKON
BRITISH COLUMBIA
N.W.T.
ALBERTA
ST. ELIAS & INSULAR BELT
COAST & CASCADES BELT
INTERMONTANE BELT
OMINECA BELT
MACKENZIE & ROCKY MOUNTAIN BELT
N
100 0 100 300 500KM

modal proportions, textures, and the mineral compositions of the xenoliths. Although each suite is distinctive, the five groups of xenoliths are shown to be similar or complementary in many respects. Compositional variations seen in the pyroxenes and in the calculated whole-rocks show that most of the xenolith samples are related by varying degrees of partial melting of a single parent mantle composition that is common to all the localities. This common petrogenetic trend can be demonstrated despite the presence in the Nunivak Island suite of a significant volatile component that is absent in the four Cordilleran localities. The results of this study are used to speculate on the causes of the variable degrees of depletion observed in each suite, on the nature of lithospheric heterogeneity beneath this area of western North America and on the variations in regional tectonics as implied by the xenolith populations.

2. FIELD RELATIONS

REGIONAL GEOLOGY OF THE CORDILLERA

In Canada, the Rocky Mountain Cordillera reflects the formation of a constructive plate margin to the west of the North American craton in Paleozoic time, followed by the subduction of the adjacent oceanic plate beneath the volcanic arc of an easterly dipping subduction zone, with the arc eventually colliding and accreting onto the craton in Mesozoic time (Atwater 1970, Templeman-Kluit 1979). The northern Cordillera has been divided by Tipper et al. (1981) into five major belts that trend northwest through British Columbia, Yukon and eastern Alaska (Fig. 1). In the east, the Cordillera consists of Paleozoic and Mesozoic miogeosynclinal and continental shelf sediments that have been folded and thrust over the craton to form the Mackenzie-Rocky Mountain Belt. To the west, this tectonic belt is separated by the Northern Rocky Mountain Trench - Tintina fault system from the Omineca Belt, which comprises a geanticlinal core-zone of Paleozoic and late Precambrian schists and gneisses cut by granitic stocks of Mesozoic age. Further to the west, the Teslin-Pinchi fault system separates the Omineca Belt from the Intermontane Belt, a broad tectonic depression containing a thick pile of Mesozoic and late Paleozoic eugeosynclinal volcanic and sedimentary rocks. The western margin of the Intermontane Belt is abruptly terminated by the Coast and Cascades Belt, a complex of predominantly Mesozoic quartz

dioritic batholiths and crystalline metamorphic rocks. The Coast and Cascades Belt is in turn bounded by the Denali-Yalakom fault system, which separates it from the St. Elias and Insular Belt of eugeosynclinal volcanic and sedimentary rocks in southeastern Alaska and the outer islands of northern British Columbia. Were it not for the intervening emplacement of the predominant Coast Plutonic complex of the Coast and Cascades Belts, the Intermontane and the St. Elias and Insular Belts would be largely indistinguishable in western Canada (Tipper et al. 1981).

The five tectonic belts are continuous into eastern Alaska, but their extension becomes complex within 300 km of the Canadian border in central Alaska. Churkin et al. (1980) have tentatively correlated Paleozoic continental sedimentary rocks from three key areas adjacent to the Yukon-Tanana upland province of the Omineca Belt in eastern and central Alaska. They proposed that the continental margin in the Brooks Range of northern Alaska is related to that seen in the Mackenzie-Rocky Mountain Belt and has been offset along the Porcupine megashear. The reconstruction of Churkin et al. (1980) suggests that the transition (equivalent to the Omineca Belt) between the miogeosynclinal rocks of the Mackenzie-Rocky Mountain Belt and the eugeosynclinal rocks of the Intermontane Belt follows a deformed arcuate trend from east-central to southwestern Alaska (Fig. 1).

In Canada, these five Cordilleran belts have formed the relatively stable western margin of the North American

tectonic plate throughout Cenozoic time. During this period, significant plate motion was restricted to dextral transcurrent offset along the Fairweather-Queen Charlotte fault system, which separates the St. Elias and Insular Belt from the Pacific tectonic plate, and to subduction of the Pacific plate beneath the Aleutian trench (Atwater, 1970, Bevier et al. 1979). Cenozoic tectonic activity also resulted in the eruption of locally voluminous volcanic rocks throughout the Intermontane Belt. The studies of Bevier et al. (1979) and Souther (1977) suggest that this reflects the resolution of motion between the North American and Pacific plates into north-south-trending tensional components as represented by the Mt. Garibaldi, Stikine and Wrangell Volcanic Belts, or in block faulting associated with east-west-trending transcurrent faulting, as represented by the Anaheim Volcanic Belt. Whereas the Garibaldi and Wrangell belts are thought to be calc-alkaline, the Stikine and Anaheim Volcanic Belts have distinctly alkaline affinities and contain basalts that are compositionally equivalent to isolated alkaline basalt shields and cinder cones of Quaternary and late Tertiary age that occur in areas adjacent to the boundary between the Omineca and Intermontane Belts along the length of the Cordillera. These alkaline basalts span the compositional range alkali olivine basalt, basanite, nephelinite, and ankaramite (Nicholls et al. 1982).

The five xenolith localities considered in this study all occurring at Recent to late Tertiary alkaline eruption centers

are restricted to a narrow band parallel to the deformed Cordilleran structure for a distance of 3300 km. The Jacques Lake, Fort Selkirk and Prindle Volcano cinder cones lie either within the Omineca Belt or close to its border, within the Intermontane Belt. The Castle Rock locality, part of the Mount Edziza Complex, also occurs within the Intermontane Belt. Whereas this volcanic complex may be related to the Stikine arch, which cross-cuts the Intermontane Belt in a northeasterly direction (Souther 1977), the Mount Edziza Complex also lies on a southeasterly extension of the Teslin fault system (Templeman-Kluit 1980). The Castle Rock locality may therefore be tectonically related to the Fort Selkirk and Prindle Volcano localities, both of which lie close to the Teslin fault. In contrast, the relatively young age and distinctly oceanic character of the Nunivak Island basement suggest that the lithosphere beneath this locality may be much thinner than that beneath the Cordilleran xenolith localities.

JACQUES LAKE

The Jacques Lake cinder cone (Long. 121,05°W, Lat. 52,58°N: map ref.: Horsefly, B.C., 1:50,000 sheet, 93A/6) lies 2.5 km south of Quesnel Lake and just north of the smaller Jacques Lake in eastern British Columbia. The basement rocks in this area consist of Precambrian to early Paleozoic quartzite, phyllite and limestone, covered by flows of alkali-rich basalt and andesite of Mesozoic age (Campbell 1961, Tipper et al.

1974). These were later intruded by hornblende-biotite granite, granodiorite, diorite and syenite. The local eruption of basalt flows of mid-Tertiary age was followed by isolated eruptions of alkali olivine basalt as breccia and tuff in late Tertiary to Quaternary time. The latest phase of volcanic ativity in this area appears to have been centered southeast of Jacques Lake, in Wells Gray Provincial Park.

The relatively recent cinder cone at Jacques Lake rises 210 m to an elevation of 1120 m, and has a diameter of 0.8 to 1.2 km. The cone is built of successive layers of coarse tuff, which are well exposed on its southern flank. Contemporaneous lava flows were not observed. Xenoliths occur sparsely through the upper third of the cone, becoming more common in the uppermost units. Most of the 88 xenolith samples counted are small (2 to 5 cm) fragments of initially larger xenoliths. In the Jacques Lake (JL) suite, spinel lherzolite is the predominant xenolith lithology (Table 1); minor proportions of harzburgite, websterite and basement rocks also occur. Small (1 to 10 cm) basalt fragments and anorthoclase megacrysts are also commonly found in the tuff.

CASTLE ROCK

The Castle Rock cinder cone (Long. 130,13°W, Lat. 57,51°N; map ref.: Klastline River, B.C.; 1:50,000 sheet, 104G/16 west) is a satellite vent of the Mt. Edziza Volcanic Complex, lying about 52 km east of Telegraph Creek, British Columbia. In this area of the Intermontane Belt, a basement complex of

Table 1: LITHOLOGIES PRESENT IN THE XENOLITH SUITES

	JACQUES LAKE	CASTLE ROCK	FORT SELKIRK	PRINCE VOLCANO	NUNIVAK ISLAND*
Dunite and Harzburgite	8.0%	7.4%	14.1%	14.5%	6.8%
Spinel Lherzolite	84.1%	83.9%	80.8%	69.5%	84.4%
Websterite	4.6%	1.2%	3.7%	7.8%	0.3%
Clinopyroxenite	-	0.6%	-	2.2%	-
Orthopyroxenite	-	1.2%	0.2%	1.9%	-
Plagioclase Lherzolite	-	0.9%	-	3.9%	-
Mafic Granulite	-	0.6%	0.8%	0.5%	0.8%
Felsic Granulite	-	2.7%	0.4%	-	0.1%
Gabbro	-	-	-	-	7.6%
Other crustal Lithologies	3.4%	1.5%	-	-	-
Total samples Counted	88	338	512	642	3297

* Data for the Nunivak Island xenolith suite, taken from Francis (1974), include iddingsitized equivalents where appropriate.

predominantly Mesozoic sandstone, conglomerate and intermediate volcanic rocks was intruded in the late Mesozoic by granodiorite and quartz diorite plutons. Throughout most of the late Cenozoic, Mt. Edziza and the adjacent Spectrum Range erupted to form a volcanic complex covering an area of nearly 2000 sq. km. Souther (1972, 1977) and Souther & Symons (1974) have shown that the basal shield of the Mt. Edziza Complex consists of thin, flat-lying flows of columnar basalt that formed during Pliocene time. The main composite cone of the Mt. Edziza Complex was built up of a series of eruptions, each of which began with alkali basalt; these were later followed by more fractionated magmas, including trachyte and thick flows of sodic rhyolite. In recent times (since 10,000 years), volcanic activity has been reflected in the development of over thirty satellite cinder cones of porphyritic alkali olivine basalt. These occur around the flanks of the main volcano, along Mess Creek Valley, west of the Mt. Edziza, and on the Klastline plateau, east of Mt. Edziza.

Castle Rock is the largest vent on the Klastline plateau (Plate 2), rising 200 m on the northern edge of the plateau, to an elevation of 1860 m. The locality consists of a volcanic neck surrounded by a cone of vesicular, subglacial pillow basalt and tuff breccia, largely stripped away to the north. Xenoliths were found in the uneroded remnants of the volcanic neck and along the surface of the cinder cone, near the summit. Some areas to the east of the summit contain as many as fifty fragments and intact xenoliths per square meter. Most of

Plate 2: CASTLE ROCK LOCALITY

Includes a remnant volcanic neck (center right) partially surrounded by dark basalt tuff (view to the southwest). Xenoliths are included in the neck and are locally very abundant in some areas near the top of the cinder cone (center).

Plate 3: FORT SELKIRK LOCALITY

Located on the southwest side of the cinder cone within 50 m of the top, this exposure shows an increase in the proportion and size of fragments included in the tuff (layering is inclined at about 40 degrees, from upper right to lower left; field assistant is about 1.5 m in height). Xenoliths are common in a 10 m horizon composed of 2 to 25 mm sized lithic basalt fragments.

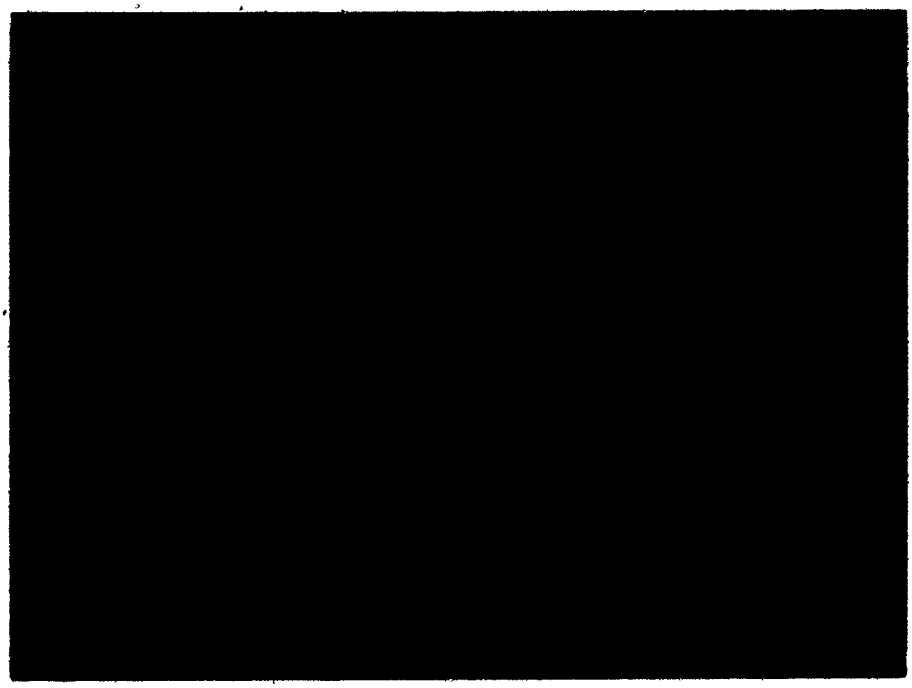

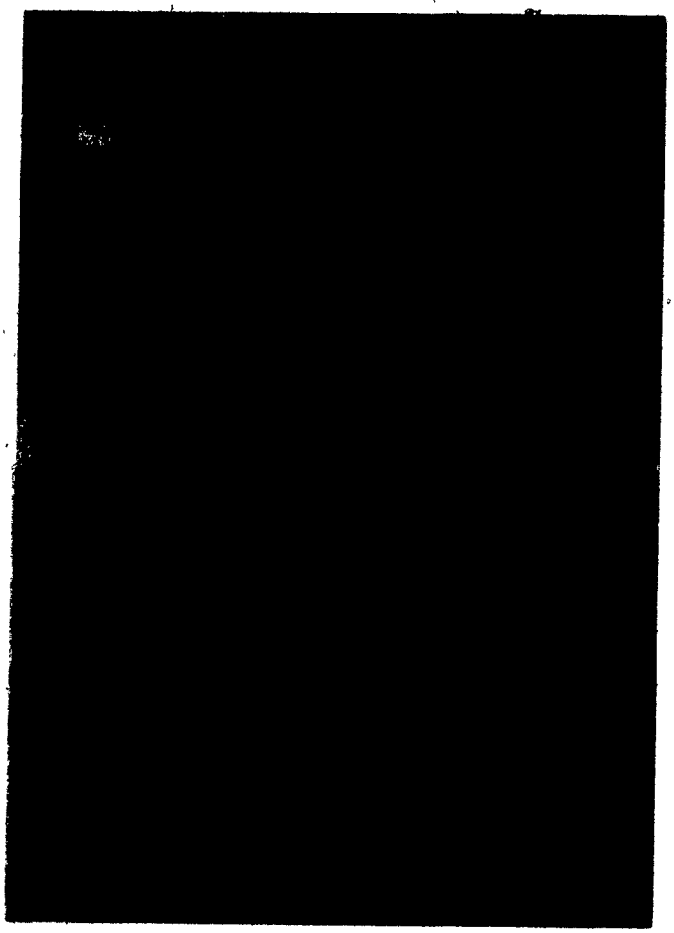

COLOURED PICTURES
Images en couleur

the 338 xenolith samples counted were found to be intact, with an average diameter of 5 to 6 cm. They are typically ellipsoidal, often flattened, and occasionally twisted, giving the impression of plastic deformation. In the Castle Rock (CR) suite, spinel lherzolite is the predominant rock type (Table 1). Smaller quantities of websterite, harzburgite, ortho- and clinopyroxenite, plagioclase lherzolite, mafic and felsic granulite and basement rocks are also included in the CR xenolith suite.

FORT SELKIRK

The Fort Selkirk cinder cone (Long. 137,15°W, Lat. 62,45°N; map ref.: Dark Creek, Yukon and Volcano Mountain, Yukon; 1:50,000 sheets, 115I/11 and 115I/14) lies 4.5 km southeast of the junction between the Yukon and Pelly Rivers in the central Yukon Territory. The basement rocks in this area of the Yukon-Tanana Upland consist of Precambrian to late Paleozoic schist and gneiss, overlain by Mesozoic basic to intermediate volcanic rocks, and intruded by late Mesozoic granodiorite and granite plutons (Bostock 1936). The Carmacks volcanic series of basalt, andesite, dacite and trachyte flows, breccias and tuffs were erupted on this basement in the Tertiary. They were succeeded by the late Tertiary to Quaternary Selkirk series of basalt flows, breccias and tuffs (Sinclair et al. 1978).

The Fort Selkirk cinder cone rises 170 m to an elevation of 710 m, with a diameter of 1.5 to 2.2 km. It is composed

of thin stratified tuff-sheets built upon a platform of vesicular Selkirk basalt flows. Distal portions of the original cone have been partially eroded by the Yukon River, whereas remnants of the volcanic neck are exposed west of the present summit. Several excellent exposures of the cinder cone's cross-section show that although absent in most of the stratigraphic section, xenoliths appear and become common in the upper 50 m of the volcanic ejecta (Plate 3). Lithic fragments of basalt, the most common fragment type, rapidly increase in size from 1 cm to 2 m upward. Xenoliths become common where these fragments average 4 to 6 cm. Most of the 512 samples counted from Fort Selkirk (FS) are xenolith fragments found in the tuff sheets and also in remnants of the volcanic neck. Intact xenoliths average 3 to 5 cm in diameter and typically are ellipsoidal in shape. The FS xenolith population (Table 1) consists predominantly of spinel lherzolite with a smaller proportion of harzburgite, and rarer websterite and mafic and felsic granulite.

PRINDLE VOLCANO

Prindle Volcano (Long. 141,40°W, Lat. 63,43°N; map ref: Tanacross, Ak., 1:63,360 sheet, C-2) lies 65 km northeast of Tetlin Junction from the Alaska Highway in eastern Alaska. In this area of the Yukon-Tanana Upland, the basement rocks consist of Precambrian or Paleozoic quartz-biotite schist and gneiss, quartz-serioite schist and quartzite. This basement is overlain by Mesozoic conglomerate and sandstone, and was

later intruded by large plutons of Mesozoic diorite, biotite granodiorite and granite (Foster 1970, Foster et al. 1966, Mertie 1931, 1937). Tertiary volcanism formed locally widespread felsic and mafic lavas, breccias and tuffs. These were succeeded by smaller isolated flows and breccias of late Tertiary to Quaternary olivine basalt. Prindle Volcano appears to be among the most recent in this area.

Prindle Volcano (Plate 4) is unglaciated and consists of a cinder cone of basalt breccia and tuff rising 100 m above an upland ridge to an elevation of 1250 m, with a diameter of 0.9 to 1.2 km. The well-preserved central crater has been breached to the south by a small flow of alkali olivine basalt that extends down-slope for 6.5 km to the southeast before turning southwest and continuing for another 4.5 km along the west side of the East Fork of the Dennison River. Xenoliths are common on and near the top of the cinder cone rim and in exposed cross-sections of the breached southern flank of the cone. Rare xenoliths were found sparsely scattered along the base of the lava flow up to 4.0 km from the cinder cone, and also rarely as bombs. Most of the 642 xenolith samples counted are fragments, many of which suggest originally intact xenoliths with an average diameter of 4 to 6 cm (Plate 5). Where observed, intact xenoliths typically were found to be either flattened ovoid or crudely rectangular in shape. The xenolith population determined from field studies at Prindle Volcano (Table 1) shows that spinel lherzolite is predominant, however, harzburgite and websterite

Plate 4: PRINDLE VOLCANO

In this view taken to the southeast, the breached crater wall can be seen (lower and right of center). Xenoliths are commonly found in exposed areas within 10 m of the rim.

Plate 5: XENOLITH SIZE AND SHAPE

A representative group of lherzolite xenolith samples found at Prindle Volcano. The red increments on the scale are 5 cm in length. Note the often twisted oblate and rectangular sample shapes.

COLOURED PICTURES
Images en couleur

also are common. Plagioclase lherzolite, clinopyroxenite, orthopyroxenite and mafic granulite are present in minor proportions. A number of the ultramafic xenoliths counted are distinctly reddish, presumably due to pervasive idding-sitization.

NUNIVAK ISLAND

Nunivak Island (Long. 166°W, Lat. 60°N; map ref.: Cape Mendenhall, AK., 1:63,360 sheets, D-3 and D-4) is located approximately 50 km from the western coast of Alaska, southwest of the floodplains of the Yukon and Kuskokim Rivers. The geology of the island was studied by Hoare et al. (1968), and it differs from that of the four Cordilleran localities in several respects. Where exposed on the island and on the mainland nearby, the basement rocks are middle Mesozoic in age, considerably younger than the basement at the other localities. These rocks consist of sandstone, conglomerate and siltstone, with lesser amounts of andesitic volcanic rocks. The volcanic history of Nunivak is dominated by the late Tertiary (<6.1 Ma) to Quaternary eruption of thin, widespread flows of olivine tholeiite basalt that now cover most of the island. Numerous small alkali basalt cinder cones and minor flows of basanite have been shown to have low $^{87}Sr/^{86}Sr$ ratios (0.7025 - 0.7033), similar to that in the more voluminous olivine tholeiites (Mark 1971). Recent rare-earth-element studies have suggested that these basalts were not contaminated by continental crust and that their

source is isotopically similar to that of modern oceanic basalts (Menzies & Murthy 1980, Roden 1982).

Ultramafic and granulite xenolith suites collected from over thirty alkali basalt cinder cones and maars on Nunivak Island have been described by Francis (1974, 1976a, b, c, 1978). The overall xenolith population, based on nearly 3,300 samples (Table 1) is shown for comparison with the Cordilleran localities. The Nunivak Island xenolith population is dominated by spinel lherzolite, with lesser quantities of harzburgite and pyroxene granulite, and minor proportions of clinopyroxenite, wehrlite and websterite.

3. PETROGRAPHY

Sample groups were chosen from the field samples collected (Table 1) at the four Cordilleran localities and Nunivak Island to represent the relative proportions of ultramafic xenolith lithologies at each site. Almost all of the Cordilleran samples were found to consist of the four-phase assemblage olivine + orthopyroxene + clinopyroxene + spinel, with spinel absent or rare in only three samples from the Castle Rock suite (CR5, CR47, and CR49). The Nunivak Island suite (described separately in Chapter 6) is distinct in that many xenoliths contain either amphibole, mica, or most commonly fine-grained zones of olivine, clinopyroxene, spinel, glass, amphibole and/or mica.

MODAL COMPOSITION

Most members of the sample groups were point-counted to determine modal composition (Appendix 1) using an automated traversing stage. The ultramafic xenolith populations of the four Cordilleran suites are very similar in their range of dominant lithologies and in their average modal composition (listed in Appendix 1 and shown recalculated without spinel or minor phases in Fig. 2). Most xenoliths range compositionally from harzburgite to spinel lherzolite, with variable but lesser proportions of either pyroxene-rich spinel lherzolite or olivine websterite (Fig. 2) also present, following the classification system suggested by Streckeisen

Figure 2: XENOLITH MODES

Modal compositions determined from point-counting; traverses included at least 80% of the area of each section, with an average of 1500 points counted for fine-grained samples and 3000 points counted for coarse-grained samples. The modal compositions shown are recalculated without spinel or other minor phases. Nunivak Island ultramafic xenoliths were recalculated in terms of anhydrous equivalents using the proportions of olivine, clinopyroxene, spinel and glass reported by Francis (1974, Table 6-13). Samples that are not ultramafic or that appear substantially inhomogeneous on a thin-section scale were not counted.

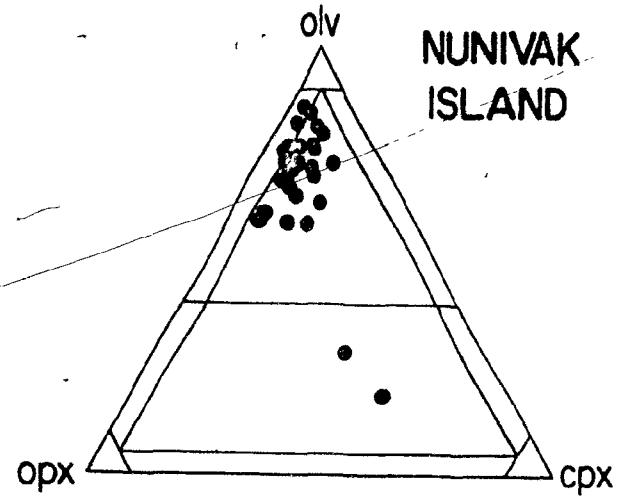

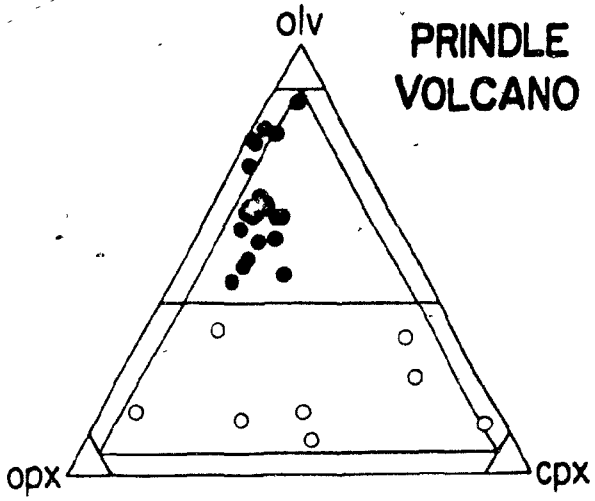

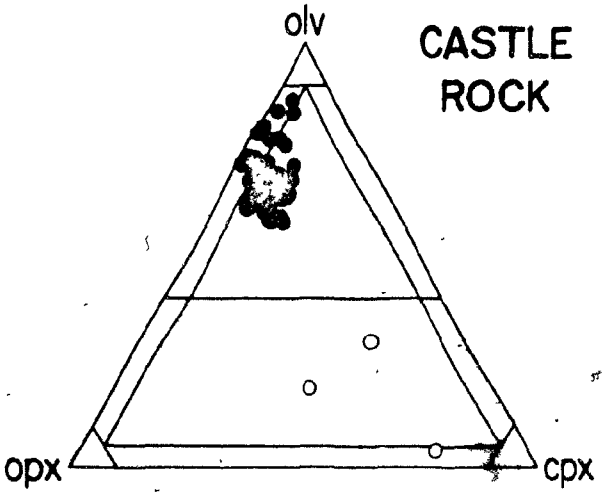

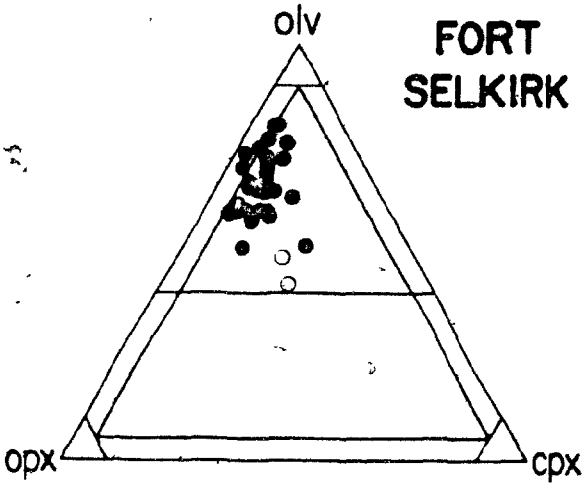

XENOLITH MODES

Recalculated to 100%

- ● **Cr-diopside series**
- ○ **Ti-augite series**

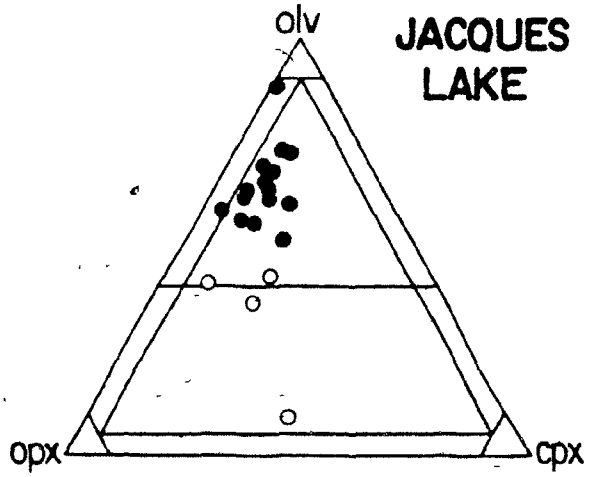

(1976).

Spinel lherzolite (Table 2) is the predominant xenolith lithology at each of the four Cordilleran localities. In the CR suite (and also in the NI suite) pyroxene-rich lithologies are comparatively rare, and there is a more limited modal range of olivine-rich harzburgite to spinel lherzolite. The JL, FS and PV suites, in contrast, are characterized by smaller proportions of harzburgite, which may form a distinct group, separate from the dominant spinel lherzolite lithology at PV. In addition, the PV suite contains a relatively large variety of pyroxene-rich lithologies including orthopyroxenite, websterite and clinopyroxenite, which constitute 12% of the suite (Table 1). The JL and FS suites are similar to PV, with lesser, but significant proportions of pyroxene-rich lithologies broadening the modal range in each suite.

The ultramafic xenolith samples from each of the Cordilleran suites can be divided into groups, based largely on the modal proportion of olivine. Although the groups defined vary from the classification of Streckeisen (1976), they subdivide the xenolith lithologies into categories which correlate with variations in their phase chemistry and appear petrogenetically significant:

> Group 1. Harzburgite (olivine > 76 modal %): clinopyroxene-poor peridotites in which the primary modal variation is the ratio olivine vs. orthopyroxene, with little change in modal clinopyroxene.
>
> Group 2. Lherzolite (olivine + 60 to 76 modal %): peridotites characterized by a large modal variation in the ratio of olivine to orthopyroxene + clinopyroxene, with little variation in the ratio of

Table 2: AVERAGE MODAL COMPOSITION OF XENOLITH SUITES

	OLIV	OPX	CPX	SPINEL
JACQUES LAKE	56.5	28.1	13.4	2.0
CASTLE ROCK	64.2	23.7	10.6	1.5
FORT SELKIRK	63.3	24.0	10.8	1.9
PRINDLE VOLCANO	51.5	28.2	17.7	2.6
AVERAGE MODE FOR CORDILLERA	59.9	25.4	12.8	1.9
NUNIVAK ISLAND*	67.2	20.0	11.1	1.7

* Includes Nunivak Island hydrous peridotites recalculated to 100% using proportions of anhydrous equivalent phases reported by Francis (1974, Table 6-13).

orthopyroxene to clinopyroxene.

Group 3. Pyroxene lherzolite (olivine = 30 to 60 modal %): comparatively clinopyroxene-rich samples that are gradational to group 2 lherzolite xenoliths in the CR and NI suites, where they appear to be only extreme members of group 2 lherzolites. However, a distinction between xenoliths of group 2 and 3 in the other suites is strongly suggested by the chemistry of the lherzolite pyroxenes (Chapter 4).

Group 4. Websterite (olivine < 30 modal %): pyroxenites with a large modal range in the ratio of orthopyroxene to clinopyroxene. This group is equivalent to Ti-augite xenoliths (group II) described by Frey & Prinz (1978) which are characterized by the green color of their clinopyroxenes. Although several peridotite xenoliths are present in each suite, they are not the primary focus of this study.

COMPOSITE XENOLITHS

Several types of composite xenoliths, similar to those described by Irving (1980) and Scarfe et al. (1982) are included in the sample groups, particularly in the CR and PV suites. In one variety, sharp bands 1 to 2 mm thick of diopsidic websterite typically cut olivine-rich lherzolite xenoliths (Plate 6A). In the other variety, the composite nature ranges from irregular modal heterogeneity on a 10-to-20 mm scale to xenoliths containing two distinct rock types (Plate 6B). Boundaries between rock types in such larger composite samples range from gradational over a distance of 1 cm, to sharp, with widths less than 1mm. These latter composite samples are typically pyroxene-rich lherzolite or olivine websterite, distinctly enriched in clinopyroxene relative to the banded olivine-rich composites.

Plate 6: COMPOSITE XENOLITHS

A. PV8: Lherzolite cut by diopsidic websterite vein, approximately 1.5 mm in thickness (field of view = 25 mm).

B. CR22: Contact between lherzolite (upper right) and websterite, each forming distinct lithologies on a hand specimen scale (field of view = 22 mm).

Plate 7: XENOLITH TEXTURES

A. FS8: Coarse equant texture with very few olivine porphyroclasts in a sample with distinct harzburgitic affinities (field of view = 25 mm in each), with virtual absence of spinel.

B. FS3: The porphyroclastic texture occurs with an increasing proportion of subordinate neoblasts and in the modal proportion of pyroxene and spinel.

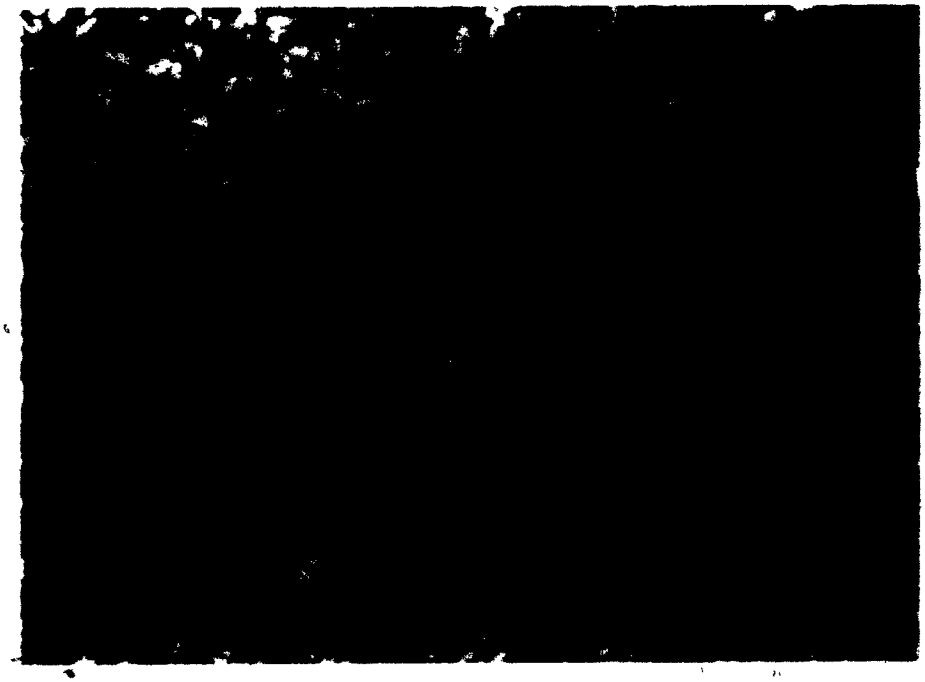

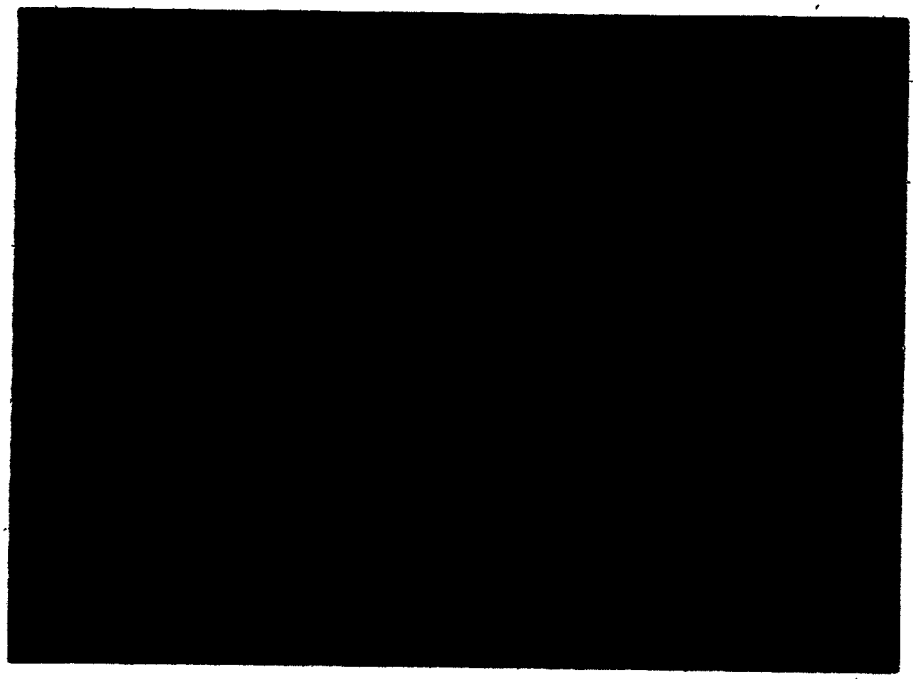

COLOURED PICTURES
Images en couleur

TEXTURES

Xenolith textures were studied using the classification schemes of Mercier & Nicolas (1976) and Harte (1977). Both studies defined textures in terms of predominant grain-size and the ratio of porphyroclasts (3 to 4 mm grains) to neoblasts (grains < 1 mm). These studies support a deformational spectrum of xenolith textures in which coarse-grained equant (CE) textures anneal, via increase in the growth of neoblasts, to the porphyroclastic (POR) texture, mosaic porphyroclastic (MP) texture (Harte 1977: olivine porphyroclasts < 10%) and granulablastic (GE: equant; GT: tabular) textures in which porphyroclasts are very rare or absent.

The samples in each suite show a range of textures (Table 3) that vary continuously in the ratio of porphyroclasts to neoblasts (Plate 7). Few samples contain less than 10% of either porphyroclasts or neoblasts. This prompted the redefinition of the mosaic porphyroclastic class of Harte (1977) in this study to include samples with up to 30% olivine porphyroclasts (Table 3). The JL and FS xenolith suites are generally coarser-grained, with textures ranging from CE (olivine porphyroclasts > 4 mm) to predominantly POR and rarely MP textures. GE textures are not developed in the JL and FS suites. In contrast, the CR and PV xenolith suites are comparatively finer-grained, with textures ranging from coarse POR to GE, with MP texture being predominant.

With few exceptions, a distinct texture is typically associated with each of the compositional groups defined for

COLOURED PICTURES
Images en couleur

Plate 7: XENOLITH TEXTURES (Cont.)

C. CR54: The mosaic porphyroclastic texture is associated with predominant neoblast proportions and is often characterized by elongate spinel grains and groups of grains.

D. NI69: A fine-grained texture composed almost entirely of neoblasts is commonly associated with the most pyroxene-rich lithologies.

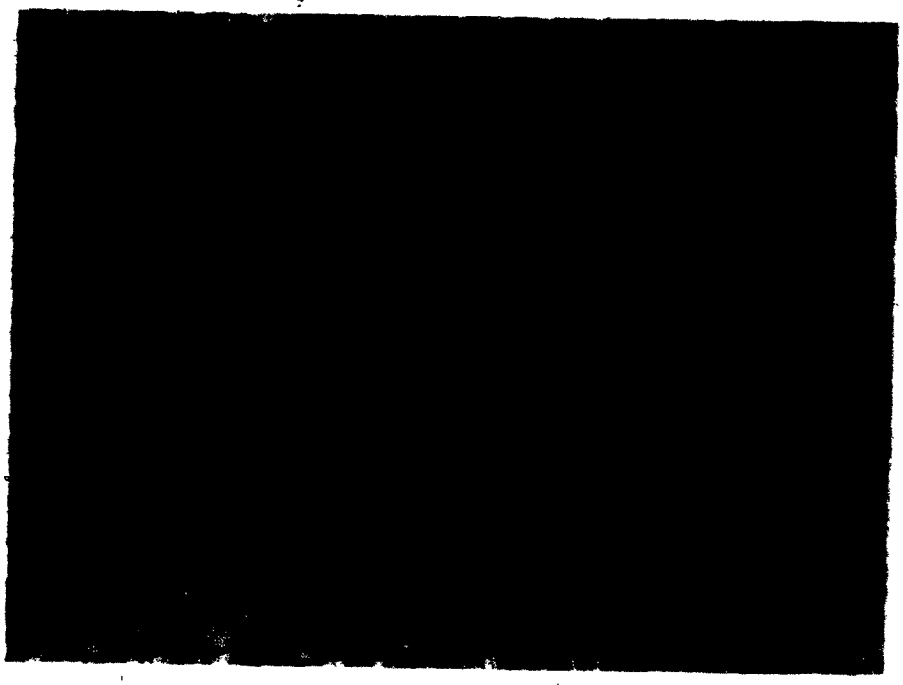

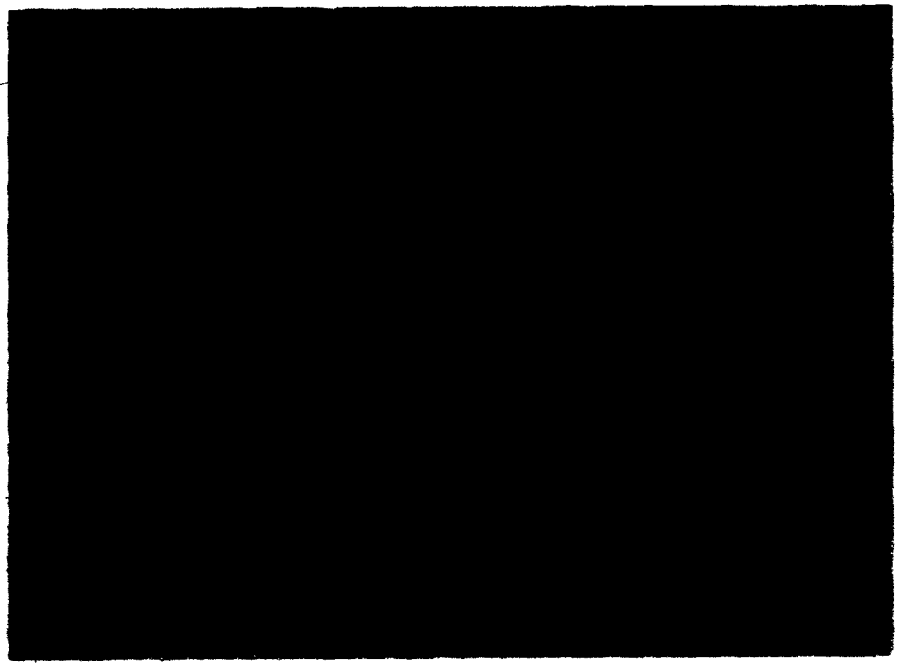

COLOURED PICTURES
Images en couleur

Table 3: CLASSIFICATION OF XENOLITH TEXTURES

	Coarse Equant	Porphyroclastic	Mosaic Porphyroclastic	Granuloblastic
% Olivine Porphyro-blasts	<90%	70%	30%	>10%
Olivine Porphyro. Grain sz.	4 mm	3-4 mm	2-3 mm	>2 mm
Preferred Olivine Orientatn.	absent	slightly elongate ‖ to foliation	variably elongate ‖ to foliation	equant: None tabular: ‖ to foliation
Olivine Optical Variations	kink bands + some wavy extinction	well-develop. kink bands ‖ to foliation	kink bands/wavy extinct. only in oliv. porphyrc.	predominantly strain-free neoblasts
Spinel Habit (see below)	"holly-leaf" w/in or btw. orthopyroxene grains	condensed holly leaf, often ‖ to foliation + interstitial	interstitial	interstitial
Spinel Color	dark red, brown or reddish brown	dark red, brown to medium brown and tan	medium brown to light brown	light brown to olive green
Rock Type	Harzburgite & cpx-poor Sp. Lherz.	Harzburgite to Sp. Lherz.	Sp. Lherz. to cpx-rich Sp. Lherz.	cpx-rich Sp. Lherz. to Olv. Websterite

the Cordilleran suites (Fig. 3). In each suite, the harzburgite samples are the coarsest-grained samples, typically with CE or relatively coarse POR textures. The larger range of modal compositions observed in the lherzolite samples is reflected by the range of their textures, predominantly between POR and MP with lesser GE. However, the textures of lherzolite samples are finer-grained than those of harzburgite, and are typically intermediate in texture between the POR and MP classes. The pyroxene lherzolite samples are typically the finest-grained xenoliths at each locality. Although their textures can range from POR to GE, the majority of the pyroxene lherzolite samples exhibit MP or GE textures. Pyroxene lherzolite samples with CE textures are absent. The textural ranges of group 3 and group 2 lherzolites appear to overlap, but the finer-grained nature of the former is apparent in each suite.

MINERALOGY

In the ultramafic xenoliths studied, olivine is light green and occurs as both equant to elongate porphyroclasts (2.0 to 4.0 km) and as equigranular to tabular neoblasts (0.5 to 0.9 mm). Kink bands are typically developed in all olivine porphyroclasts, but are characteristically absent in neoblasts. In a number of xenoliths, earlier kink bands have been subject to a later deformation, as suggested by the bending or kinking of earlier structures. An anomalous wavy extinction, reflecting the development of subgrains is

Figure 3: COMPARISON OF XENOLITH MODES AND TEXTURES

The modal dependence of xenolith textures is shown compared to the modal percent of olivine in the point-counted samples from each xenolith suite. A predominant trend towards finer-grained textures with decreasing modal olivine characterizes each of the suites. Y axis indicates the modal olivine content.

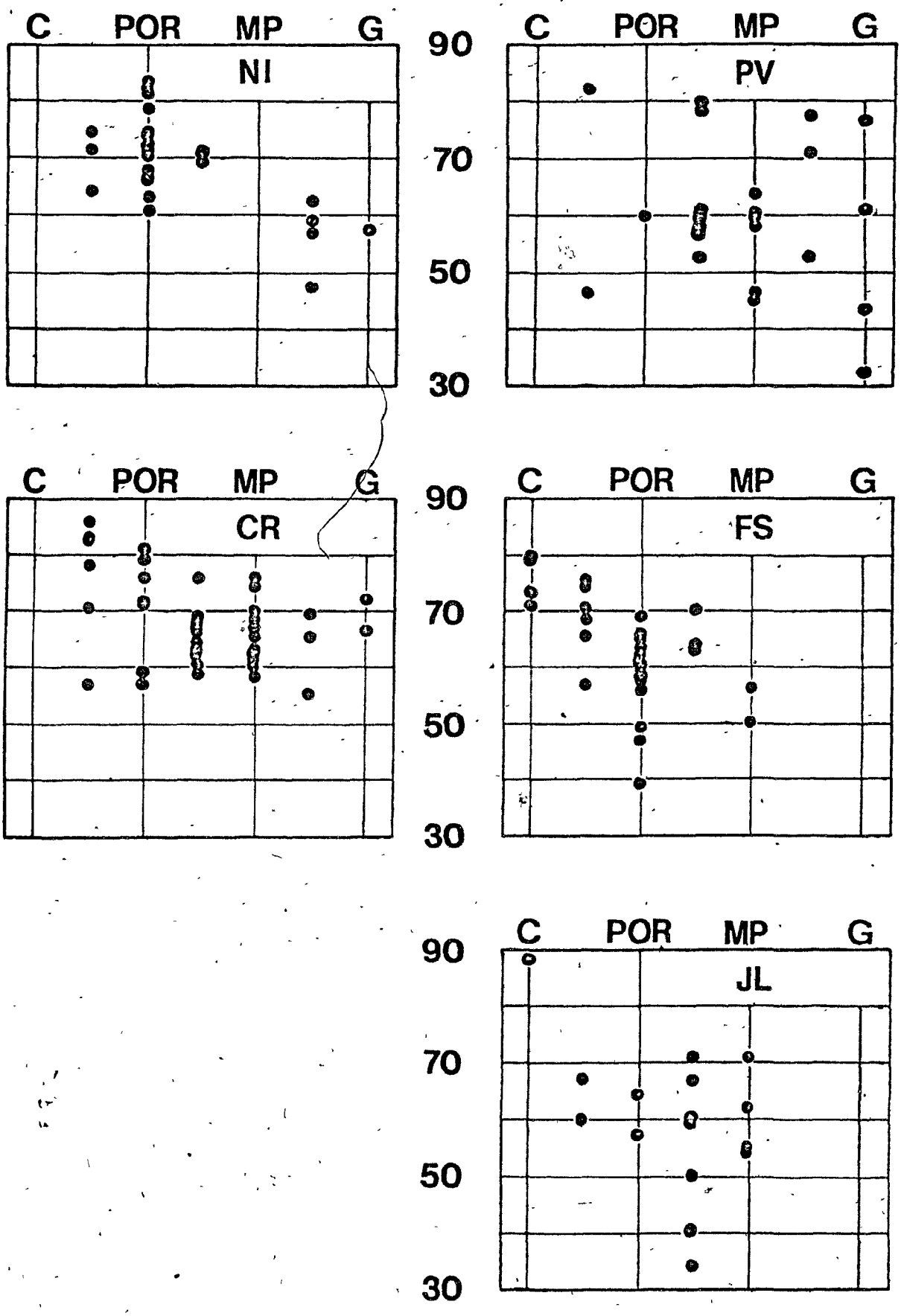
C
POR
MP
G
NI
PV
CR
FS
JL
90
70
50
30

observed in olivine with well-developed kink bands. Alteration is preferentially developed in the olivine porphyroclasts. Here, reddish-brown iddingsite, generally with a fine-grained opaque phase, commonly occurs as veins replacing olivine along grain margins or subgrain boundaries, and as masses at triple junctions. In contrast, olivine neoblasts are altered only in the few samples that show pervasive iddingsitization.

Orthopyroxene, light to dark brown in color, exhibits habits similar to those of olivine in the ultramafic xenoliths. It forms porphyroclasts (2 to 4 mm), typically smaller and more equant than coexisting olivine, and equigranular neoblasts (0.5 to 0.9 mm). In many samples, a fine-grained recrystallization assemblage after orthopyroxene is observed along the outer (0.01 to 0.02 mm) margins of the grains. This feature is particularly apparent in orthopyroxene in direct contact with the enclosing basalt, suggesting a reaction between the orthopyroxene and the host basalt (Plate 8). In addition, some orthopyroxene porphyroclasts contain exsolved clinopyroxene lamellae parallel to their (100) planes. In a few samples, spinel forms equant inclusions in orthopyroxene porphyroclasts. Neither exsolution features nor inclusions were found in orthopyroxene neoblasts.

In the Cordilleran peridotite xenoliths, clinopyroxene is typically a bright green diopside, in contrast to the clinopyroxene of websterite samples which are typically a dark green augite. In the peridotite samples, clinopyroxene is subordinate in grain size to the other silicate phases,

Plate 8: XENOLITH-BASALT CONTACT

Signs of a breakdown reaction involving the three silicate phases (FS6) in contact with the host basalt. In this picture, individual olivine grains (on the left and right margins) show little reaction, whereas both orthopyroxene (center) and clinopyroxene (left of center) are characterized by a fine-grained margin of breakdown products.

Plate 9: BREAKDOWN OF CLINOPYROXENE

Signs of disequilibrium along grain boundaries and fractures in clinopyroxene (JL5) in the interior of the xenolith sample (field of view = 3.5 mm).

COLOURED PICTURES
Images en couleur

most commonly occurring as neoblasts (0.5 - 1.5 mm), and only rarely as porphyroclasts (2.0 - 2.5 mm). In samples with CE and coarse POR textures, clinopyroxene typically occurs adjacent to orthopyroxene porphyroclasts. This spatial association of pyroxenes declines in samples with increasingly finer-grained textures. A close spatial association is also evident between clinopyroxene and spinel in samples with CE, POR and MP textures, but again is not observed in those with GE textures. An apparent breakdown of clinopyroxene along grain boundaries (Plate ?), similar to that previously described in orthopyroxene, is common. However, in clinopyroxene this reaction rim is not limited to grains near the margin of the xenoliths, but is found throughout the samples. It is particularly well-developed in grains adjacent to fine alteration veins (described below). Exsolution lamellae of orthopyroxene in rare clinopyroxene porphyroclasts are occasionally encountered. In a few instances, orthopyroxene forms two distinct sets of intersecting lamellae, parallel to the (100) and (001) planes of the host clinopyroxene grain, respectively.

Among the xenolith suites studied, spinel shows the greatest variation in appearance and habit (Plate 7). Spinel colors range from nearly opaque, dark red and brown to medium brown, tan and light olive green. In the Cordilleran peridotites, spinel is found with the following habits, in order of decreasing frequency: (1) isolated, interstitial grains with anhedral shapes (0.5 - 1.5 mm); (2) groups or

"trains" of irregular grains, parallel to the foliation of the xenolith and probably derived from a single, much larger, parent grain; (3) the distinctive "holly-leaf" habit (Mercier & Nicolas 1976), in which spinel grains (1 - 2 mm) are intergrown with orthopyroxene + clinopyroxene (Plate 10); (4) occasional, subrounded blebs as inclusions (0.2 - 0.8 mm) within olivine or orthopyroxene; (5) very rare poikilitic grains enclosing orthopyroxene inclusions. In about 20% of the peridotite xenoliths, especially those with coarser-grained textures, an opaque rim is observed on the margins of interstitial spinel grains. This feature is not found in any of the samples with finer-grained textures.

Fine veins, 0.2 - 0.8 mm in thickness, commonly cut the ultramafic xenoliths. The veins consist of fine-grained (0.2 - 0.5 mm) olivine, clinopyroxene and light brown glass, with or without plagioclase (Plate 11). Spinel may also be present as small (0.05 - 0.10 mm) grains within veins. In a websterite sample (CR48), several small (0.5 mm) grains of yellowish-brown phlogopite occur in similar fine-grained zones (Plate 12). Silicate grains adjacent to the veins exhibit the best-developed alteration of the types previously described (i.e., iddingsitization in olivine, breakdown of grain boundaries in pyroxene). Spinel adjacent to the veins is rimmed by the opaque alteration. These veins appear to be derived from a source external to the xenoliths, as their thickness typically increases toward the xenolith margins. However, the alteration reflected by the veins and iddingsite

Plate 10: "HOLLY-LEAF" SPINEL TEXTURES

This distinctive spinel texture is found in coarse-grained samples (CR3) intergrown with large orthopyroxene porphyroclasts, occasionally with smaller clinopyroxene grains present (field of view = 3.5 mm).

COLOURED PICTURES
Images en couleur

Plate 11: ALTERATION VEINS

In many samples, cross-cutting veins are found that increase in thickness toward the xenolith margin. The breakdown of large orthopyroxene porphyroclasts (left of center) and darkened coronas around spinel can be seen in FS15 (field of view = 3.5 mm).

Plate 12: THE LONE PHLOGOPITE

A websterite xenolith from the Castle Rock suite (CR48) contains the only traces of a hydrous phase in the 180 samples studied from the four Cordilleran suites. In this sample, pleochroic yellow-brown spinel is occasionally found in fine-grained zones (field of view = 1.75 mm).

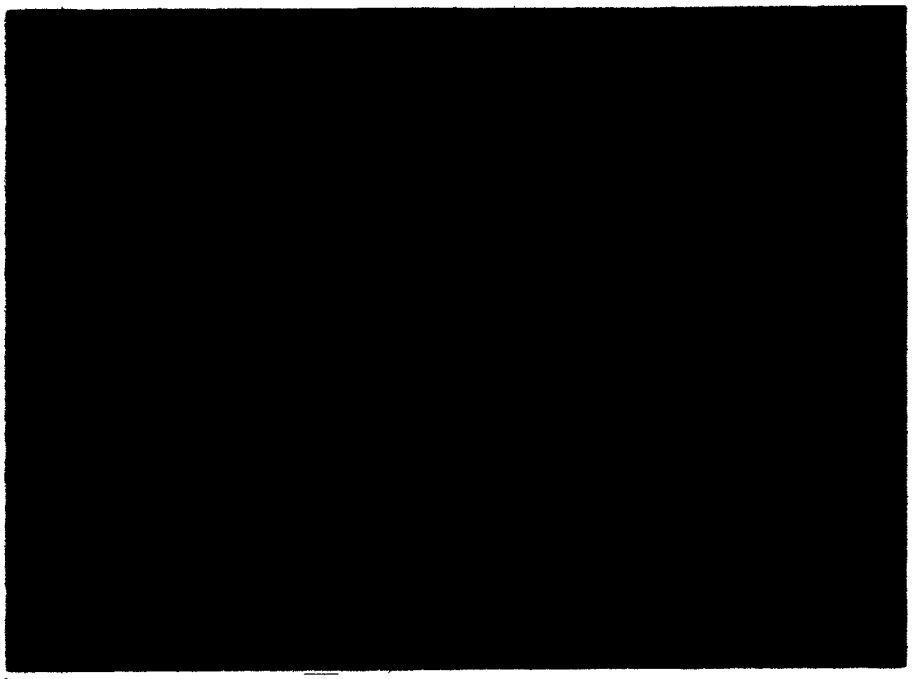

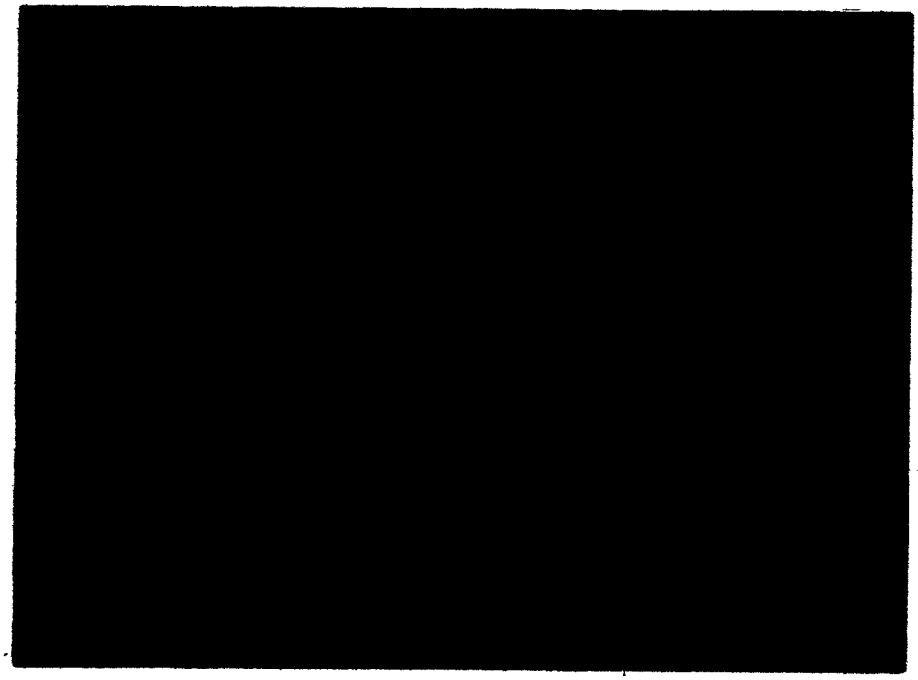

COLOURED PICTURES
Images en couleur

may be unrelated to the transport of the xenoliths in the host basalt. This view is supported by the preferential development of iddingsitize in samples with abundant olivine porphyroclasts. In coexisting annealed neoblasts most iddingsitization appears to be only a relic of the larger parent olivine grains.

4. MINERAL CHEMISTRY

Forty ultramafic xenoliths were chosen from the four Cordilleran localities for chemical analysis of their major mineral phases. The xenolith samples chosen for analysis span the range of textures and modal compositions found at each Cordilleran locality. The mineral analyses were performed with an M.A.C. electron microprobe, equipped with Krisel automation, at the Geophysical Laboratory, Carnegie Institute of Washington, D.C. Standard operating conditions included a filament current of 1200 nA at 15 kV and a beam diameter of approximately 15 μm. Matrix corrections were made using the Bence-Albee technique (Bence & Albee 1968), with alpha factors taken from Albee & Ray (1970). Analyses for which either total cations or weight percent oxides differed by more than $\pm$1.5% from the expected ideal values were discarded. The accepted mineral compositions are compiled in Appendix 2. Mineral compositions from a group of 11 Nunivak Island ultramafic xenoliths are also included in Appendix 2 for comparison (Francis 1974, unpublished data).

Although the range of major element concentrations are almost equivalent at each locality, as seen by the ratio (100 X Mg)/(Mg + Fe) or "Mg number" of the xenolith minerals (Fig. 4), they are distinctive for each of the xenolith groups. Harzburgite samples are characterized by the most magnesian olivine, orthopyroxene and clinopyroxene; the coexisting spinel compositions are the most iron- and

chromium-rich. The silicates in the lherzolite samples have lower Mg numbers in comparison to those of the harzburgite group, whereas spinel is more magnesian than those of group 1. In pyroxene lherzolite samples the silicate minerals are uniformly the least magnesian, whereas the coexisting spinel is the most magnesian. The few group 4 peridotite samples analyzed are characterized by low Mg numbers for all of the phases, including spinel.

OLIVINE

Olivine is the predominant mineral present in the xenolith samples. The individual compositions reported for olivine (Appendix 2) represent the average of 2 or 3 spots from at least 3 grains per sample. Olivine is homogeneous, both across individual grains and within samples. For 23 of the 25 samples analyzed, the Mg number, or forsterite content of olivine, ranges from 88.5 to 91.7 (Fig. 4). These olivine compositions are similar to those found in many other suites of spinel lherzolite xenoliths (Carswell 1980, Frey & Prinz 1978) and they are Mg-rich compared to most estimates of olivine (88.0 - 89.5) compositions in the primitive upper mantle (Carter 1970, Ringwood 1966). The olivine contained in the harzburgite samples are consistently the most Mg-rich (Fig. 4), whereas those of the pyroxene lherzolite samples lie within the estimated range of primitive olivine compositions. The lherzolite samples contain olivine with intermediate compositions. The two group 4 samples analyzed (CR37,

Figure 4: Mg NUMBERS OF XENOLITH MINERALS

The Mg numbers (100 X Mg/(Mg + Fe)) of the four coexisting minerals in samples from the Cordilleran suites. Note that the left-hand scale (increasing toward the top) is used for the silicate phases, whereas the right-hand scale (decreasing toward the top) used for spinel is inverted to maintain consistency with the distribution of silicate phases. Legend: 5 Jacques Lake; 4 Castle Rock; 3 Fort Selkirk; 2 Prindle Volcano; 1 Nunivak Island.

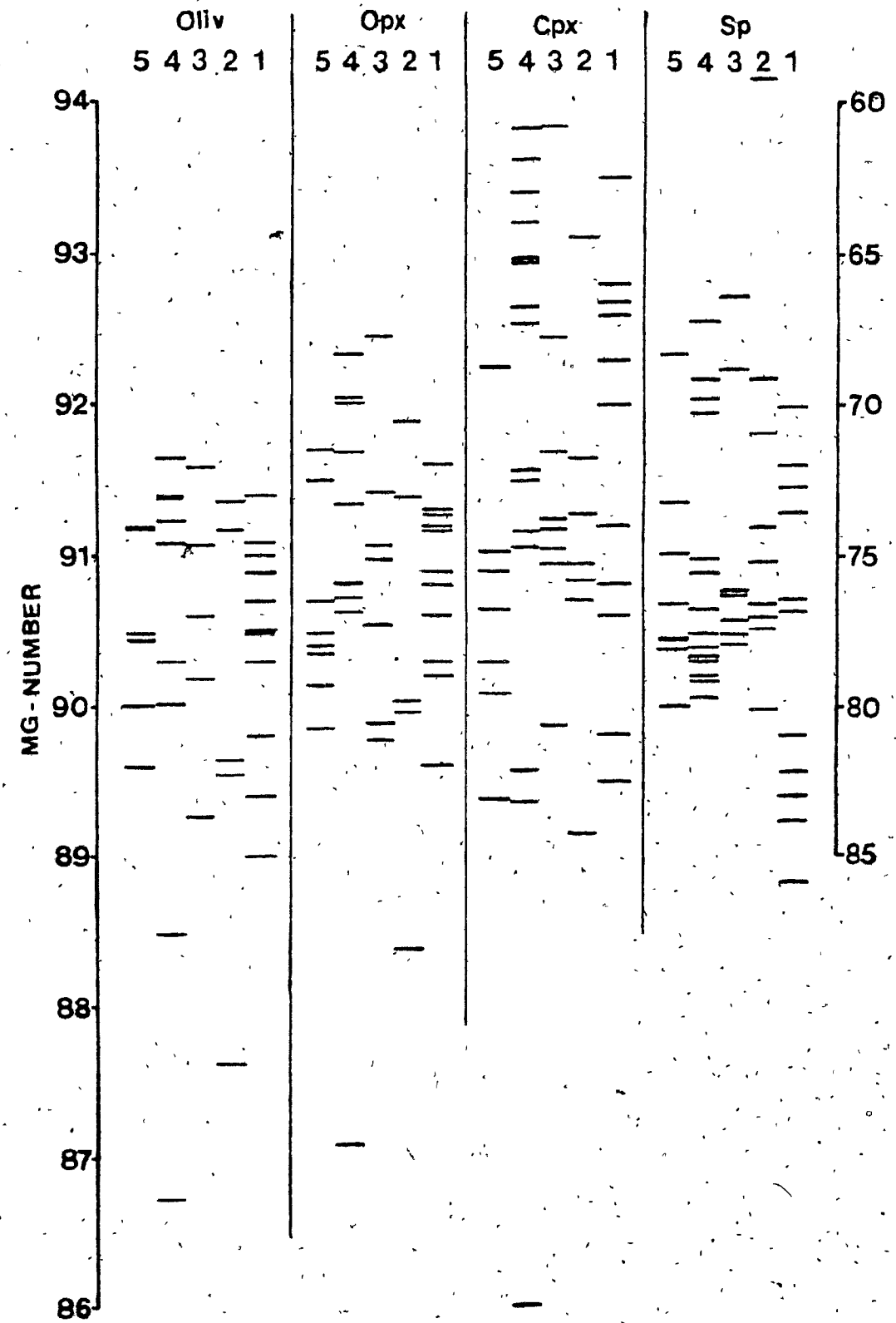
Oliv
5 4 3 2 1
Opx
5 4 3 2 1
Cpx
5 4 3 2 1
Sp
5 4 3 2 1
MG-NUMBER
94
93
92
91
90
89
88
87
86
60
65
70
75
80
85

PV39) contain olivine with Mg numbers (86.7, 87.6, respectively) lower than this range. The Mg-Fe distribution of olivine is further considered in Chapter 7.

Although olivine does vary in major-element compositions, very little minor-element substitution was found in the samples analyzed. Nickel and manganese concentrations are low but relatively constant between samples (average: 0.35 - 0.40 wt.% NiO, 0.10 - 0.16 wt.% MnO). Calcium is present in variably low concentrations, ranging from only 0.05 to 0.16 wt.% CaO.

ORTHOPYROXENE

Orthopyroxene is the more common and abundant of the two inosilicate phases in the Cordilleran xenolith samples. The compositions reported for orthopyroxene (Appendix 2) represent the average of at least 4 spots for each of 3 grains per section. The majority of the compositions from 29 Cordilleran xenoliths have slightly higher Mg numbers (89.9 to 92.4) than the coexisting olivine (Fig. 4), although the range of compositions observed in these two phases is nearly identical. Most orthopyroxene in xenoliths forms a narrow, well-defined cluster with low calcium concentrations, in the enstatite field of the pyroxene quadrilateral ($CaSiO_3$-$MgSiO_3$-$FeSiO_3$, Fig. 5). The peridotite group 4 samples are again exceptional with CR37 and PV39 containing distinctly iron-rich orthopyroxenes. In addition, the group 4 samples JL1, JL19, CR30, and CR37 are slightly calcic compared to the predominant cluster

Figure 5: PYROXENE QUADRILATERAL

The compositions of coexisting orthopyroxene and clinopyroxene in the analyzed xenolith samples plotted in terms of the relative proportion of the end-member components in the system $CaSiO_3$-$MgSiO_3$-$FeSiO_3$.

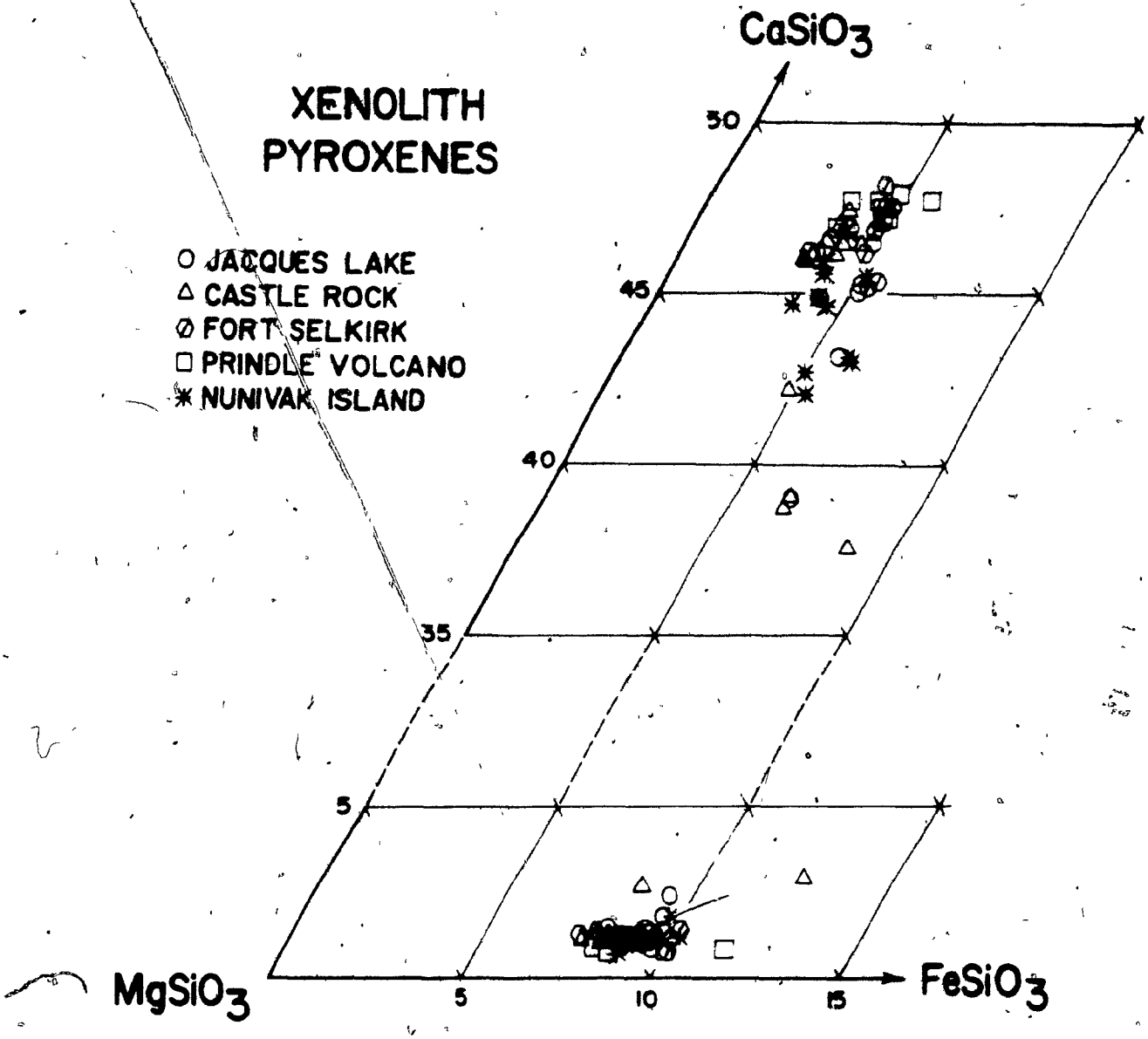
XENOLITH
PYROXENES
○ JACQUES LAKE
△ CASTLE ROCK
⌀ FORT SELKIRK
□ PRINDLE VOLCANO
✱ NUNIVAK ISLAND
CaSiO3
50
45
40
35
5
MgSiO3
5
10
15
FeSiO3

of orthopyroxene compositions in Figure 5.

The orthopyroxene structure consists of two octahedral (M1 and M2) and two tetrahedral (A and B) crystallographic sites, with the M2 site somewhat larger and more distorted than the M1 site (Deer et al. 1978). Compared to the structure of olivine, in which both the M1 and M2 octahedral sites are very similar, significant substitution of elements other than Mg and Fe can be expected in orthopyroxene in the octahedral sites. Ganguly & Ghose (1979) showed that aluminum substitutes for both Mg and Si, shortening of the M1-O and M2-O bond distances suggests that Al is distributed between both octahedral sites, with a strong preference to enter M1. Overall charge balance of an Al-orthopyroxene is thought to be preserved by equal substitution of Al in the tetrahedral and octahedral sites according to $2Al^{6+} = (MgSi)^{6+}$, in which case $X(Al)^{iv} = X(Al)^{vi}$ (Ganguly & Ghose 1979).

Assuming that sufficient aluminum must be preferentially added to silicon to fill the stoichiometric tetrahedral site, with the remaining Al substituting into the octahedral site, the distribution of aluminum between tetrahedral and octahedral sites approximates a 1:1 slope in the xenolith orthopyroxene (Fig. 6). However, there is some scatter and a regression line, through the distribution in Figure 6, intersects the Al^{iv} axis at approximately 0.05 atoms Al^{iv} 4 cations indicating the presence of tetrahedrally coordinated aluminum in excess of octahedrally coordinated aluminum. An

Figure 6: DISTRIBUTION OF Al^{iv} and Al^{vi} IN ORTHOPYROXENE

This shows the distribution of tetrahedrally and octahedrally coordinated aluminum calculated for orthopyroxene by assuming that Al_{iv} equals the difference between the available tetrahedral sites (based on 4 cations) and the concentration of silica. The difference between total aluminum and Al_{iv} is assigned to the octahedral site. Color code: red harzburgite; green lherzolite; yellow pyroxene lherzolite; uncolored group 4 peridotites.

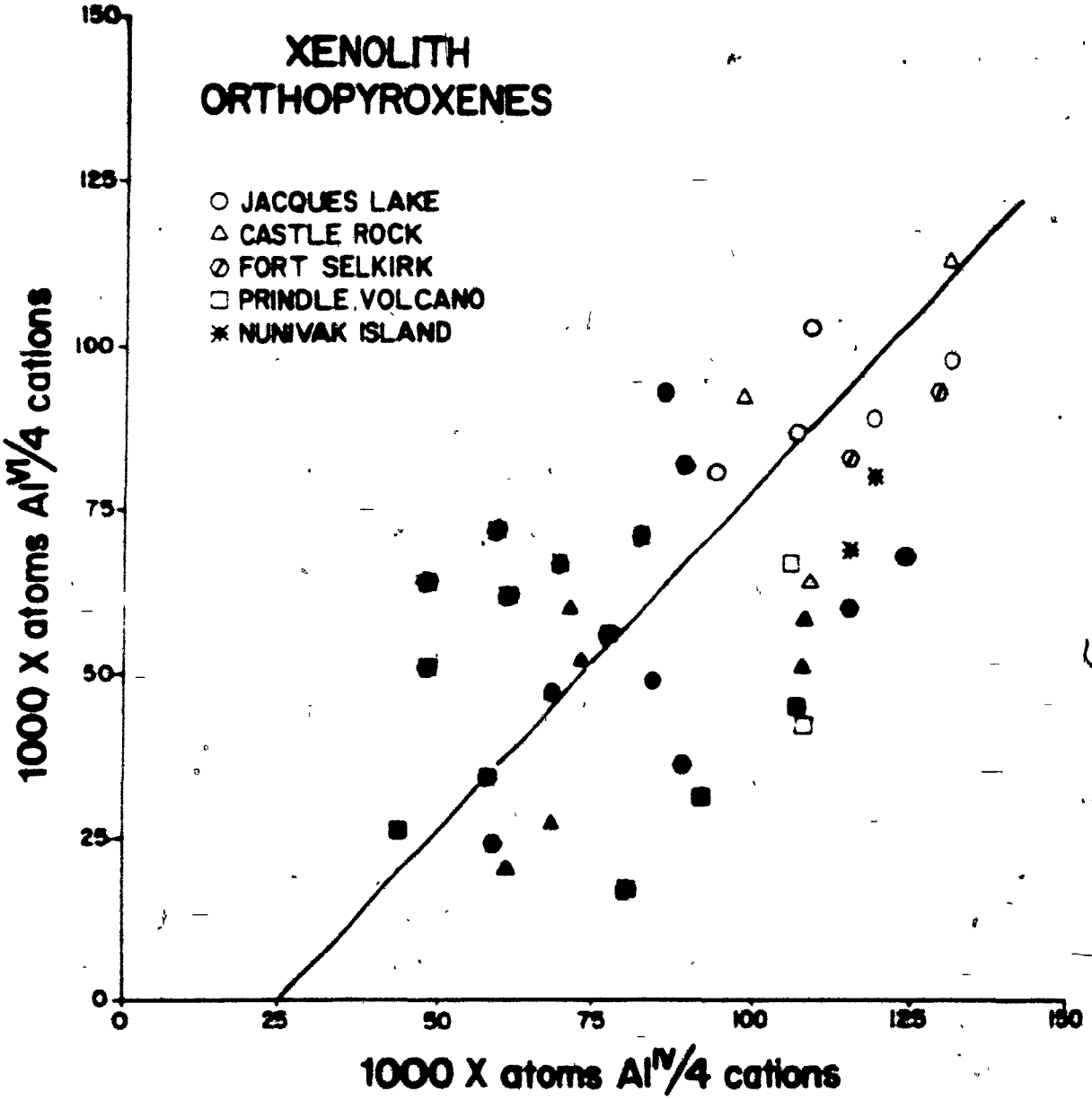
XENOLITH
ORTHOPYROXENES
JACQUES LAKE
CASTLE ROCK
FORT SELKIRK
PRINDLE VOLCANO
NUNIVAK ISLAND
1000 X atoms AlVI/4 cations
1000 X atoms AlIV/4 cations
0
25
50
75
100
125
150

equivalent range of concentrations is observed in each suite, with aluminum in orthopyroxene increasing in the sequence harzburgite to lherzolite to pyroxene lherzolite. The orthopyroxenes analyzed from group 4 xenolith samples (CR37 and PV39) have uniformly high aluminum contents, comparable to those of the pyroxene lherzolite samples.

If compared to the survey made by Stephens & Dawson (1977), which included 1-9 orthopyroxenes from kimberlite xenoliths, most of the Cordilleran orthopyroxene samples would be assigned to the Cr-Al-enstatite group largely on the basis of their Al contents. Stephens & Dawson suggested that the compositions of the Cr-Al-enstatite group imply some garnet component in solid solution with the orthopyroxene (further discussed in Chapter 5).

The concentrations of titanium and sodium, although low in the orthopyroxene of xenoliths, are positively correlated with aluminum content (Fig. 7) and progressively increase in the above sequence of xenolith groups. Chromium content, in contrast, is inversely correlated to that of aluminum in the xenolith orthopyroxenes (Fig. 7). The sum of other than pyroxene quadrilateral components ("others component", Cameron & Papike 1981, $Al^{VI} + Fe^{3+}$ (calculated from stoichiometry in Appendix 2) + Cr + Ti substituting in the octahedrally coordinated crystallographic sites in orthopyroxene are low for the Cordilleran xenoliths.

The manganese concentration in orthopyroxene appears to be independent of both aluminum concentration (Fig. 7) and

Figure 7: MINOR ELEMENTS IN ORTHOPYROXENE

A comparison of minor elements with the concentration of total alumina based on 4 cations for orthopyroxene. Color code: red harzburgite; green lherzolite; yellow pyroxene lherzolite; uncolored group 4 peridotites.

A. mole Al/4 cations vs. mole Ti/4 cations

B. mole Al/4 cations vs. mole Na/4 cations

C. mole Al/4 cations vs. mole Cr/4 cations

D. mole Al/4 cations vs. mole Mn/4 cations

▲ NUNIVAK ISLAND
+ PRINDLE VOLCANO
× FORT SELKIRK
● CASTLE ROCK
◆ JACQUES LAKE

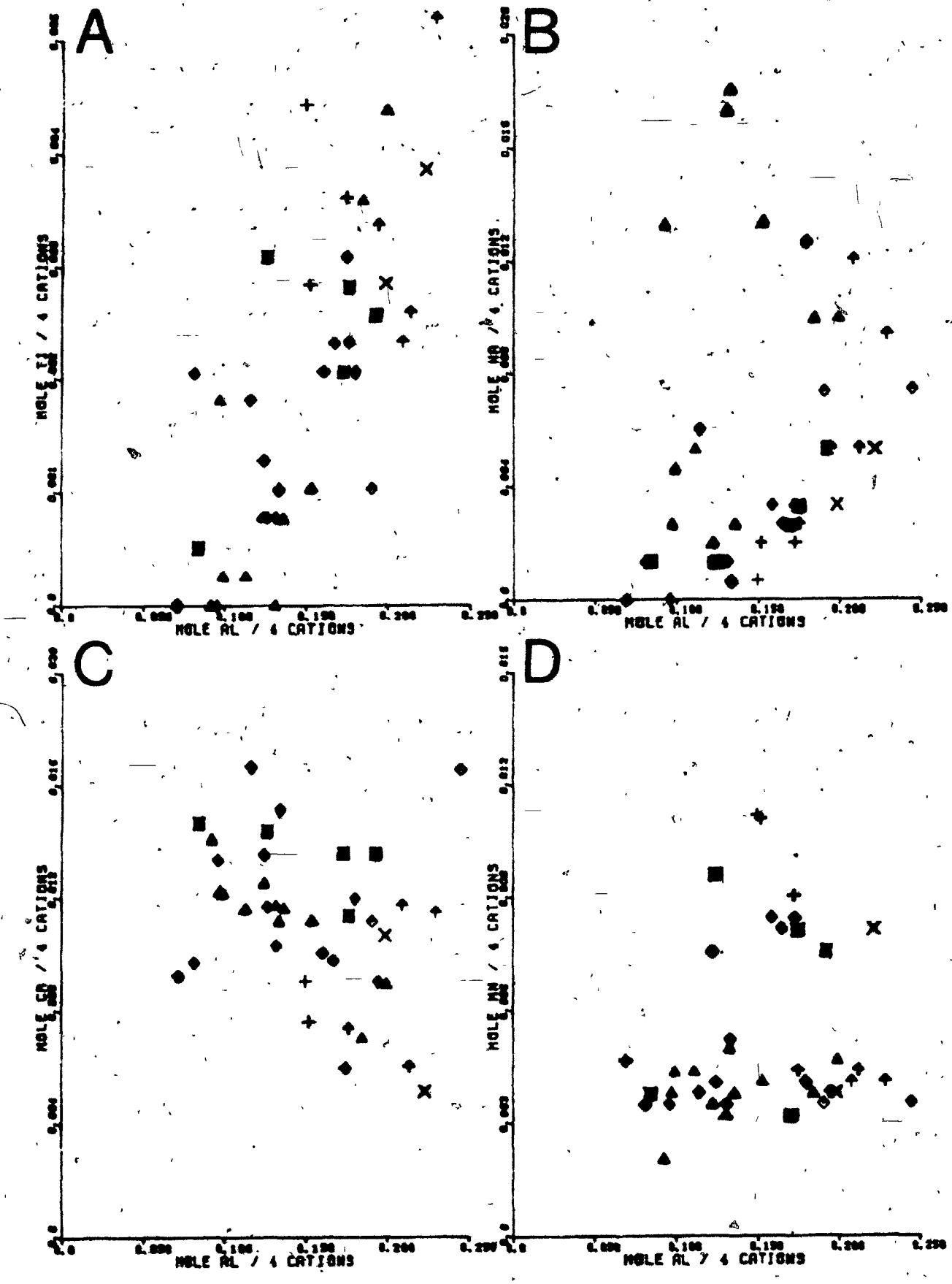
A
B
C
D
MOLE TI / 4 CATIONS
MOLE NB / 4 CATIONS
MOLE CR / 4 CATIONS
MOLE MN / 4 CATIONS
MOLE AL / 4 CATIONS
MOLE AL / 4 CATIONS
MOLE AL / 4 CATIONS
MOLE AL / 4 CATIONS

Mg number (Appendix 2). Orthopyroxene from the JL suite is uniformly low in Mn content, similar to many of the samples from the other suites. However, in the CR, FS and PV suites, Mn concentration appears to be bimodal (Fig. 7), with many of the lherzolite and pyroxene lherzolite samples containing nearly twice the Mn observed in the majority of xenolith orthopyroxenes.

CLINOPYROXENE

A variable, but typically low proportion of clinopyroxene is present in most of the Cordilleran xenolith samples. The clinopyroxene compositions (Appendix 2) represent the averages of at least 5 spots for each of 3 grains per sample. The clinopyroxene in xenoliths exhibit greater compositional variation than that seen in either olivine or orthypyroxene. Mg numbers of clinopyroxene are higher (89.9 to 93.8) than those of coexisting silicate phases (Fig. 4). Although the majority of the analyzed clinopyroxenes form a distinct cluster in the diopside field of the pyroxene quadrilateral (Fig. 5), many of the clinopyroxenes from the JL and CR xenolith suites are endiopside in composition. The clinopyroxene contained in the group 4 peridotite samples plot in the augitic fields of the pyroxene quadrilateral (Fig. 5).

Another illustration of the compositional variation of clinopyroxene in the xenoliths (Fig. 5) is obtained by comparing the ratio Ca/(Ca + Mg) with the aluminum content (Fig. 8). The clinopyroxene compositions form a band along

Figure 8: COMPARISON OF Ca/(Ca + Mg) VS. Al IN CLINOPYROXENE

The variation in the pyroxene quadrilateral components Ca and Mg is shown to be comparatively small compared to the concentration of coexisting total aluminum between the xenolith samples. Color code: red harzburgite; green lherzolite; yellow pyroxene lherzolite; uncolored group 4 peridotites.

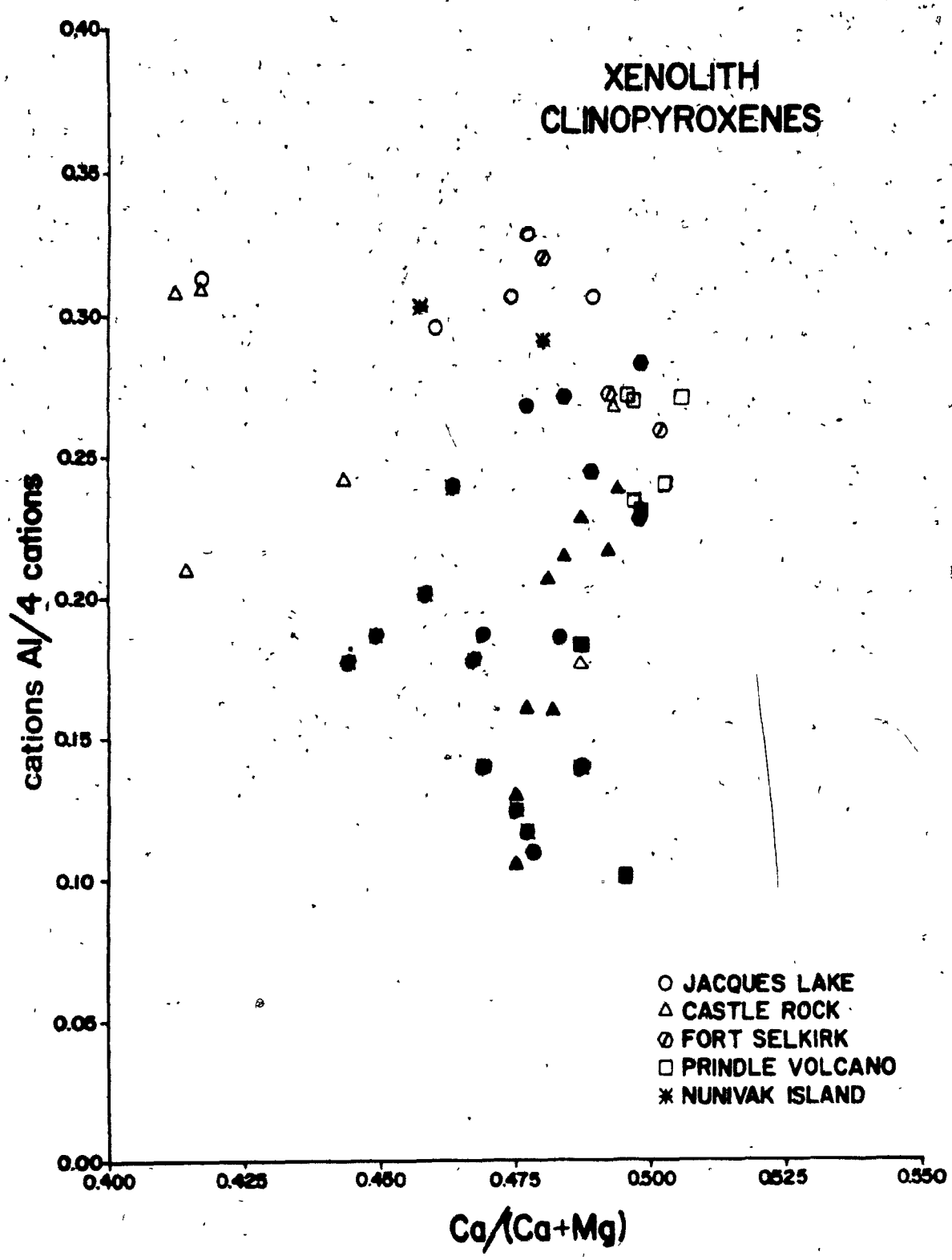
XENOLITH
CLINOPYROXENES
cations Al/4 cations
0.40
0.35
0.30
0.25
0.20
0.15
0.10
0.05
0.00
0.400
0.425
0.450
0.475
0.500
0.525
0.550
Ca/(Ca+Mg)
O JACQUES LAKE
△ CASTLE ROCK
⌀ FORT SELKIRK
□ PRINDLE VOLCANO
✱ NUNIVAK ISLAND

which the aluminum content progressively increases from the harzburgite to the lherzolite and pyroxene lherzolite groups with little change in the Ca/(Ca + Mg) ratio. In contrast, the augitic group 4 clinopyroxene samples JL1, CR1, CR37 and CR55 have comparatively high aluminum contents, but exhibit a range of Ca/(Ca + Mg) values.

The variation of aluminum contents of clinopyroxene in the xenoliths is accompanied by a wide range of the aluminum distribution between tetrahedral and octahedral sites (Fig. 9). The experiments of Herzburg (1978) support a charge balance model for $CaMgSi_2O_6$-$CaAl_2SiO_6$ solid solutions in which Al and Mg mix randomly in the M1 octahedral site; Al in the tetrahedral site is coupled to its nearest neighbor Al in the M1 site; and Si and Al in the tetrahedral sites are ordered. The expression of Jenkins & Newton (1979) for the activity of $CaMgSi_2O_6$ assumes "one-site" ideal mixing of Mg and Al on the M1 octahedral site, with the octahedral and tetrahedral Al atoms linked and not substituting independently. Unlike Al^{vi}/Al^{iv} ratios in coexisting orthopyroxene, those of clinopyroxene are typically greater than 1 in the Cordilleran xenolith samples. The more aluminous clinopyroxenes, predominantly from the JL and FS suites, have a higher proportion of octahedrally coordinated aluminum than that typical of the CR-PV suites.

Although the pyroxene lherzolite xenoliths include clinopyroxenes with major element compositions that overlap those of the lherzolite xenoliths, the compositional identity

Figure 9: DISTRIBUTION OF Al^{iv} and Al^{vi} IN CLINOPYROXENE

This shows the distribution of tetrahedrally and octahedrally coordinated aluminum calculated for clinopyroxene by assuming that Al^{iv} equals the difference between the available tetrahedral sites (based on 4 cations) and the concentration of silica. The difference between total aluminum and Al^{iv} is assigned to the octahedral site. Color code: red harzburgite; green lherzolite; yellow pyroxene lherzolite; uncolored group 4 peridotites.

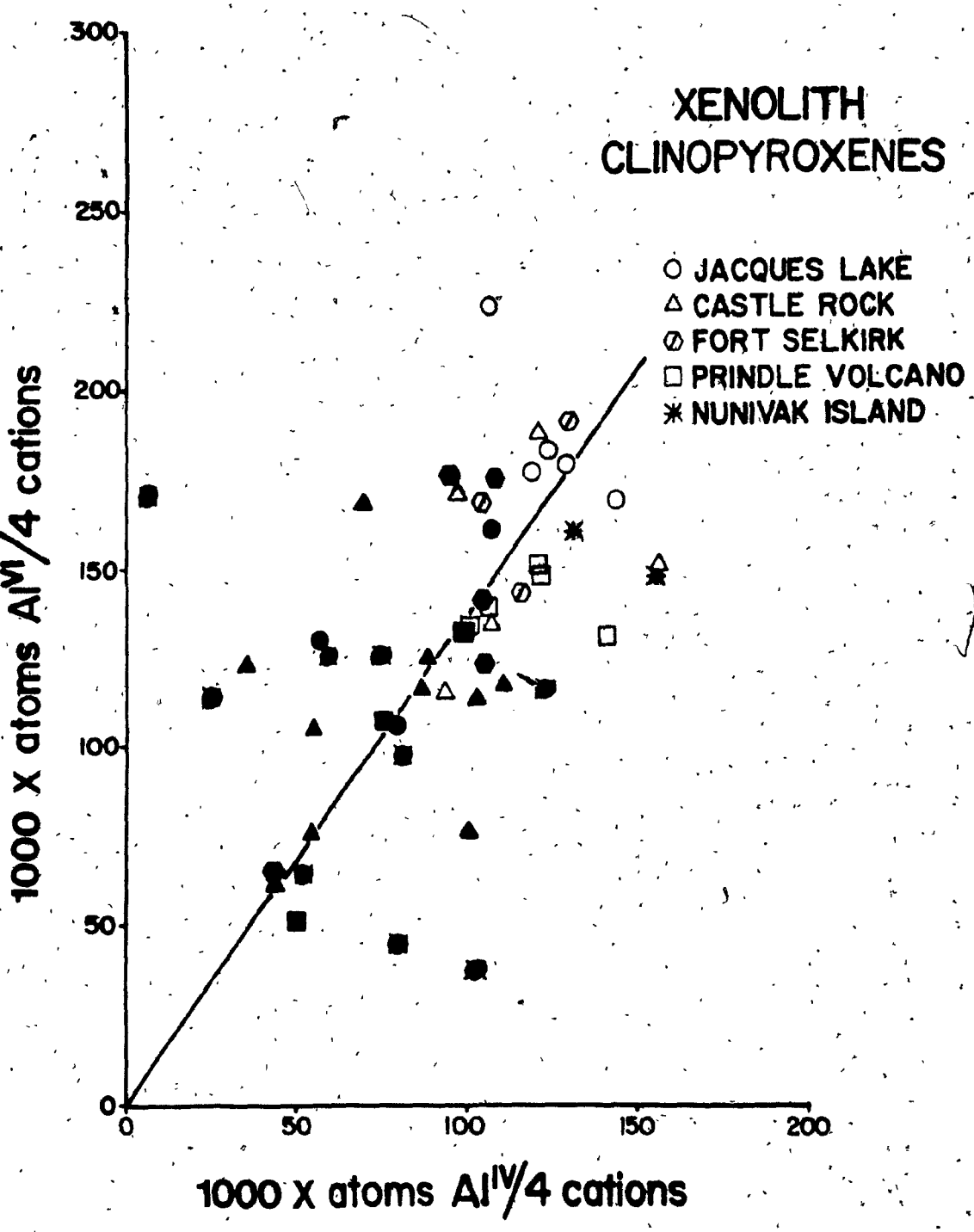
XENOLITH
CLINOPYROXENES
JACQUES LAKE
CASTLE ROCK
FORT SELKIRK
PRINDLE VOLCANO
NUNIVAK ISLAND
1000 X atoms AlVI/4 cations
1000 X atoms AlIV/4 cations
0
50
100
150
200
250
300

of the group 3 xenoliths is best illustrated by the high concentrations of Al, Ti and Na (Fig. 10) in their clinopyroxene. The minor cations in clinopyroxene can be evaluated in terms of the mole percent of the "others components" (Camerson & Papike 1981) Na, R3 (the sum of Al^{vi}, Fe^{3+}, Cr and Ti), and Al^{iv}. These minor elements substitute in the M2 octahedral, M1 octahedral and tetrahedral crystallographic sites in clinopyroxene, respectively. The range of each of the "others components" is approximately equivalent in the four Cordilleran suites (Fig. 11) however, the proportion of each consistently increases between xenolith groups in the sequence harzburgite to lherzolite to pyroxene lherzolite.

Of the three "others components", the R3 group shows the best linear correlation with the concentrations quadrilateral components (Fig. 11), and reflects their variable concentrations in the bulk composition. The proportion of R3 component (Fig. 11) is also reflected in a concurrent variation in Al^{iv}, as seen by comparing it to correlation between Al^{vi} and Al^{iv} (Fig. 9). This is supported by the models of coupled substitution of the aluminum in clinopyroxene between the octahedral and tetrahedral crystallographic sites.

Among the "others components" the greatest variation is observed between the Na and Al^{iv} components in the Cordilleran clinopyroxenes. Although Na and Al^{iv} approximate a positive linear correlation increasing in the sequence harzburgite to lherzolite to pyroxene lherzolite, two minor groups of samples depart from the trend. The group 4

Figure 10: MINOR ELEMENTS IN CLINOPYROXENE

A comparison of minor elements with the concentration of total aluminum based on 4 cations for clinopyroxene. Color code: red harzburgite; green lherzolite; yellow pyroxene lherzolite, uncolored group 4 peridotites.

A. mole Al/4 cations vs. mole Ti/4 cations

B. mole Al/4 cations vs. mole Na/4 cations

C. mole Al/4 cations vs. mole Cr/4 cations

D. mole Al/4 cations vs. mole Mn/4 cations

▲ NUNIVAK ISLAND
+ PRINDLE VOLCANO
× FORT SELKIRK
◇ CASTLE ROCK
✦ JACQUES LAKE

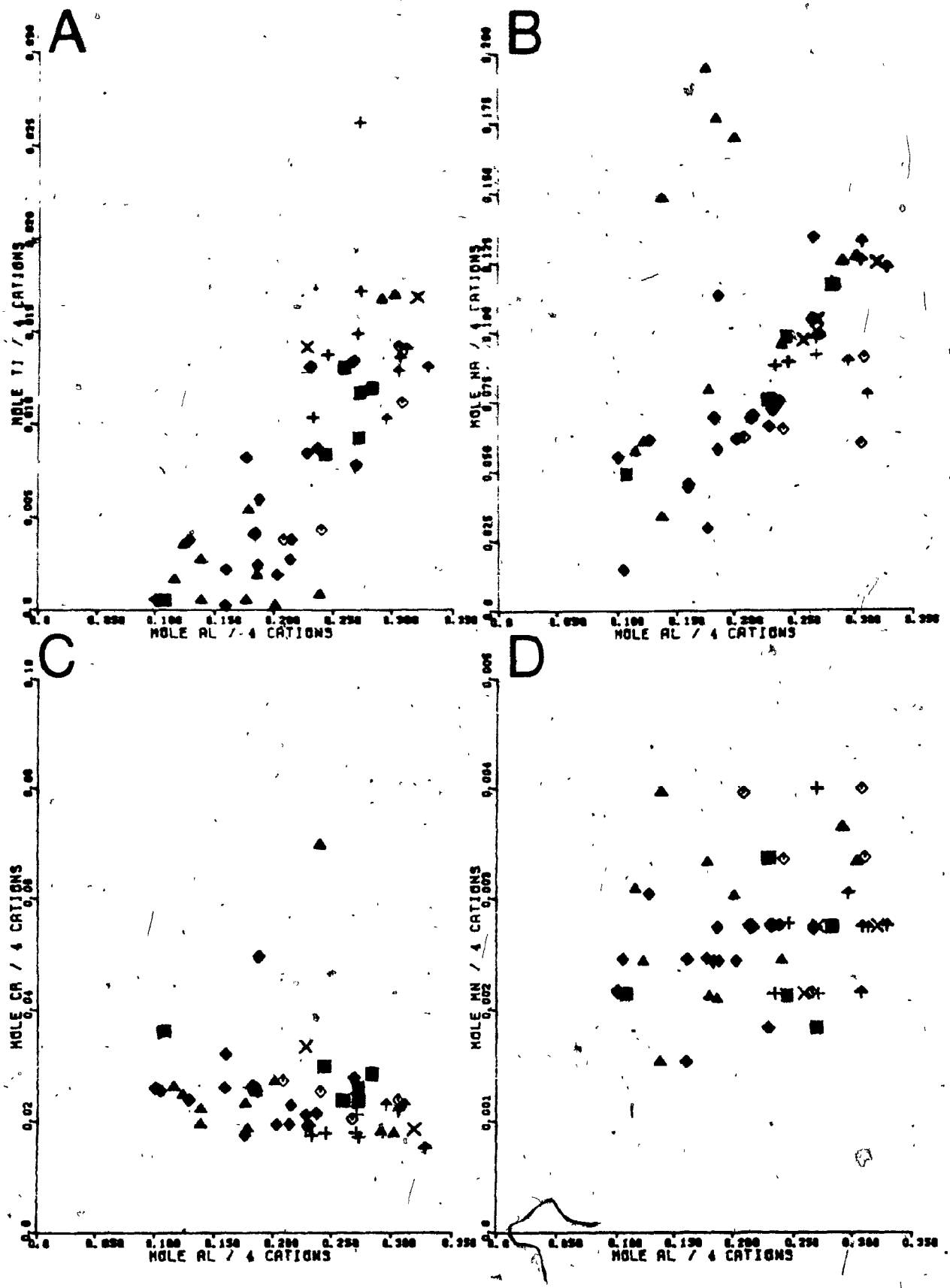
A
MOLE TI / 4 CATIONS
MOLE AL / 4 CATIONS
B
MOLE NA / 4 CATIONS
MOLE AL / 4 CATIONS
C
MOLE CA / 4 CATIONS
MOLE AL / 4 CATIONS
D
MOLE MN / 4 CATIONS
MOLE AL / 4 CATIONS

Figure 11: "OTHERS COMPONENTS" IN CLINOPYROXENE

A comparison of "others components" (other than pyroxene quadrilateral components: Cameron & Papike 1981) in mole percent for clinopyroxene. Color code: red harzburgite; green lherzolite; yellow pyroxene lherzolite; uncolored group 4 peridotites.

A. quad components v. R3 (sum of Al^{vi} + Ti + Cr + Fe^{+3})

B. quad components vs. Na

C. quad components vs. Al^{iv}

D. Na vs. Al^{iv}

▲ NUNIVAK ISLAND
+ PRINDLE VOLCANO
× FORT SELKIRK
◆ CASTLE ROCK
♦ JACQUES LAKE

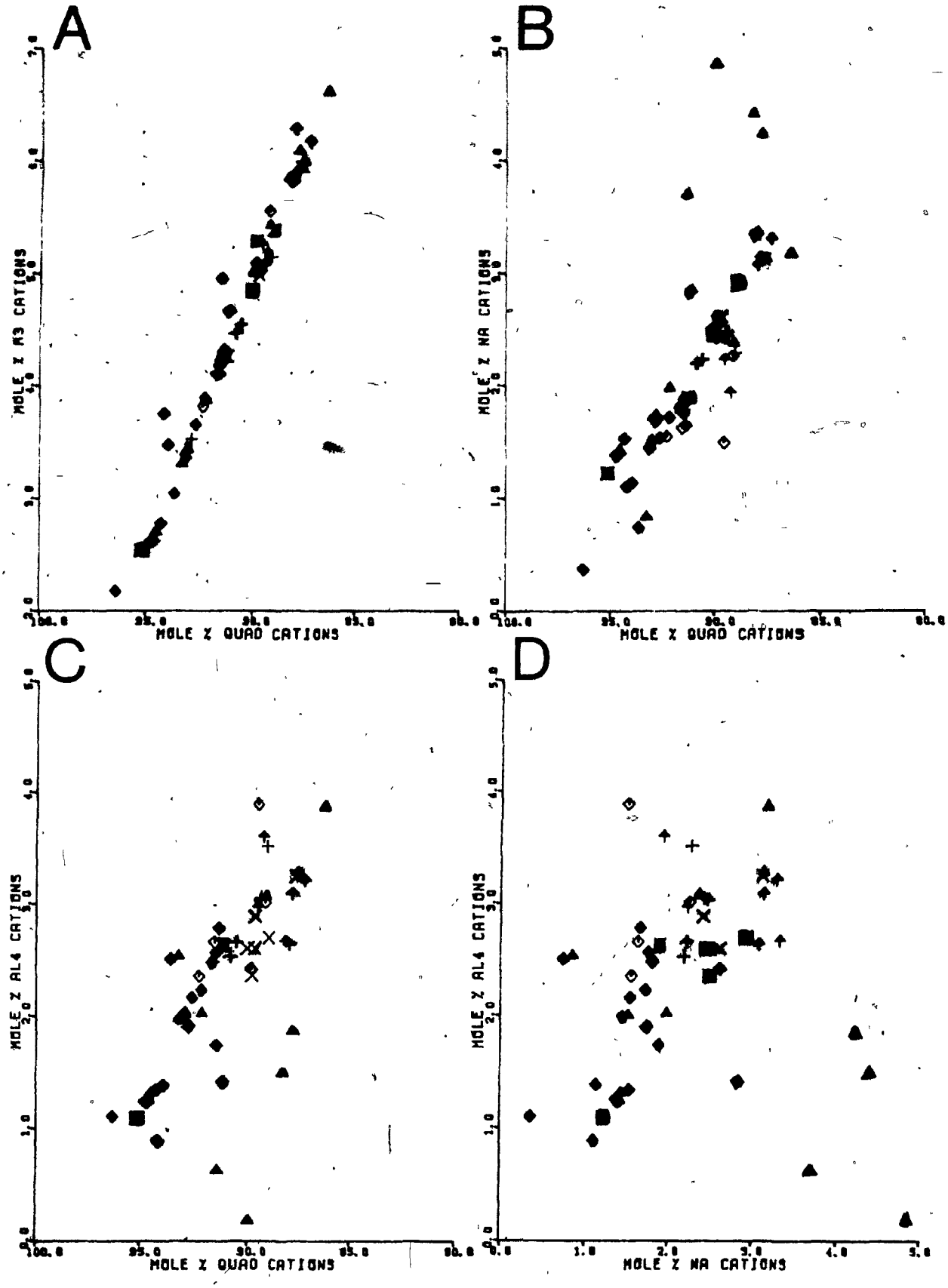
A
MOLE % K3 CATIONS
MOLE % QUAD CATIONS
B
MOLE % NA CATIONS
MOLE % QUAD CATIONS
C
MOLE % AL4 CATIONS
MOLE % QUAD CATIONS
D
MOLE % AL4 CATIONS
MOLE % NA CATIONS

clinopyroxenes are relatively enriched in Al^{iv} component, whereas clinopyroxenes from the hydrous Nunivak Island xenoliths are much more enriched in Na component (discussed further in Chapter 6).

A comparison of the behavior of a compatible minor element (Cr) with respect to a readily fusible element (Na) in the clinopyroxenes is presented in Figure 12. Stosch (1981) noted that Cr^{3+} has an ionic radius similar to that of Mg^{2+} and should be readily incorporated into the M2 site in clinopyroxene. A large increase in Na is accompanied by only a slight decrease in Cr (Fig. 12) in the sequence harzburgite to lherzolite to pyroxene lherzolite. The average chromium content of clinopyroxenes from the FS suite appears to be uniformly greater than that from the other three suites.

SPINEL

Spinel is present as a ubitquitous minor phase in the Cordilleran xenoliths. The spinel compositions reported (Appendix 2) represent the average of at least 5 spots for each of 3 grains per sample. Spinel shows the greatest compositional variation of the four phases analyzed (Fig. 13). The Mg numbers of spinel are inversely correlated to those of the coexisting silicate phases, with the spinel mg numbers increasing in the sequence harzburgite to lherzolite to pyroxene lherzolite. The mole proportions in Appendix 2 were calculated by assuming that iron in excess of that required to fill the octahedral site was present as Fe.

Figure 12: COMPARISON OF Cr VS. Na IN CLINOPYROXENE

The distribution of chromium and coexisting sodium based on 4 cations in clinopyroxene shows the variation in compatible vs. fusible components. Color code: red harzburgite; green lherzolite; yellow pyroxene lherzolite; uncolored group 4 peridotites.

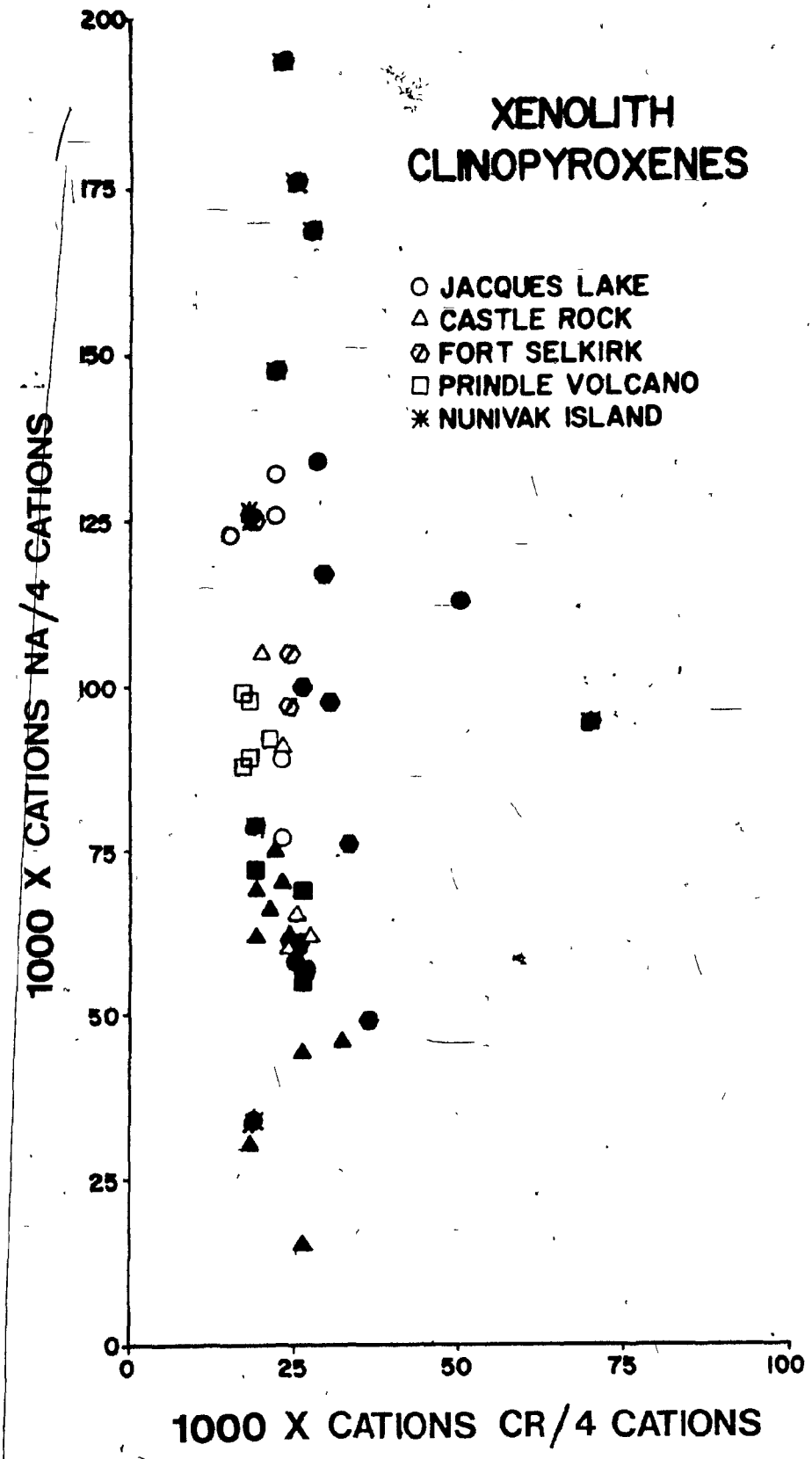
XENOLITH
CLINOPYROXENES
O JACQUES LAKE
△ CASTLE ROCK
⊘ FORT SELKIRK
□ PRINDLE VOLCANO
✳ NUNIVAK ISLAND
1000 X CATIONS NA/4 CATIONS
1000 X CATIONS CR/4 CATIONS
0
25
50
75
100
125
150
175
200

Figure 13: COMPARISON OF Mg/(Mg + Fe) VS. Cr/(Cr + Al) IN SPINEL

The distribution of the two solid-solution series that comprise the major elements in spinel. Note the large proportion of aluminous spinel compositions present in the Cordilleran suites. Color code: red harzburgite; green lherzolite; yellow pyroxene lherzolite; uncolored group 4 peridotites.

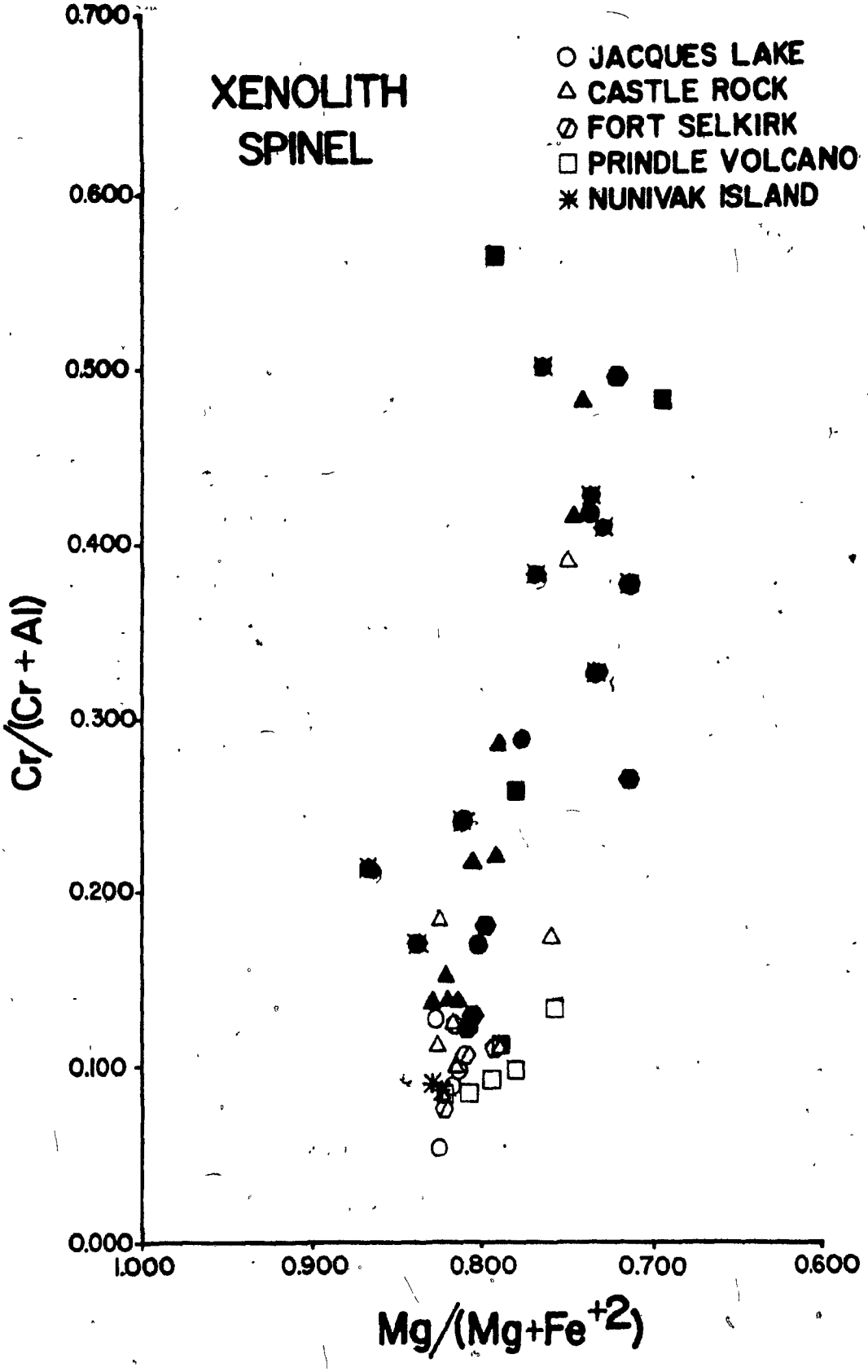
XENOLITH
SPINEL
JACQUES LAKE
CASTLE ROCK
FORT SELKIRK
PRINDLE VOLCANO
NUNIVAK ISLAND
0.700
0.600
0.500
0.400
0.300
0.200
0.100
0.000
Cr/(Cr+Al)
1.000
0.900
0.800
0.700
0.600
Mg/(Mg+Fe+2)

There is a strong correlation between spinel color (as observed in thin section) and the ratio Cr/(Cr + Al); the highest values being found in the dark red and brown spinel, intermediate values in medium brown spinel, and the lowest values in greenish brown spinel. The ratio Cr/(Cr + Al) decreases in spinel with increasing Mg numbers in the sequence harzburgite to lherzolite to pyroxene lherzolite. The pyroxene lherzolite and many of the lherzolite xenoliths contain spinel compositions that form a prominent group within the pleonaste field (Fig. 13). However, in each suite, the spinel population extends to Cr- and Fe-rich compositions along a linear trend ranging from picotite to magnesio-chromite. The majority of the CR spinels (similar to the CR clinopyroxenes) are depleted in aluminum compared to those of the JL, FS and PV suites.

The concentrations of the minor elements titanium, manganese and nickel are correlated with variations in the major element contents of spinel in the Cordilleran xenoliths (Fig. 14). Titanium contents are low, but increase slightly from the harzburgite to the lherzolite and pyroxene lherzolite spinels. However, the titanium content of spinel in many of the group 4 samples and also in the harzburgite samples JL15 and CR44 are significantly higher than the majority of spinel compositions. The manganese content of spinel exhibits a reciprocal relationship to that of titanium being relatively concentrated in the harzburgite spinel, and decreasing in the lherzolite and pyroxene lherzolite spinel.

Figure 14: MINOR ELEMENTS IN SPINEL

A comparison of minor elements based on 24 cations with the ratio of Cr/(Cr + Al) for spinel. Color code: red harzburgite; green lherzolite; yellow pyroxene lherzolite; uncolored group 4 peridotites.

A. Cr/(Cr + Al) vs. mole Ti/24 cations

B. Cr/(Cr + Al) vs. mole Mn/24 cations

C. Cr/(Cr + Al) vs. mole Ni/24 cations

▲ NUNIVAK ISLAND
\+ PRINDLE VOLCANO
× FORT SELKIRK
◇ CASTLE ROCK
✦ JACQUES LAKE

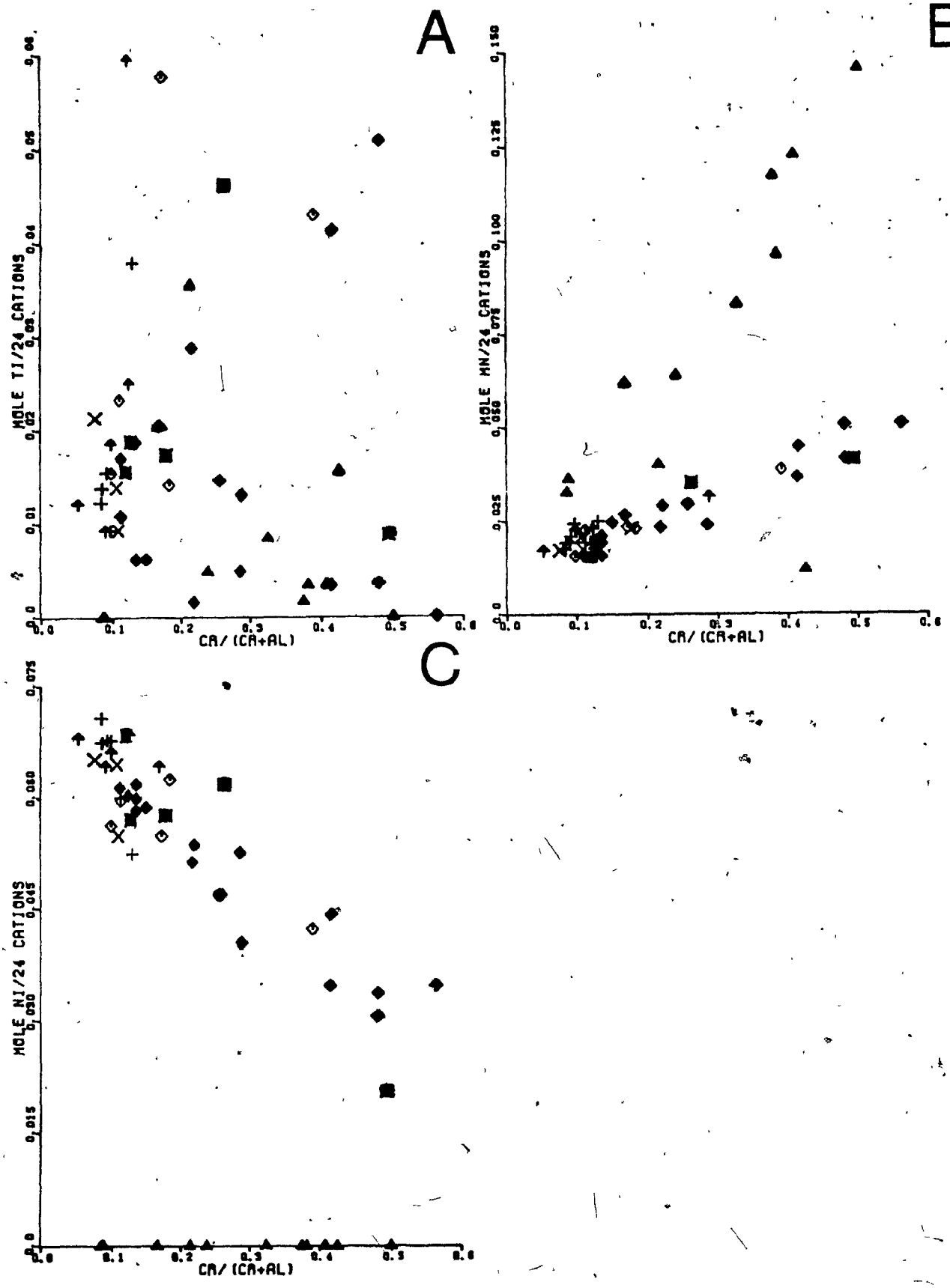
A
B
C
MOLE TI/24 CATIONS
MOLE MN/24 CATIONS
MOLE NI/24 CATIONS
CA/ (CA+AL)
CA/ (CA+AL)
CA/ (CA+AL)

In contrast, however, the most Ni-rich compositions are the most aluminous with Ni decreasing in spinel from pyroxene lherzolite samples to lherzolite and harzburgite samples! From single ionic-radii criteria, it is expected that Ni^{2+} would be a compatible element in spinel, substituting for Mg or Fe in the tetrahedral position. However, Burns (1973) suggested that Ni^{2+} may favor octahedral coordination in spinel as it will attain even higher crystal field stabilization energy in this position.

5. GEOTHERMOBAROMETRY

Estimations of the temperature and pressure conditions of equilibrium for ultramafic xenoliths are based on experimental studies of the phase equilibria observed for simplified analogues of natural lherzolite compositions. Most recent studies have dealt with the four-component CaO-MgO-Al_2O_3-SiO_2 (C-M-A-S) system. Since the greatest variation in the compositions of xenolith minerals occurs in the pyroxenes, special emphasis has traditionally been focused upon the diopside-enstatite solvus. Several of these approaches are reviewed in this chapter and applied to the Cordilleran xenolith compositions. As most thermodynamic or experimentally based estimates of equilibrium pressure for spinel-bearing lherzolite compositions are only useful at the pressure-dependent phase-transformation boundaries, other criteria including petrographic and geophysical information, must be used to obtain estimates of equilibrium pressure for the Cordilleran xenolith samples.

DIOPSIDE-ENSTATITE SOLVUS RELATIONS

The pioneering studies of Davis & Boyd (1966) examined the temperature relations of the diopside-enstatite solvus in the system $MgSiO_3$-$CaMgSi_2O_6$ at 30 kbar. Concerning coexisting pyroxenes from kimberlite xenoliths, these experiments showed that the extent of solid-solution between Mg-rich clinopyroxenes and calcic orthopyroxenes is propor-

tional to temperature and relatively insensitive to pressure. The experiments of Mori & Green (1975) and Lindsley & Dixon (1976) determined the diopside-enstatite solvus between approximately 900 and 1500°C and 5 to 40 kbar pressure. Both studies confirmed the temperature dependence of the solvus and emphasize the greater extent of mutual solid-solution in diopside compared to that in enstatite. Mori & Green (1975) observed that at low temperatures (< 900°C) there is little perceptible pressure effect on the pyroxene solvus. However, at higher temperatures (> 1200°C) the pyroxene solvus widens considerably with increasing pressure.

Wells (1977) has revised the pyroxene geothermometer of Wood & Banno (1973) using the diopside-enstatite solvus determinations of Lindsley & Dixon (1976) with the empirical expression:

$$T(K) = \frac{7341}{3.355 + 2.44X^{cpx}_{Fe^{+2}} - \ln\left(\frac{a^{cpx}_{MgSiO_3}}{a^{opx}_{MgSiO_3}}\right)}$$

With this equation, Wells (1977) was able to reproduce most experimentally determined temperatures to within 70°C, and his geothermometer has been widely cited in the recent literature.

THE SOLUBILITY OF ALUMINUM IN PYROXENES OF THE LHERZOLITE ASSEMBLAGES

Aluminum substitution in coexisting enstatite and diopside solid solutions has a significant effect on the pyroxene solvus and thus on the equilibrium temperatures estimated from the pure enstatite-diopside solvus. The calculation of Al solubility in orthopyroxene presented by Wood & Banno (1973) assumes a model of activity-composition relations in which octahedral Al in orthopyroxene is restricted completely to the smaller M1 octahedral site, whereas tetrahedral Al is restricted completely to the neighboring Si(B) site. Ganguly & Ghose (1979) showed that Al may substitute for a maximum of one half of the Si atoms in the Si(B) sites, or one quarter of the total Si atoms, leading to the end-member stoichoimetry of $(Mg_3Al)^{vi}(AlSi_3)^{iv}O_{12}$ or $Mg_3Al_2Si_3O_{12}$ (the stoichoimetric composition of pyropic garnet) for Al-orthopyroxene.

Obata (1976) examined the solubility of Al_{203} in orthopyroxene for simplified lherzolite assemblages and showed that aluminum isopleths are insensitive to pressure in the spinel lherzolite field of stability. However, the experiments described by Danckworth & Newton (1978) show that the high Cr content of spinel may extend its stability to greater temperatures (up to 70°C) and lower pressures than in the simple C-M-A-S system. They concluded that spinel must have a very high molar content of $MgAl_2O_4$ to warrant use of enstatite isopleths as a geothermometer. In addition,

Herzberg (1978) showed that the solubility of aluminum, as the calcium tschermak component $CaAl_2SiO_6$, in complex diopside-CaTs-enstatite clinopyroxene solid solutions in spinel lherzolite can be represented:

$$\underset{\text{diop}}{CaMgSi_2O_6} + \underset{\text{sp}}{MgAl_2O_4} = \underset{\text{CaTs}}{CaAl_2SiO_6} + \underset{\text{fo}}{Mg_2SiO_4}$$

and for garnet lherzolites:

$$\underset{\text{gar}}{Ca_2MgAl_2Si_3O_{12}} = \underset{\text{diop}}{CaMgSi_2O_6} + \underset{\text{CaTs}}{CaAl_2SiO_6}$$

Herzberg (1978) noted that the high content of aluminum in clinopyroxene in the spinel lherzolite field strongly reduces the amount of $Mg_2Si_2O_6$ that can be dissolved in clinopyroxene, and failure to take this into account can result in temperature uncertainties of up to 150°C.

OTHER GEOTHERMOMETERS

Because of uncertainties caused by aluminum in the pyroxene solvus geothermometers, several other geothermometers have been proposed. Hervig & Smith (1980) proposed a geothermometer based on sodium exchange between coexisting Ca-poor orthopyroxene and Ca-rich clinopyroxene. A complex distribution between pyroxenes is theoretically expected, as Na couples with Al, Cr and Fe^{3+}. Surprisingly, the distribution coefficient (K_D) for sodium contents between coexisting clinopyroxene and orthopyroxene has a linear

relation to the reciprocal of the estimated (Wells 1977) temperature. Consequently, the Hervig & Smith (1980) geothermometer:

$$T(^{o}C) = \frac{7525}{3.16 + \ln K_D} - 273$$

is expected to be accurate to within $\pm 100^{o}C$. Particularly important is the expected increase in sensitivity of the Na geothermometer with decreasing temperature, in contrast to those based on diopside-enstatite solvus.

Fujii & Scarfe (1982) used experiments near the solidus temperature of spinel lherzolite compositions at 10 kbar to recalibrate the olivine-spinel geothermometer developed for layered mafic intrusions (Jackson 1969, Roeder et al. 1979). Assuming a reciprocal solution model for spinel and a simple solution model for olivine, the equilibrium temperature for the partitioning of Fe and Mg between olivine and spinel can be obtained from the equation:

$$RT\ln K - 4.0X^{Sp}_{Fe^{3+}} + 1000(1-2X^{Ol}_{Mg}) = 2941 - 1.87T + (3644 - 0.15T)X^{Sp}_{Cr}$$

The experimental temperatures determined by Fujii & Scarfe (1982) are lower than the temperatures calculated using the Wells (1977) geothermometer for lherzolite compositions.

EQUILIBRIUM TEMPERATURE OF THE CORDILLERAN XENOLITHS

Equilibrium temperatures were calculated for the samples from the four Cordilleran xenolith suites and for those from Nunivak Island (Table 4) using the geothermometers of Wells (1977), Hervig & Smith (1980) and Fujii & Scarfe (1982). The geothermometers based on Al_{203} isopleths were not used in this study because of the large uncertainty that remains in the application of the experimental data calibrated in 3- or 4-component systems to natural assemblages. The results obtained using the olivine-spinel geothermometer of Fujii & Scarfe (1982) are suspiciously low, with many of the calculated temperatures in the range of 400 to 700°C. However, the variation between Fe and Mg in spinel is small compared to that between Cr and Al. The effects of the latter substitution are not included in the calculation of this geothermometer. The Hervig & Smith (1980) geothermometer yields temperatures whose values and range much more closely approximate those from the Wells (1977) geothermometer. Uncertainties in the strict application of the results from the Hervig & Smith (1980) geothermometer arise at present owing to the lack of experimental calibration.

Calculated equilibrium temperatures of coexisting Cordilleran pyroxene samples (Table 5) range from 861°C to 1207°C using the Wells (1977) geothermometer. The temperatures calculated for xenolith groups 1, 2 and 3 define a narrow temperature range of 60 to 100°C at each locality. The average pyroxene temperature for the JL, CR and NI suites

Table 4: CALCULATED EQUILIBRIUM TEMPERATURES

SAMPLE	GROUP	TEMPERATURE (C) WELLS (1977)	HERVIG & SMITH (1980)	FUJII & SCARFE (1982)
10001	1	947	925	845
10007	1	966	1053	417
10010	1	1029	1194	482
10002	2	989	1100	422
10004	2	1013	1251	758
10006	2	1001	700	488
10008	2	928	1047	605
10013	2	972	1121	492
10016	2	927	887	398
10068	3	970	1048	747
10069	3	1038	1046	758
20038	1	859	-	366
20015	2	946	785	504
20029	2	-	-	617
20008	3	899	809	-
20046	3	934	792	666
20039	4	903	659	608
30008	1	971	839	387
30006	2	953	839	559
30020	2	992	962	603
30028	2	932	772	-
30003	2	928	847	-
30012	3	997	919	756
30022	3	960	867	645
40003	1	1010	-	432
40015	1	1012	851	518
40044	1	969	803	412
40017	2	1005	856	541
40054	2	973	885	-
40061	2	972	951	660
40010	3	951	866	670
40030	4	1126	1136	629
40055	4	-	-	545
40037	4	1206	1162	643
50015	1	1005	962	422
50005	2	977	1091	603
50011	2	976	713	497
50006	3	1017	924	749
50008	3	955	801	-
50009	3	996	909	662
50001	4	1183	1155	650
50019	4	1078	1184	-

Table 5: COMPARISON OF WELLS (1977) TEMPERATURES

Temp.	Jacques Lake	Castle Rock	Fort Selkirk	Prindle Volcano	Nunivak Island
1200°C		CR37(1206)			
	JL1(1183)				
1150°C					
		CR30(1126)			
1100°C					
	JL19(1078)				
1050°C					
					NI69(1038)
					NI10(1029)
	JL6(1017)	CR15(1012)			
	JL15(1005)	CR3(1010)			NI4(1013)
1000°C	JL9(996)	CR17(1005)	FS12(997)		NI6(1001)
			FS20(992)		NI2(989)
	JL5(977)	CR54(973)			NI13(972)
	JL11(976)	CR44(965)	FS8(971)		NI68(970)
			FS22(960)		NI7(966)
950°C	JL8(955)	CR10(951)	FS6(953)	PV15(946)	NI1(947)
			FS28(932)	PV46(934)	NI8(928)
			FS3(928)		NI16(927)
900°C				PV39(903)	
				PV6(895)	
				PV38(859)	
850°C					

* calculated using the geothermometer formulated by Wells (1977)

(988, 981 and 980°C, respectively) are nearly identical. The average pyroxene temperature for the FS suite (962°C) is approximately 25°C lower, and that of the PV suite (908°C) is distinctly lower than that of the JL, CR and NI xenolith suites. These results are in general agreement with the pyroxene temperatures reported by Scarfe et al. (1982), and suggest that a rather restricted temperature range is being sampled by xenoliths from southern and central British Columbia. Nicholls et al. (1982) also showed that the temperature range represented by xenoliths from the Atlin Lake and Yukon (Fort Selkirk) localities in the northern Cordillera is lower than that of more southern localities in British Columbia.

The calculated pyroxene temperatures support a surprisingly homogeneous distribution of the xenolith groups at most of the localities. Based on the temperature dependence established for the diopside-enstatite solvus, the distribution of clinopyroxenes in Figure 9 would predict temperatures of equilibrium to decrease in the sequence harzburgite to lherzolite to pyroxene lherzolite. Only in the Castle Rock suite does the distribution of temperatures approximate the order expected. In the remaining suites, the temperature range of the xenolith groups 1, 2 and 3 largely overlap. The group 4 peridotite samples have the highest calculated temperatures, in the range 1000 to 1200°C. Of all the xenolith samples, only these have temperatures that approach the magmatic temperatures of basalt. The much

lower temperatures calculated for groups 1, 2 and 3 most reflect subsolidus re-equilibration within the lithosphere.

PRESSURE INDICATIONS FROM PYROXENE COMPOSITIONS

Several attempts have been made to establish the equilibration pressure of ultramafic xenolith assemblages based on their pyroxene compositions. Bell & Davis (1965, 1967) investigated the diopside-jadeite solid solution series at high pressures (30 to 40 kbar) and found that the jadeite content of clinopyroxene solid solutions increases significantly with pressure, accompanied by a smaller decrease in the proportion of Ca-Tschermaks components. Although the Na content of clinopyroxene (Fig. 12) has an overlapping range of values in the four Cordilleran suites, the average value for the clinopyroxenes in each suite increases in the sequence CR to PV to FS to JL. This suggests that the comparatively jadeite-rich JL and FS clinopyroxene compositions have equilibrated at comparatively higher pressures than those of the other xenolith suites. However, in the anhydrous lherzolite xenoliths, there is no other phase present that can buffer Na in clinopyroxene. In addition, Na increases from the harzburgite to the lherzolite and pyroxene lherzolite clinopyroxenes. Alternately, the variation in Na contents may simply represent variations in bulk composition of the xenoliths.

A possible pressure discriminant lies in the ratio of Al^{iv} to Al^{vi} in clinopyroxenes. Wood (1976) showed

experimentally that in $CaMgSi_2O_6$-$CaAl_2SiO_6$ solid solutions coexisting with anorthite and quartz, an increasing mole fraction of $CaAl_2SiO_6$ is directly associated with increasing pressure (10 to 25 kbar). The majority of the Cordilleran samples (Fig. 9) fall on a line that intercepts the Al^{vi} axis at 0.10 atoms $Al^{vi}/4$ cations, whereas some of the pyroxene-rich lherzolite (group 3) samples and the Nunivak hydrous lherzolite group appear to be shifted to higher concentrations of Al^{vi}. The higher content of octahedral aluminum may indicate higher equilibration pressures for the pyroxene lherzolite (group 3) and the NI hydrous lherzolite xenoliths compared to the majority of the samples. However, this distribution could reflect the higher Na contents of these clinopyroxenes, which would require higher Al^{vi}/Al^{iv} ratios to stabilize them in the pyroxene structure.

PETROGRAPHIC INDICATIONS OF PRESSURE OF EQUILIBRIUM

Another approach, useful in estimating the range of equilibrium pressure of spinel lherzolite xenoliths, utilizes the appearance of assemblages transitional to stable higher or lower pressure ones. The distinctive "holly-leaf" texture of spinel (Plate 10) intergrown with enstatite, observed in several of the coarse-textured Cordilleran xenoliths, has been related in other suites to the breakdown of relict garnet in recrystallized garnet lherzolite. Reid & Dawson (1972) described garnet coronas in ultramafic xenoliths from the Lashaine (Tanzania) carbonatite volcano. They suggested

that if the reaction had gone to completion, the original garnet probably would have been replaced by clusters of two pyroxenes + spinel. Reid & Dawson (1972) noted that these coronas, if formed as a result of incorporation in the rising host magma, are unusual in that the garnet reaction occurred in a "dry" carbonatitic ankaramite without the addition of H_2O.

Smith (1977) described two pyroxene - spinel clusters in spinel peridotite xenoliths from the Green Knobs kimberlite diatreme in Colorado. In these rocks, pyroxene - spinel aggregates (6.0 mm) consist of equant, anhedral enstatite and diopside with interstitial spinel, occasionally present as coarse blebs or "fingers" within diopside and enstatite. Smith (1977) suggested that the pyroxene - spinel clusters form from the reaction of olivine and garnet. The variable proportion of spinel is explained by relating it to the amounts of tetrahedral Al in the parent and product pyroxenes. Smith (1977) proposed that the transition from garnet to spinel peridotite indicated by this texture probably reflects a decrease in pressure, either during tectonic uplift following erosion or during upward mantle convection.

Those Cordilleran xenolith samples that contain "holly-leaf" spinel textures or show spatial association between pyroxene and spinel could possibly represent equilibrium pressures near the maximum of the spinel lherzolite stability field. In addition, the presence of plagioclase lherzolite and granulite xenoliths in the CR, PV and NI suites (Table 1)

indicates that xenoliths from at least several suites may have equilibrium at the minimum pressure of the spinel lherzolite stability field. Thus the only constraint on the pressure range which these xenoliths sampled is the experimentally determined stability field for spinel-bearing lherzolite, between the garnet- or plagioclase-bearing lherzolite stability fields.

EQUILIBRATION OF LHERZOLITE ASSEMBLAGES

Early estimates of pressure of equilibration for ultramafic xenolith compositions relied on the pyroxene-calibrated P-T grid of O'Hara (1967). Using experimental results in the system CaO-MgO-Al_2O_3-SiO_2, O'Hara (1967) showed that an anhydrous spinel lherzolite assemblage was stable between 10 and 25 kbar pressure, with plagioclase lherzolite stable at lower pressures, and garnet lherzolite stable at higher pressures. Later experimental results, however, illustrated important problems with the simplified compositions used by O'Hara because of the solubility of aluminum in pyroxene.

Danckwerth & Newton (1978) employed hydrothermal reversals to facilitate the attainment of equilibrium in the reaction of spinel lherzolite to garnet lherzolite in the system MgO-Al_2O_3-SiO_2. Their experimental isopleth data show that the mass-balanced equation for the univariant equilibrium is:

$$2\ en + 0.754\ sp = gt + 0.754\ olv$$

Ganguly & Ghose (1979) showed that the transition represented by this reaction can be rewritten:

$$\underset{\text{opx}}{Mg_4Si_4O_{12}} + \underset{\text{sp}}{MgAl_2O_4} = \underset{\text{opx}}{Mg_3Al_2Si_3O_{12}} + \underset{\text{olv}}{Mg_2SiO_4}$$

The introduction of CaO causes little change in the equilibrium constants for the 3-component system. Obata (1976) found that in the C-M-A-S system, the reaction cpx + opx + sp = gt + fo curves significantly and is nearly vertical below 800°C, whereas the reaction an + fo = cpx + opx + sp curves in the opposite direction in temperature and pressure space. In the petrogenetic grid of Herzberg (1978) the intersection of the aluminum isopleths for clinopyroxene in lherzolite assemblages limits the minimum stability of garnet lherzolite at a pressure of 16 kbar and the maximum stability field of plagioclase lherzolite at a pressure slightly above 8 kbar.

Jenkins & Newton (1979) employed hydrothermal reversals in their experimental determinations of the spinel lherzolite to garnet lherzolite inversion. Calculation of the dT/dP slope of this reaction in the C-M-A-S system support the mass balanced equation:

1.500 opx + 0.500 cpx + 0.760 sp = 1.000 gt + 0.760 olv

Jenkins & Newton (1979) suggested that natural peridotitic compositions can retain garnet-bearing assemblages in the presence of free H_2O at depths as low as 30 to 40 km within

the lower continental crust. They conclude that the subcontinental upper mantle will be in the spinel lherzolite field of stability only in exceptional areas of high geothermal gradiant.

CORDILLERAN GEOTHERM

Ranalli (1980) adopted a unique approach to estimates of equilibrium pressure and temperature in the Cordilleran lithosphere by applying microrheological equations of olivine deformation to rheological properties. Geotherms for the Canadian shield and Cordillera are constructed by combining estimates of surface heat-flow and geochemical models with pyroxene equilibration temperatures. Additional constraints assume Rao's & Jessop's (1975) estimate of T = 400 to 500°C at a depth of 40 km under the shield, from an average heat flow of 0.94 HFU, and Caner's (1970) estimate of temperature of 750°C at a depth of 35 km beneath the southern Canadian Cordillera where heat flow is approximately 2 HFU.

To best approximate the range of equilibrium conditions represented by the Cordilleran xenolith samples, the sample groups are superimposed on Ranalli's (1980) Cordilleran geotherm (Fig. 15) using the temperatures calculated from Well's (1977) geothermometer. All samples fall in the pressure range of the spinel lherzolite stability field and the distribution in Figure 15 supports the suggestions of O'Neill (1981) and Scarfe et al. (1982) that xenolith suites may reflect a very limited range of equilibration conditions.

Figure 15: APPLICATION OF THE CORDILLERAN GEOTHERM

The distribution of samples from each xenolith suite on the Cordilleran geotherm of Ranalli (1980). The temperatures assumed are those calculated using the geothermometer of Wells (1977). The pressure-dependent phase-transformation boundaries result from the experiments of Herzberg (1978).

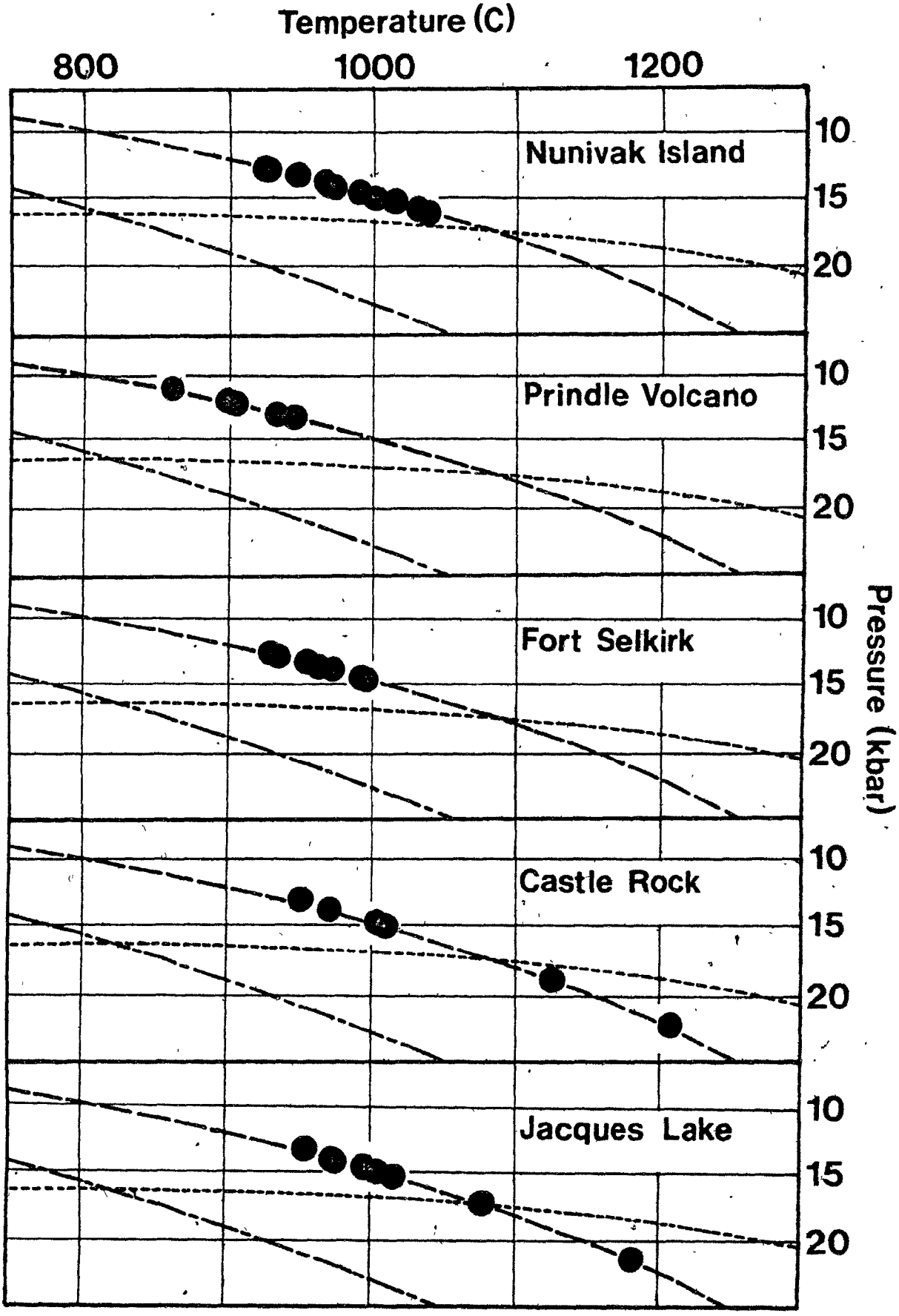
Temperature (C)
800
1000
1200
Nunivak Island
Prindle Volcano
Fort Selkirk
Castle Rock
Jacques Lake
10
15
20
Pressure (kbar)

The majority of the samples from each locality and all those from xenolith groups 1, 2 and 3 are confined to the pressure range of 11 to slightly less than 16 kbar, assuming this geotherm. However, it appears that the Cordilleran xenoliths suites have sampled an average depth that decreases in the sequence JL - CR - FS - PV, although this correlation clearly is a direct reflection of the calculated temperatures. The presence of significant plagioclase lherzolites in the PV suite agrees with it's lower estimated pressure. Application of Ranalli's (1980) geotherm is also supported by the apparent maximum equilibration depth of about 16 km for the xenolith samples. This is in close agreement with the experimentally determined minimum stability of garnet lherzolite. Only the group 4 peridotite samples yield anomalously great depths. However, the major-element compositions of these samples is sufficiently distinct to assume they may not be appropriate to a hypothesis of equilibration using the assumed geotherm.

6. ULTRAMAFIC XENOLITHS FROM NUNIVAK ISLAND

The suite of ultramafic xenoliths studied by Francis (1974, 1976a, b, c, 1978) from alkali basalt cinder cones and maars on Nunivak Island, Alaska, consists almost entirely of samples of harzburgite and spinel lherzolite, approximately half of which contain amphibole, mica or more commonly fine-grained zones after these phases. Nunivak Island is unique in that it is the only basaltic xenolith locality throughout Alaska or the entire Canadian Cordillera in which hydrous, Cr-diopside-bearing ultramafic xenoliths have been documented. A representative group of 29 Nunivak Island (NI) ultramafic xenoliths were included in the present study. Although important differences exist between the NI xenolith suite and those of the four Cordilleran localities, the xenoliths from these five areas do appear to be similar in many respects.

Two distinct groups of anhydrous ultramafic xenoliths can be recognized in the NI suite: 1) harzburgite and olivine-rich (>76 modal % olivine) spinel lherzolite, and 2) pyroxene-rich spinel lherzolite. In terms of modal composition, these two NI groups are equivalent to the harzburgite and pyroxene lherzolite groups of the Cordilleran xenolith suites. In addition, ultramafic samples containing hydrous phases make up nearly 50% of the Nunivak Island xenolith suite. The modes of these samples were recalculated in terms of anhydrous equivalents (Fig. 2), using the proportions of

olivine, clinopyroxene, spinel and glass reported by Francis (1974, Table 6-13). Whereas the olivine enrichment in the hydrous NI samples may partially result from the recalculation of hydrous to anhydrous components, these xenoliths are typically enriched in clinopyroxene compared to the harzburgite (group 1), and cluster around the average of NI modal compositions. The resulting average modal composition of the Nunivak Island suite, 67.2% oliv, 20.0% opx, 11.2% cpx and 1.7% spinel, is considerably more refractory than the average modal composition at each of the four Cordilleran suites (Table 2), despite the evidence for a relatively abundant volatile component in the Nunivak Island suite.

Xenolith textures in the Nunivak Island suite were classified by Francis (1974, 1976a, b, c, 1978) into three basic groups: coarse equant, coarse tabular and granuloblastic. Francis adopted the coarse tabular texture, in preference to the porphyroclastic category of Mercier & Nicolas (1976), owing to the high porphyroclast/neoblast ratio of such rocks in the NI suite (Harte 1977). Xenolith textures were assigned to the NI suite in Figure 3 by comparing the predominant size of olivine porphyroclasts in these samples with those of the Cordilleran xenoliths. At Nunivak, anhydrous harzburgite and olivine-rich lherzolite have coarse equant or coarse tabular textures, equivalent to those of the Cordilleran harzburgite samples, whereas the anhydrous pyroxene lherzolite samples have finer-grained textures, equivalent to those of the pyroxene lherzolite

group. These granuloblastic xenoliths comprise approximately 10% of the NI xenolith population (Francis, 1981, pers. comm.) compared to 60% coarse equant and 30% coarse tabular xenoliths.

The hydrous NI peridotite samples are predominantly coarse tabular in texture, although hydrous peridotite xenoliths with coarse equant texture are not uncommon, and at least two hydrous peridotite xenoliths with find-grained textures (NI10067 and NI10211) are also included in the Nunivak Island suite (Plate 13). Francis (1976a) noted the distinct orthorhombic to monoclinic symmetry of the fabric defined by the porphyroclasts in both coarse textural groups. There appears to be a continuous gradation between xenoliths with coarse textures at Nunivak. Nevertheless, Francis (1974, 1976a, b, c, 1978) recognized the significant departure of the Nunivak Island suite from the continuous spectrum of textures in mantle xenoliths described by Mercier & Nicolas (1976). These authors proposed a continuous sequence of coarse to porphyroclastic to granuloblastic textures with increasing degree of deformation of the xenoliths. Whereas xenoliths with coarse textures appear to be gradational (Fig. 3), an abrupt textural discontinuity exists between xenoliths with coarse tabular texture and those in which granuloblastic textures are developed.

The mineral compositions of the Nunivak Island xenolith suite complement those of the Cordilleran suites in many respects; this is especially evident in the pyroxene and

Plate 13: NUNIVAK ISLAND AMPHIBOLE LHERZOLITE

NI67 is shown here as an example of the contrasting appearance of the hydrous Nunivak Island samples compared to that of the anhydrous Cordilleran samples (Plate 7). In this sample, yellowish brown amphibole is a conspicuous minor phase. This sample is unusual in that it also represents a comparatively rare variety of NI hydrous samples characterized by fine-grained textures (field of view = 25 mm).

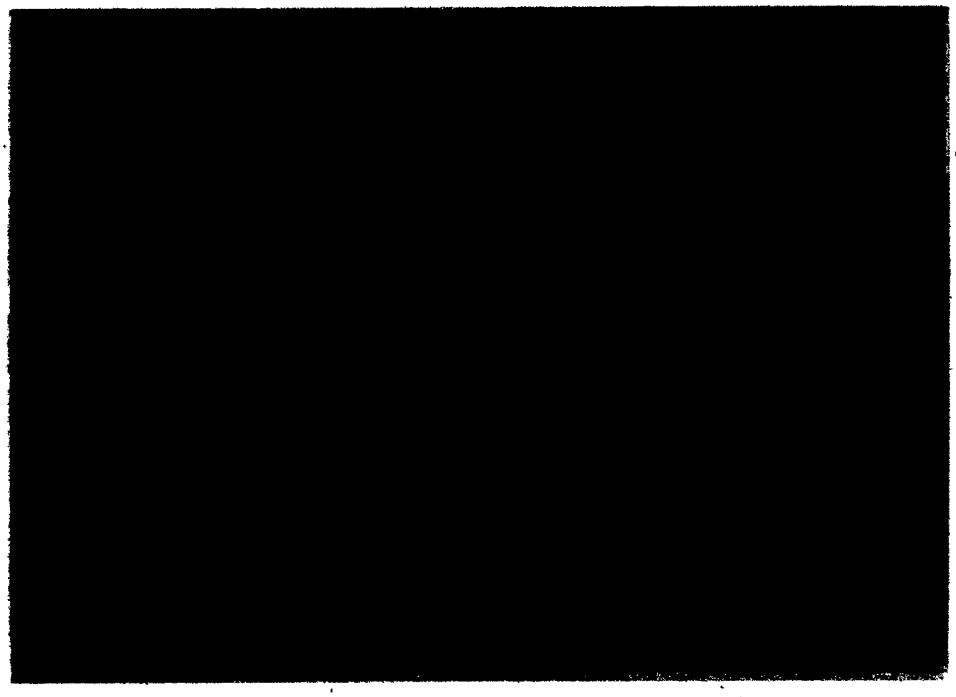

COLOURED PICTURES
Images en couleur

spinel compositions. The distribution of aluminum in NI orthopyroxene is comparable to that of the Cordilleran orthopyroxene for the harzburgite and pyroxene lherzolite samples (Fig. 6), with Al^{iv} approximately equal to Al^{vi}. However, in the Nunivak Island suite, orthopyroxenes with intermediate aluminum content are characterized by a higher ratio of Al^{vi}/Al^{iv} than orthopyroxenes with equivalent aluminum contents from the Cordilleran suites. Most of the NI orthopyroxenes with higher ratios of Al^{vi}/Al^{iv} are from hydrous xenolith samples with coarse tabular textures. The concentrations of both Ti and Cr in Nunivak Island orthopyroxenes are equivalent to those of the Cordilleran group of samples (Fig. 7), and manganese concentrations are uniformly low in the NI orthopyroxenes, comparable to that in the JL suite. However, Na contents of orthopyroxenes from Nunivak Island harzburgite and hydrous lherzolite samples are distinct from those of the Cordilleran suites, with Na increasing to comparatively high concentrations independent of the aluminum content.

A comparison of clinopyroxene compositions shows that the Nunivak Island clinopyroxenes are consistently more magnesian and less calcic (Fig. 5) than those from the equivalent Cordilleran xenoliths. The distribution of aluminum between tetrahedral and octahedral sites in the NI clinopyroxenes (Fig. 9) follows that seen in the coexisting orthopyroxene, with the aluminum distribution shifted to higher ratios of Al^{vi}/Al^{iv} in the clinopyroxene of hydrous

NI lherzolites with intermediate aluminum concentrations. Between the hydrous lherzolite and the pyroxene-rich NI xenoliths, Francis (1978) noted a population gap in terms of aluminum concentrations in NI clinopyroxenes. Nearly half of the clinopyroxenes analyzed from the four Cordilleran suites fall within this gap. The concentration of Ti and Cr vary with total aluminum content (Fig. 10) over the range of NI clinopyroxene compositions, similar to that seen in the Cordilleran suites. The clinopyroxene from NI hydrous peridotite samples are, however, anomalously enriched in Na, compared to the Cordilleran samples (Fig. 11).

Spinel compositions in Kunivak Island ultramafic xenoliths are largely equivalent to those of the Cordilleran xenoliths, with spinel contained in coarse-textured NI samples comparatively rich in Fe^{2+} and Cr, and that contained in the granuloblastic-textured NI xenoliths rich in Mg and Al (Fig. 14). In NI xenoliths with coarse textures, equant to elongate (0.2 to 0.5 mm) spinel inclusions are common in olivine, orthopyroxene and amphibole. Similar spinel inclusions are rare in the coarse-grained xenoliths from the Cordilleran suites and absent altogether in xenoliths with granuloblastic textures from any of the localities. The spinel inclusions contained in olivine and orthopyroxene are both more aluminous and more magnesian (similar to spinel compositions in the pyroxene lherzolites) than coexisting interstitial spinel in these rocks. In contrast, spinel inclusions in amphibole are enriched in Fe and Cr with respect to interstitial spinel

or spinel inclusions in coexisting silicate phases.

The most obvious distinction of the Nunivak xenoliths from the Cordilleran samples is the presence of a hydrous component, indicating a metasomatic event in the mantle beneath this locality. The hydrous NI xenoliths are similar in many respects to the Cordilleran lherzolite samples. Although the coarse textures most often associated with the hydrous NI xenoliths have higher porphyroclast/neoblast ratios and a better defined penetrative foliation than the Cordilleran group 2 samples, both of these xenolith groups are intermediate in grain size and in major-element composition between the harzburgite and the pyroxene lherzolite groups. Two important distinctions that can be made between these two groups include the high ratio of Al^{vi} to Al^{iv} and the Na-rich character of pyroxenes in the NI population, perhaps reflecting higher pressures (Francis 1976a). Whereas the origin of this hydrous component is uncertain, the compositional zoning in spinel inclusions in amphibole and the lack of deformation in larger amphibole grains suggest a late-stage metasomatic component (Francis 1974, 1976a, b). Roden (1982) has proposed that even the clinopyroxene compositions reflect this process. It is possible that the anomalously high Al^{vi}/Al^{iv} ratios and Na concentrations of the clinopyroxene in the NI hydrous lherzolites are also a reflection of the metasomatic event, and do not indicate higher pressures. Thus, the hydrous xenoliths may correspond to Cordilleran-type lherzolite xenoliths of group 2 that were

subsequently affected by the introduction of a volatile phase.

7. BULK COMPOSITION OF ULTRAMAFIC XENOLITHS

The bulk compositions of 23 Cordilleran and 11 Nunivak Island samples were calculated (Appendix 3) using their modes (from point-counted thin sections) and mineral compositions. The proportion and average composition of hydrous minerals and fine-grained zones and glass in NI1, NI2, NI6, NI10, NI13 and NI16 were included in the calculation of their bulk compositions. In this chapter the major and minor element variations in these calculated compositions are described, and the possible factors controlling these variations are reviewed.

MAJOR ELEMENT DISTRIBUTION

Among the major elements, the concentration of silicon is comparatively uniform in the xenolith samples, ranging from 34.7 to only 39.1 cation % Si for 32 of the 34 calculated bulk compositions. The relative variation of Fe (total iron) is similar to that of Si, with Fe concentrations typically ranging from 5 to 6 cation % in the harzburgite, lherzolite and pyroxene lherzolite samples. In contrast to both Si and Fe, a much greater variation occurs in Mg concentrations, with magnesium ranging from 40 to almost 60 cation % in the bulk compositions of the xenoliths. Because Mg is the predominant element in each of the calculated bulk compositions, yet shows the greatest major-element variation between the xenolith samples, the distribution of the less concentrated

elements is compared to that of Mg.

The distribution of Mg and Fe in the xenolith bulk compositions is shown with that of the analyzed mineral compositions in Figure 16A. Superimposed on Figure 16A is a "sail" diagram, which has been used by Hanson & Langmuir (1978) and Langmuir & Hanson (1980) to relate the compositions of various mafic volcanic rocks (considered quenched liquids) to primitive mantle compositions with which they could have equilibrated. A complementary sail diagram (Fig. 16B) related the compositions of partially melted residues to temperature and degree of depletion from any initial mantle composition. Both diagrams can be constructed by assuming the Mg and Fe concentration and Fo content of the olivine in a mantle source and a value for the olivine Fe/Mg Kd (Hanson & Langmuir 1978). The position of the calculated residual field on the Mg-Fe distribution is critically dependent on the composition of the assumed primitive mantle (point P in Fig. 16B). The residual field in Figure 16B is calculated for pyrolite-1 (Ringwood 1966), a widely accepted hypothetical composition proposed to represent pristine mantle.

Two trends are observed in the Mg-Fe distribution of the xenolith bulk compositions in Figure 16. The majority of xenolith samples from each locality, including the harzburgite, lherzolite and some members of the pyroxene lherzolite group lie within the residual field of pyrolite in the said diagram. The Mg-Fe distribution of these samples follows a hyperbolic curve (trend A in Fig. 16B) with respect to the

Figure 16: COMPARISON OF Fe VS. Mg IN BULK COMPOSITIONS

A. Fe-Mg distribution for minerals and rocks. Mineral (solid circles) from analyzed compositions, whereas rocks (open circles) are calculated compositions. Sail diagram for melt field calculated assuming a pyrolite source by the method of Hanson & Langmuir (1978) and Langmuir & Hanson (1980). P indicates Pyrolite mantle, C indicates Carter's mantle.

B. Residual field calculated assuming a pyrolite source. Color code: red harzburgite; green lherzolite; yellow pyroxene lherzolite; uncolored group 4 peridotites.

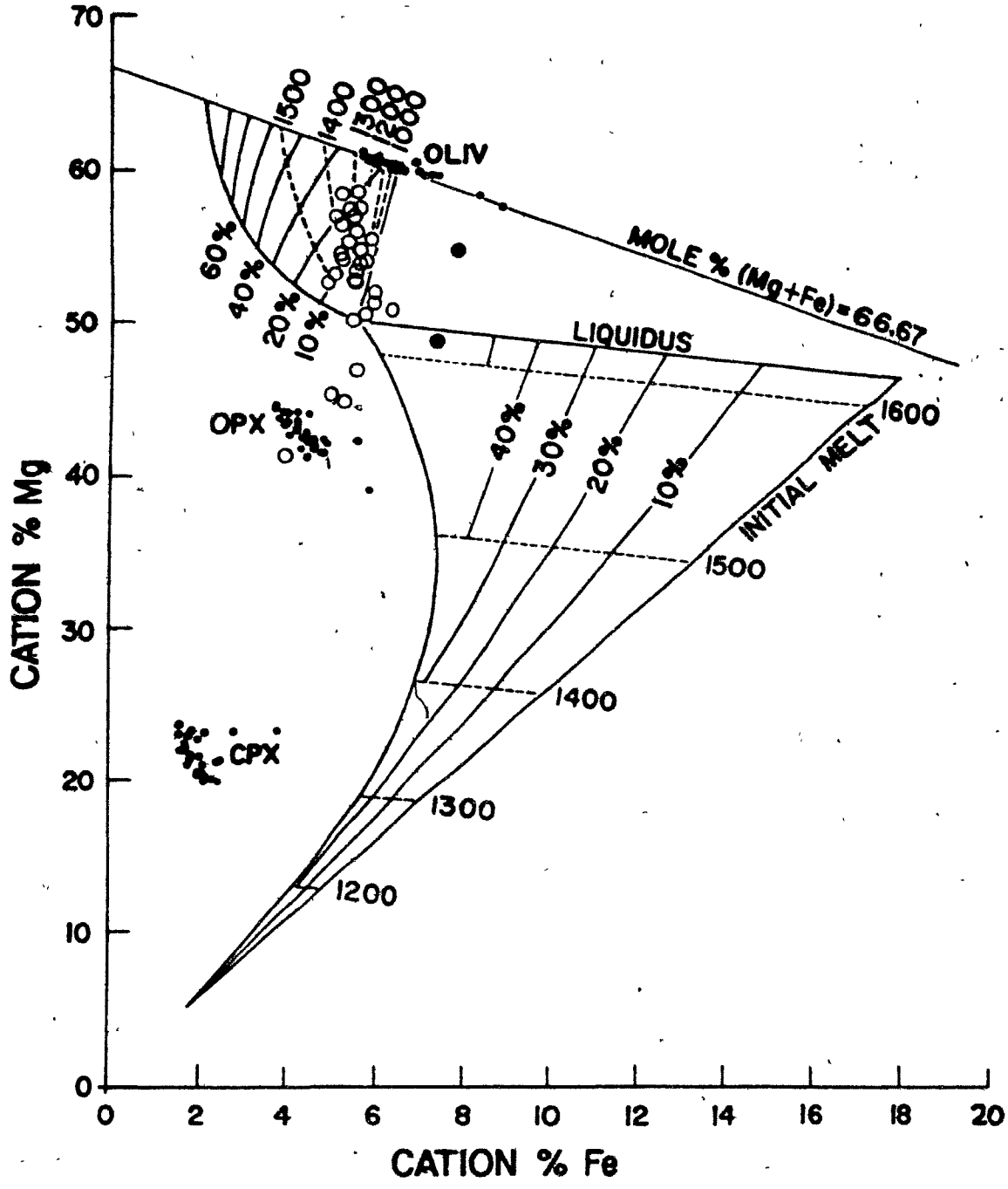
70
60
50
40
30
20
10
0
0
2
4
6
8
10
12
14
16
18
20
CATION % Mg
CATION % Fe
OLIV
MOLE % (Mg+Fe)=66.67
LIQUIDUS
OPX
CPX
INITIAL MELT
1500
1400
1300
1200
1600
60%
40%
20%
10%
40%
30%
20%
10%

ULTRAMAFIC XENOLITHS

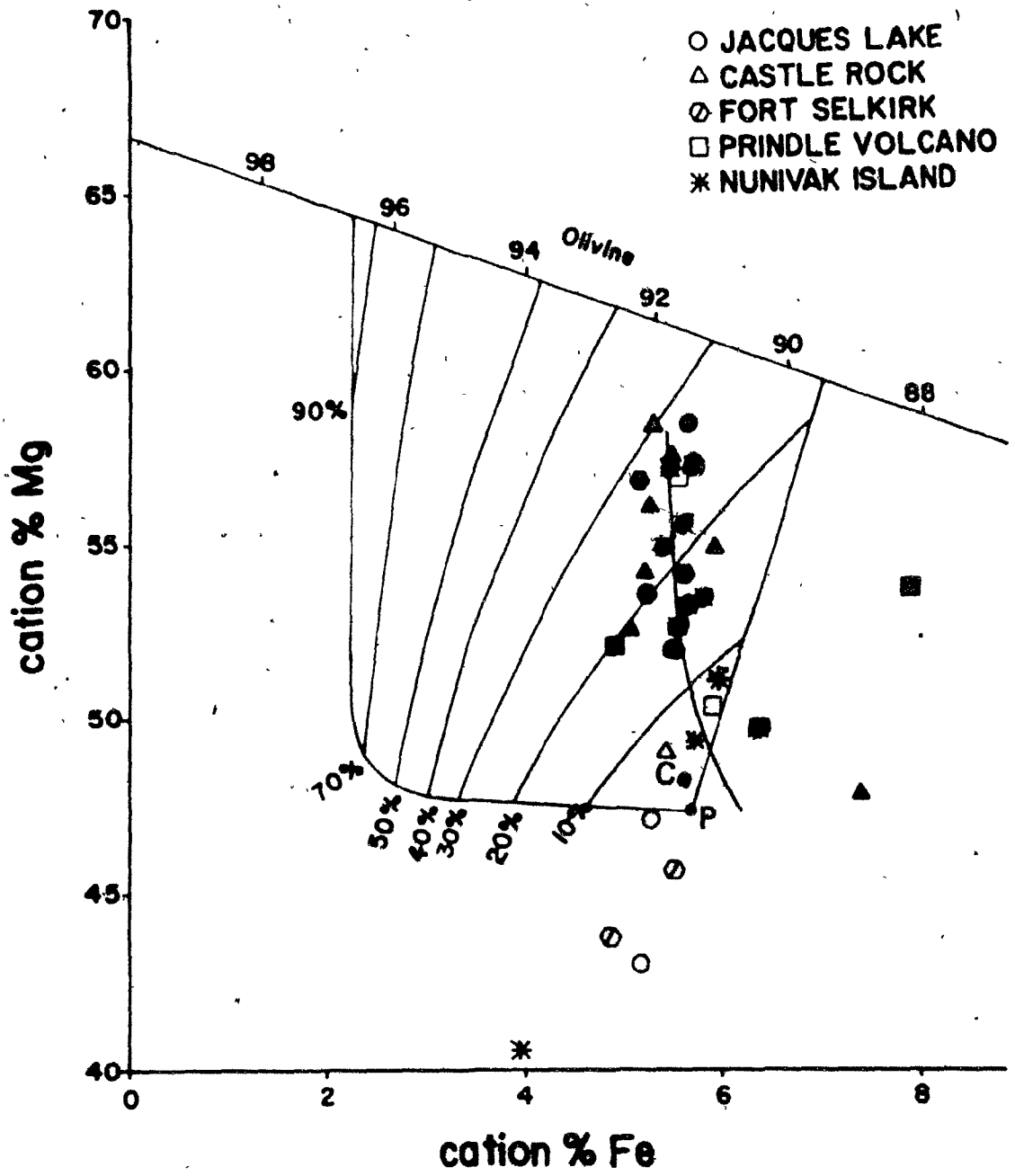

origin. The Nunivak Island xenoliths, including the hydrous lherzolites, are indistinguishable with respect to their Mg-Fe distribution from those of the Cordilleran suites. If trend A is produced by partial melting, then its coherent character would suggest that the majority of the xenolith samples represent varying degrees of depletion of mantle sources with a common composition at each of the five localities. Assuming a pyrolite initial composition, the harzburgite bulk compositions would correspond to residues formed by 20 to 30% partial melting, whereas the lherzolite bulk compositions would correspond to 15 to 25% partial melting and those pyroxene lherzolite bulk compositions that lie within the residual field would reflect up to 15% partial melting. Although these numbers are somewhat dependent on the assumed mantle composition, trend A approximates an isothermal melting line for a reasonable mantle model. This suggests that if this compositional variation is produced by partial melting, it approximates an isothermal process.

Whereas the bulk compositions of some pyroxene lherzolite samples plot within the residual field, the compositions of several other pyroxene lherzolite samples are comparatively Mg-poor. These samples lie outside of the residual field and appear to define a distinct trend B in Figure 16B. Trend B appears to be linear and confined to a uniform band of Mg-Fe distributions that extends from the origin and includes the compositional ranges of the coexisting olivine, orthopyroxene and clinopyroxene. Consequently, the bulk

composition variations that define trend B appear to represent a mixing line towards larger proportions of pyroxene with respect to olivine.

The Mg-Fe distributions of the calculated xenolith compositions are essentially a function of the relative abundance of olivine and orthopyroxene (O'Neill 1981) in the xenoliths. Al_2O_3 and CaO, however, are controlled by the compositions as well as the abundance of the pyroxene phases. Even so, there is a strong linear correlation between both Ca and Al and Mg. Ca and Al uniformly increase through the sequence harzburgite, lherzolite and pyroxene lherzolite bulk compositions. This progressive enrichment of both Al and Ca parallels a regular increase in proportion of modal clinopyroxene. The transition between harzburgite and lherzolite occurs at about 1.7 cation % Al and about 6 modal % clinopyroxene, whereas the transition between lherzolite and pyroxene lherzolite occurs at about 3.5 cation % Al and about 12 modal % clinopyroxene.

MINOR-ELEMENT DISTRIBUTION

The dominance of the major elements in a calculated bulk composition has the effect of diluting many of the individual minor elements reported in the mineral analyses to trace levels. However, significant variations are apparent in the abundances of Na, Ti, Cr and Ni. These elements exhibit equivalent concentration ranges in the bulk compositions of all five xenolith suites. There is a systematic correlation

between the concentration levels of these elements and the xenolith group type.

The concentrations of Na and Ti in the calculated bulk compositions define almost identical distributions compared to Mg (Fig. 17). A wide range in concentrations of both Na and Ti occurs in the xenolith samples (Na: 0 to 1.0 mole %; Ti: 0 to 0.12 mole %). Harzburgite bulk compositions have a limited range of uniformly low Na and Ti concentrations (Na: 0 to 0.16 mole %; Ti: 0 to 0.01 mole %) comparable to many of the lherzolite samples. However, the range of abundance of Na and Ti in the lherzolite group is much larger (Na: 0.05 to 0.39 mole %; Ti: 0.00 to 0.06 mole %). The significantly higher Na contents of the hydrous NI lherzolite bulk probably reflects the metasomatism that these samples have experienced. The pyroxene lherzolite compositions associated with trend A (Fig. 16B) reflect a regular increase in the concentrations of both Na and Ti (Na: to 0.70 mole %; Ti: to 0.09 mole %) from the lherzolite group. In contrast, pyroxene lherzolite bulk compositions associated with trend B (Fig. 16B) have distinctly high and relatively uniform Na and Ti concentrations compared to regular increase seen between the lherzolite group and the former subgroup of pyroxene lherzolite samples. The abundance of Na and Ti in the calculated xenolith bulk compositions cannot be accounted for by variation in the modal proportion of clinopyroxene in the samples alone. The range from harzburgite to pyroxene lherzolite is characterized by a 4- to 6-fold increase in

Figure 17: MINOR ELEMENTS IN BULK COMPOSITIONS

A comparison of minor elements vs. Mg in cation percent. Color code: red harzburgite; green lherzolite; yellow pyroxene lherzolite; uncolored group 4 peridotites.

A. Mg vs. Ca

B. Mg vs. Al

C. Mg vs. Na

D. Mg vs. Ti

E. Mg vs. Cr

F. Mg vs. Ni

G. Mg vs. Mn

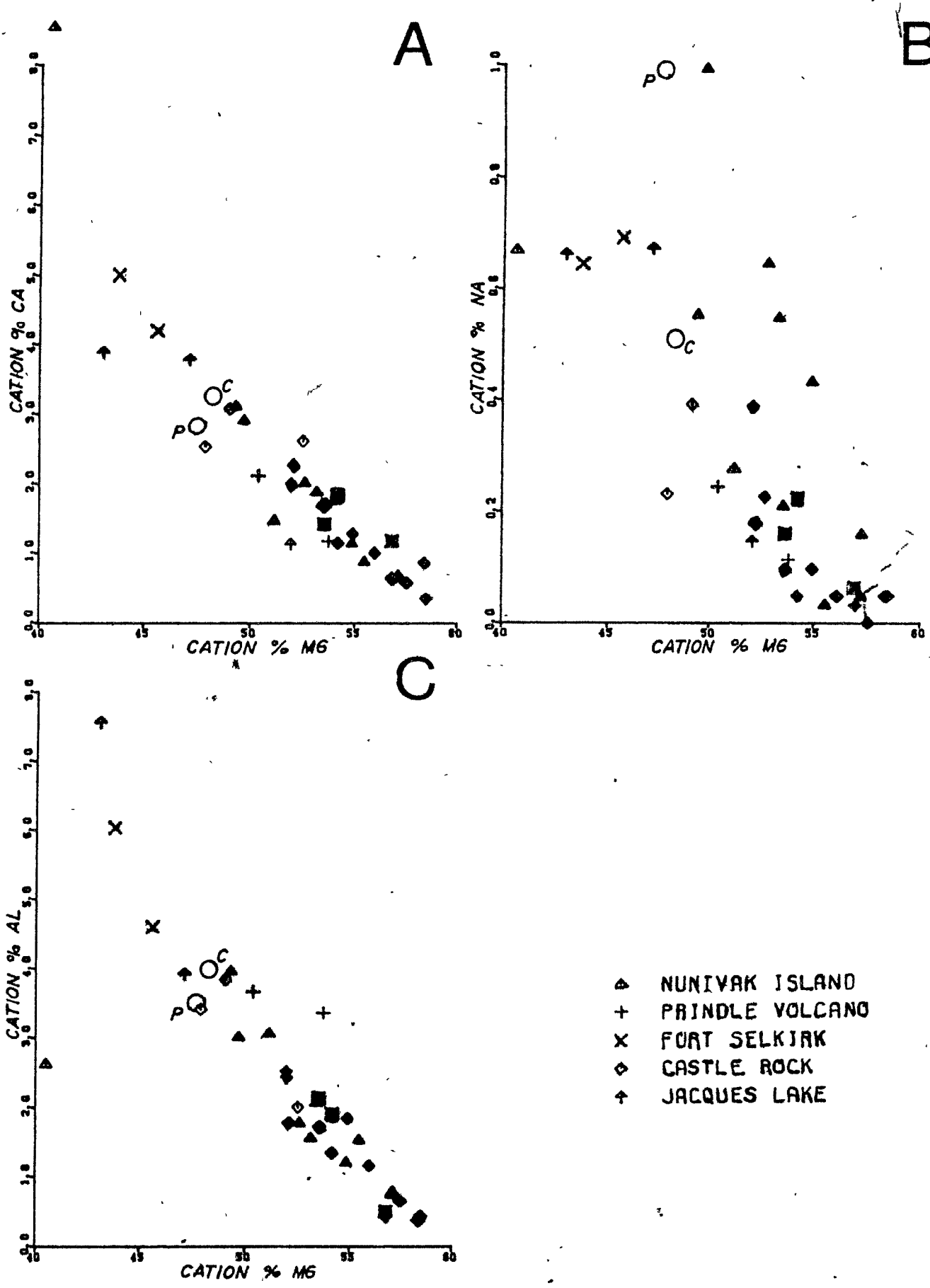
A
B
C
CATION % CA
CATION % NA
CATION % AL
CATION % MG
CATION % MG
CATION % MG
C
P
NUNIVAK ISLAND
PRINDLE VOLCANO
FORT SELKIRK
CASTLE ROCK
JACQUES LAKE

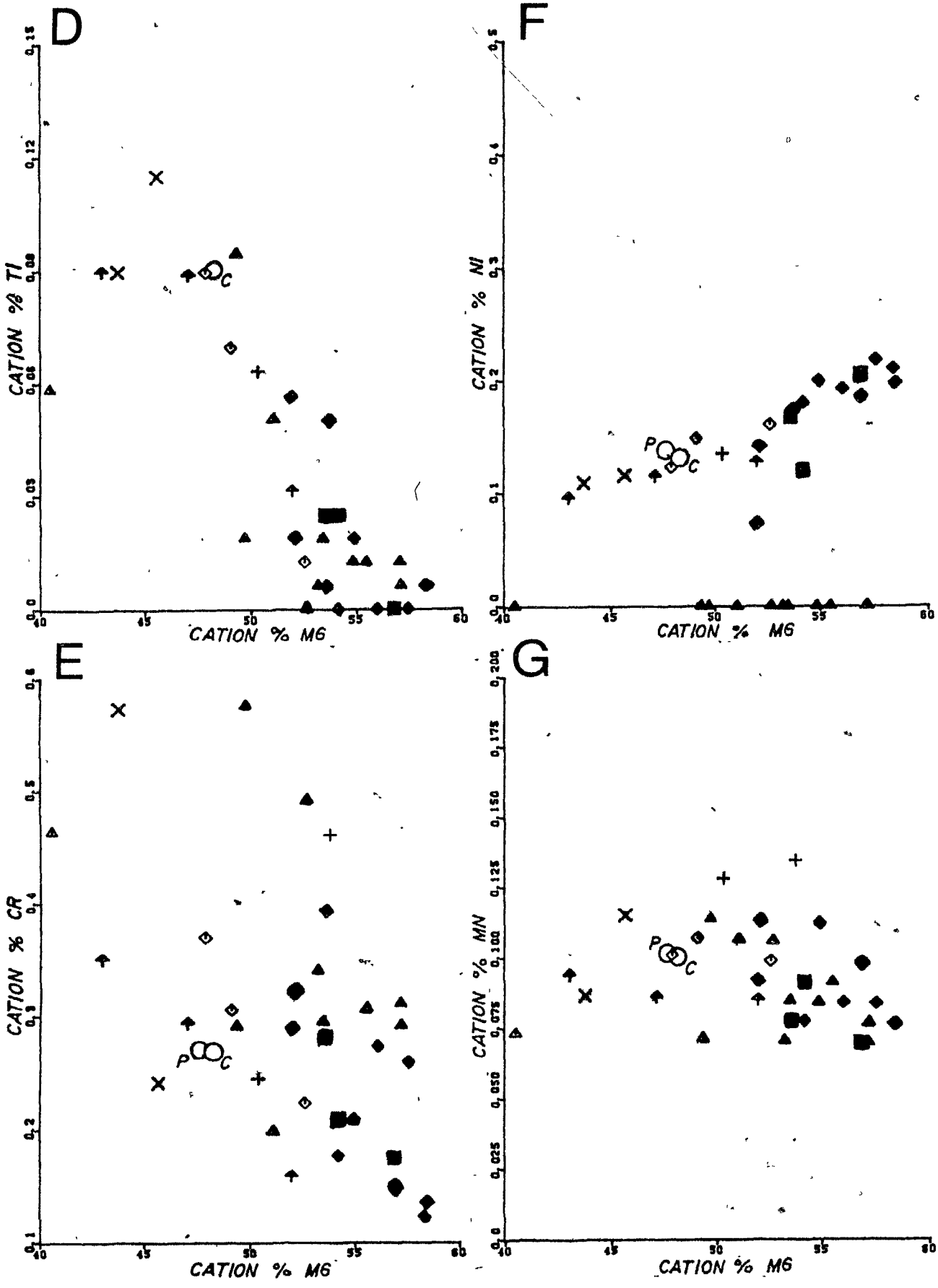
D
CATION % TI
CATION % MG
F
CATION % NI
CATION % MG
E
CATION % CR
CATION % MG
G
CATION % MN
CATION % MG

modal clinopyroxene but a 10-fold increase in the bulk concentrations of both Na and Ti. This requires that both the modal proportion and Na and Ti contents of clinopyroxene must increase.

The distribution of Cr in the calculated bulk compositions parallels that of Na and Ti. There is, however, significantly more scatter, and a poorer separation of the xenolith groups in terms of Cr. The distribution of Cr appears to be a function of the modal proportion of clinopyroxene. There is no apparent distinction in Cr contents between the xenolith samples that defined trends A and B in Mg-Fe distribution. Stosch (1981) has evaluated the possible temperature and compositional dependencies of Co, Ni, Sc and Cr partitioning under upper-mantle conditions. The variations in the olv/cpx and olv/opx partitioning coefficients for Cr appear to be temperature dependent.

Ni decreases linearly in the sequence harzburgite (0.22 to 0.19 mole % Ni) to lherzolite (0.20 to 0.11 mole % Ni) to pyroxene lherzolite (0.15 to 0.11 mole % Ni) groups. This concentration variation in bulk Ni is the reverse of the concentration variation of Ni in the spinel of the xenolith samples. As seen in Chapter 4, the most Ni-rich spinel is found in the pyroxene lherzolite samples, whereas the most Ni-poor spinel is found in the harzburgite samples. This suggests that the modal proportion of olivine is controlling the bulk Ni concentration. Stosch (1981) has proposed a compositional effect exists for the sp/olv and sp/cpx

partition coefficients. Sp/olv partition coefficients for Ni are about 1 for lherzolites that are essentially undepleted or only slightly depleted, but are significantly lower in severely depleted lherzolites or harzburgites.

In contrast to Na, Ti, Cr and Ni, the concentration of Mn appears to be relatively uniform in all of the xenoliths despite the increased concentration of Mn observed in spinels in harzburgite group xenoliths. This probably reflects the low modal proportion of spinel (0.5%) in these samples.

8. DISCUSSION

The majority of xenolith samples from all five localities display a coherent pattern of compositional variation. Therefore, it is likely that these were all formed as a result of a single petrogenetic process. The constraints that are required by applying petrogenetic models to the compositional variations described for the Cordilleran and Nunivak Island xenolith suites are reviewed in this section. The phase relations derived from experimental and theoretical melting studies of simplified and natural peridotites are evaluated in terms of the modal and chemical variations observed in the xenolith samples. These results are compared to yield a model for the evolution of the range of xenolith compositions from the five suites. Those parameters of the xenolith samples that reflect conditions at the time of their eruption with the host basalts are used to illustrate the nature of the contemporary lithosphere beneath the Canadian Cordillera and Alaska. Finally, the tectonic implications of the distribution of ultramafic xenoliths at the five localities are considered.

PETROGENETIC MODELS

Any meaning that can be drawn from the Cordilleran and the Nunivak Island xenolith suites must consider the nature of their relationship to the alkalic basalt host rocks at each locality. Two basic alternatives exist: 1) the samples

are true "xenoliths" or foreign rocks accidentally entrained in the rising host magma or 2) the xenolith samples are "cognate", and bear a direct genetic relationship with their host basalts. Although the incorporation of the xenolith samples in the basaltic hosts may be more understandable as an "accidental" relation - - - - , the diagnostic test of this alternative is the ~~lack of any~~ direct compositional relation between them.

Two principal models have been proposed for the petrogenesis of ultramafic xenoliths. Each places specific constraints on their modes and mineral and bulk compositions. The most commonly applied model assumes that the xenoliths represent the residue of a partially melted lherzolitic mantle. The more widely accepted variant of a partial melting model holds that the xenoliths represent the residue after the extraction of some magmatic component which is unrelated to the host basalts in which they are entrained. A less likely variation of the partial melting model suggests that the xenoliths represent the upper mantle residue that coexisted with the host basalts. In this case, the xenolith samples would be cognate.

O'Hara (1967) proposed a cognate origin for spinel lherzolite xenoliths, relating them to their host magma. In this model, the partial melting of garnet peridotite to depths in excess of 100 km would generate parental hypersthene-normative magmas that evolve towards nepheline-normative compositions by the separation of crystals that

form spinel lherzolite accumulates. Alternately, the xenoliths may be accidental, and yet represent crystallized accumulates formed in a manner similar to O'Hara's, prior to their entrainment in their host.

Lherzolitic assemblages are known to have fractionally crystallized and accumulated in the basal portions of layered mafic intrusions (Wager & Brown 1966). In these sequences the lithologies have distinct contrasts in modal composition. The majority of xenolith samples, however, are characterized by a uniform variation in modal composition, largely transitional in the proportion of one or both pyroxenes to olivine. Within the xenolith suites, the only samples which are characterized by the distinctive modal compositions commonly associated with accumulate origin are the few pyroxenites and rare dunites. In these samples, the modal proportion of spinel is significantly higher than in the majority of xenolith samples. However, several of the peridotite xenoliths (JL6, FS20, PV39) also contain greater than 5 modal % spinel, as compared to the typical range of 0.5 to 3.0 modal % spinel in the majority of xenolith samples (Appendix 1). An accumulate origin may be supported by modal proportions for these samples.

Little support for a cumulate model can be derived from an examination of xenolith textures. Cumulate peridotites that form by fractionation of a basaltic magma are characterized by distinctive textures (Wager & Brown 1966) which vary in the proportions of cumulus phases and phases which

have crystallized from an intercumulus liquid. Poikilitic textures are common in cumulate lithologies. However, the great majority of xenolith samples lack cumulate petrographic characteristics. Despite the range of xenolith textures observed among the five suites, most samples display equigranular textures that vary only in the ratio of porphyroclasts vs. neoblasts.

The composition of the xenolith phases are remarkably uniform, showing no evidence of the compositional zonation commonly associated with a fractionally crystallized origin (Wager & Brown 1966). The olivine contained in the majority of xenolith samples shows a small range in composition (Fo88 - Fo92) comparable to most estimates of the composition of the primitive upper mantle (olivine = Fo88 - Fo90) (Carter 1970, Ringwood 1966). Only xenoliths CR37 and PV39 have relatively Fe-rich olivines (Fo86 - Fo88) characteristic of those produced by fractional crystallization. The pyroxene compositions from the harzburgite, lherzolite and pyroxene lherzolite xenolith groups are also relatively Fe-poor. Only the group 4 samples CR37 and PV39 contain orthopyroxene which are relatively Fe-rich. The majority of the clinopyroxenes form a tight group in the pyroxene quadrilateral (Fig. 5), whereas the group 4 peridotite samples plot in the endiopside and augite fields, displaying distinctly more Fe-rich compositions. In contrast to the inverse relationship in Mg/(Mg + Fe) between coexisting silicates and spinel in the majority of xenolith samples, these group 4 peridotites are also anomalous

in having both Fe-rich silicate and spinel compositions, compatible with a cumulate model.

Further discrimination between the accumulate or partial melting models can be drawn from the distribution of compatible minor elements in the xenolith minerals. Such elements, with solid-liquid partition coefficients greater than one, are expected to concentrate preferentially in the solid phase as opposed to the coexisting melt. Assuming an initial partition coefficient of 10 in the parent composition (approximately equivalent for example, to Ni in olivine or Cr in clinopyroxene), 30% fractional crystallization will change the abundance ratio in the resulting cumulate from 10 to 3.33, whereas 30% partial melting will change their abundance ratio in the remaining residue from 1.00 to 1.38 (Frey & Green 1974). In the xenoliths, the nickel concentrations of olivine are approximately uniform (0.20 to 0.27 mole % Ni) and similar to the concentration of Cr in the coexisting clinopyroxenes (0.50 to 0.75 mole % Cr). The small range in concentration of Ni in olivine and Cr in clinopyroxene are thus more compatible with a partial melting model. Comparable variations in concentration are observed for all of the compatible minor elements in the silicate minerals. Within the xenolith suites there is a slight increase in the concentrations of compatible minor elements in the sequence pyroxene lherzolite to lherzolite to harzburgite, suggesting that this sequence may correspond to an increasing degree of partial melting.

Complementary solid-liquid partitioning relations can be expected for those minor elements with ratios less than one, which preferentially partition into a liquid as opposed to a coexisting solid phase. In the xenolith clinopyroxenes, a relatively wide range of sodium contents (Fig. 12) is accompanied by almost no change in Cr. content. This is a classic signature of a partial melting process. A fractional crystallization process would produce the inverse of the distribution seen in Figure 13. The large variation in readily fusible elements, such as Na and Ti in pyroxenes of xenolith samples with little variation in compatible element contents, does not support an origin by an O'Hara-type model. However, the gradational depletion of Na and Ti in the sequence harzburgite to lherzolite to pyroxene lherzolite can be readily accounted for by the partial melting of a primitive source with an initial composition similar to the pyroxene lherzolite samples.

A final consideration of the alternative models of petrogenetic origin may be derived from the calculated pyroxene equilibrium-temperatures. The majority of these temperatures (850 to 1000°C) are too low to have been in equilibrium with basaltic melts, which typically range in temperature from 1200 to 1500°C. Most of the calculated pyroxene equilibrium temperatures are clearly subsolidus and refute the possibility of a strict application of O'Hara's (1967) model to the majority of the xenolith samples. The only samples with distinctly higher pyroxene equilibrium

temperatures are the group 4 peridotites (JL1, JL19, CR30 and CR37) in the range of 1100 to 1200°C. These calculated temperatures are compatible with equilibration from a basaltic melt. Because of the abundance of petrographic and compositional evidence, a partial melting origin for the majority of the Cordilleran and Nunivak Island samples will be assumed in the following discussion.

THE NATURE OF THE PARTIAL MELTING PROCESS

The term "partial fusion" has been used by Presnall (1969) to indicate melting of some portion less than the whole. In a natural system, this process is probably intermediate between that of equilibrium melting and fractional melting. An equilibrium melting process is one in which a liquid produced by melting continually reacts and re-equilibrates with its depleted source. In contrast, a fractional melting process is one in which the liquid is immediately isolated from the source as it is formed. The liquid does not continue to react with the source even though the latter may continue to melt. Presnall (1969) showed that fractional melting results in a discontinuous liquid path comprising distinct eutectic compositions, approximately invariant in major-element composition. However, these liquids would exhibit a continuous range of trace-element contents because of the progressive variation of partition coefficients (Yoder 1978). Addition of heat to the system while a constant eutectic liquid is produced results in no increase in temperature

even though the depleting source continuously changes in composition. If heat is continuously supplied, the production of melt will eventually halt when one of the major phases has been consumed. Melting resumes as soon as the temperature is raised to that of the invariant point governing the initial system minus the consumed phase.

In his review of basalt genesis, Yoder (1976) supported the view that the initial melting of primitive source material in the upper mantle takes place in an invariant-like fashion. Minor melting (< 1%) of a pristine source may involve only accessory minerals and fluids located along grain boundaries and in inclusions in the silicate phases. Consequently, major melting of a mineral assemblage probably commences at the junctions of the principal silicate phases. Presnall et al. (1979) showed that discontinuities or cusps in the solidus curves for mantle materials result from their intersections, at an invariant point, with a subsolidus reaction. Melting begins at the lowest-temperature cusp, and this temperature will determine the depth of melting and control the composition of the primary melt.

Kushiro's (1969) experiments at high pressures show that up to 30% partial melting of a parent mantle composition is pseudo-invariant. The melt produced is relatively restricted in major element composition, but varies largely in fusible ("basaltic-magma-yielding") components. This eutectic-like composition is continuously generated from the residue as long as all four principal phases are still present. The

residuum from the partial fusion of an olivine-rich lherzolite is a more magnesian olivine-rich lherzolite, harzburgite or dunite.

Mysen & Boettcher (1975) have experimentally examined the phase relations of natural lherzolites at high pressure and temperature, with controlled activities of H_2O, CO_2 and H_2. The phase relations of the four sample compositions in the presence of nearly pure H_2O vapor ($X^v_{H_2O} = 1.0$) are similar. All hydrous peridotite solidi ($X^v_{H_2O} = 1.0$) exhibit temperature minima, probably related to the breakdown of amphibole, aluminous pyroxene and spinel to give a denser garnet-bearing assemblage. The addition of phlogopite in the experimental charge shows that the K-bearing phases phl + amph + liq coexist over extensive pressure intervals. In addition, phlogopite appears stable to temperatures above the upper temperature stability limit of amphibole, supporting the suggestion (Mysen & Boettcher 1975) that phlogopite is a refractory hydrous mineral in the upper mantle. Mysen & Boettcher (1975) used CO_2 to reduce $X^v_{H_2O}$ and f_{H_2O}, resulting in a shift of the solidi to higher temperatures. The mineralogy of the run products with CO_2 added differs from that in the CO_2-free charges in one important respect: modal orthopyroxene at any temperature and pressure with $X^v_{H_2O} < 0.5$ is significantly higher than with more H_2O-rich vapors. The solubility of CO_2 in silicate liquids increases and probably reaches a maximum at $X^v_{H_2O}$ 0.25 to 0.20, whereas the solubility of H_2O decreases.

In later experiments, Mysen & Kushiro (1977) determined the compositional variations with degree of partial melting for two undepleted garnet peridotite xenoliths, PHN-1611 and 66SAL-1 at 20 kbar and 35 kbar. The samples differ in solidus temperature and the temperature and degree of melting at which phase changes occur. For example, the loss of clinopyroxene occurs with 60% melting of 66SAL-1 vs. 25% melting of PHN-1611. The melting ranges at 20 kbar can be divided into three distinctly different fields according to the mineralogy of the residue: olv + opx + cpx (+sp) + L; olv + opx + L; olv + L. The derived liquids that are associated with the three melting ranges are olivine tholeiite, tholeiitic picrite and peridotitic komatiite, respectively. Mysen & Kushiro (1977) concluded that each melting range of peridotite yields a restricted melt composition that varies only within narrow compositional limits. The width of these melting intervals depends on the bulk composition of the peridotite.

Using beta-track mapping techniques, Scarfe et al. (1979) experimentally studied invariant melting behavior, emphasizing the importance of low degrees of partial melting. They found that the variation in the composition of the coexisting solid phases correlates well with the melting relationships. For example, the Mg/(Mg + Fe) content of olivine and orthopyroxene varies only slightly in the initial melting interval, but shows larger increases where a phase is lost and an inflection occurs in the melting curve. Scarfe et al. (1979) concluded that the flat slope of the melting curves at

temperatures just above the solidus and the almost constant composition of liquid and coexisting solid phases in this interval suggest that melting is approximately invariant, the composition of the liquid being determined by the phases present in the residue, not by their proportions.

Jacques & Green (1980) presented a recent experimental study of the anhydrous melting at 0 to 15 kbar pressure of pyrolite and Tinaquillo peridotite. Their results indicate the presence of a narrow field close to the solidus in which an aluminous phase coexists with olivine, 2 pyroxenes and liquid. This aluminous phase melts completely within 25 to 30°C of the solidus (in the case of aluminous spinel by continuous reaction to chrome spinel). The clinopyroxene-bearing field for these peridotites extends some 75 to 100°C above the solidus. The upper stability limit of orthopyroxene lies approximately 150 to 200°C above the solidus of both peridotites and increases slightly with pressure. The percentage of melt obtained from the melting of both peridotite samples increases rapidly in the initial stages of melting, and then increases at a steady rate, whereas the proportion of residual phases decreases regularly. Jacques & Green (1980) suggested that alkali olivine basalts and more undersaturated rocks are derived from lherzolite assemblages at low degrees of partial melting and at pressures greater than 10 kbar, and probably 15 kbar, leaving a residue of olivine + clinopyroxene +/- spinel or garnet depending on pressure.

EVOLUTION OF THE XENOLITH SAMPLES

A partial melting model may be applied to the four Cordilleran and Nunivak Island xenolith suites by highlighting the observed variations that may reflect petrogenetic control. Among the most uniform features of the five ultramafic xenolith suites is the range in modal proportions. A common trend can be seen in the distribution of lithologies from each suite (Fig. 2) defined by the predominant group of lherzolite samples and the range of either more olivine- or pyroxene-rich lithologies. Pyroxene-rich lithologies are comparatively abundant at the JL, FS and PV xenolith localities. Samples from these three suites appear to define a modal distribution which varies in the ratio of olv vs. opx + cpx. An extension of this distribution would intersect the opx-cpx axis in Figure 2 at about 60 modal % orthopyroxene. However, samples with greater than 76 modal % olivine appear to diverge from the trend. In the CR suite, samples from the harzburgite xenolith group define a linear distribution with a uniform modal clinopyroxene content but a variation in the ratio of olv vs. opx. This inflection between the modal distribution of harzburgite and lherzolite samples is also weakly apparent in the PV and FS suites.

The residue produced by the initial partial melting of a pyrolite-like mantle would have pyroxene lherzolite to lherzolite composition and would coexist with a pseudo-invariant melt. The transition from lherzolite to harzburgite residue compositions may reflect the loss of clinopyroxene

in the source at higher degrees of partial melting. According to such an interpretation, the modal clinopyroxene observed in harzburgite group xenoliths would have formed by exsolution from orthopyroxene during subsolidus re-equilibration.

The variations in mineral compositions can be readily interpreted according to a partial melting model. For the majority of samples, the Mg-Fe distributions of olivine, ortho- and clinopyroxene (Fig. 16A) and of spinel (Fig. 13) define narrow ranges. In addition, there is little variation in the ratio of Ca/(Ca + Mg) in clinopyroxenes from the harzburgite, lherzolite and pyroxene lherzolite xenolith groups (Fig. 6). However, significant compositional variations occur in the fusible element contents of both pyroxenes and spinel. This is shown by the progressive depletion of aluminum in the sequence pyroxene lherzolite to lherzolite to harzburgite for each of these three phases. The distribution of sodium and titanium closely follows that of aluminum in the xenolith pyroxenes (excluding the comparatively anomalous Na-rich clinopyroxene of the hydrous NI samples). This progressive depletion of the fusible elements Al, Ti and Na in the sequence pyroxene lherzolite to lherzolite to harzburgite is interpreted to reflect an increase in the degree of melting these xenoliths represent.

The variations in mineral chemistry between xenolith groups are reflected in the calculated bulk compositions. The distribution of the compatible major elements Mg and Fe

in the bulk compositions is derived from their solid solution in each of the four mineral phases and should therefore reflect any common petrogenetic process that affected all four. In contrast, Ca is held in pyroxene solid-solution, whereas aluminum is controlled by mutual solid-solution among both pyroxenes and spinel. The concentration of both Ca and Al in the bulk compositions is correlated with both the modal proportion of these phases and their individual compositions. A similar pattern of variation is displayed by the fusible elements Na and Ti, both preferentially partitioned into clinopyroxene. The rapid depletion of both Na and Ti (Fig. 17) in the transition from pyroxene lherzolite to lherzolite is followed by comparatively smaller degrees of depletion in the transition from lherzolite to harzburgite. In fact, the range of Na and Ti concentrations in the harzburgite bulk compositions largely overlaps the lower range of lherzolite bulk compositions. The variation of fusible minor elements in the bulk compositions suggests that Na and Ti are functionally controlled by the modal amounts of clinopyroxene.

A surprisingly similar conclusion can be drawn for Cr in the bulk compositions. In both pyroxenes and spinel, Cr contents follow the trend expected of a compatible element, typically increasing from that of the pyroxene lherzolite group. Yet the highest Cr contents in the calculated bulk compositions are from samples in the pyroxene lherzolite xenolith group. Depletion of Cr in the bulk compositions occurs predominantly in the range of pyroxene lherzolite and

lherzolite compositions. Cr concentrations in lherzolite bulk compositions overlap those of harzburgite bulk compositions in a similar manner to that seen for Na and Ti.

The compositional variations in each of the xenolith suites appear to reflect a common partial melting process, the principal differences between the suites lying in the average degree of depletion of a common primitive mantle composition which characterizes each suite. The close similarity in the composition of the pyroxene lherzolite samples and that of pyrolite-1 (Table 6) suggests that this xenolith group may approximate anhydrous undepleted upper mantle that is present in some proportion beneath each of the sample localities. The xenoliths of the lherzolite and harzburgite groups (Fig. 16B) can be related by increasing degrees of partial melting of parental compositions that are approximately equivalent to the pyroxene lherzolite group. Thus the lherzolite and the harzburgite xenolith groups represent upper mantle that is compositionally depleted and barren, respectively, in terms of fusible components, compared to a "fertile" clinopyroxene-rich lherzolite source, as represented by group 3 xenoliths. The fact that the trend defined by the hydrous peridotites at Nunivak Island (Fig. 16B) is identical to that of the anhydrous Cordilleran suites indicates that the late Na-rich metasomatic fluids had little effect on the major-element chemistry of the upper mantle beneath this locality.

THE COMPOSITION OF THE PRIMITIVE CORDILLERAN MANTLE

The high fusible element content of samples with pyroxene lherzolite compositions forms the basis for distinguishing this group from the otherwise continuous lherzolite xenolith group. Pyroxene lherzolite samples from each of the four Cordilleran and Nunivak Island suites were used to calculate an average undepleted upper mantle composition (Table 6). Although several other pyroxene lherzolite bulk compositions plot outside the residual field (Fig. 16B), these samples may be products of fractional crystallization, as shown by the Fe-rich nature of their clinopyroxene and their high modal proportions of spinel. The pyroxene lherzolite samples chosen in Table 6 (with the exception of FS12) plot within the residual field (Fig. 16B) and cluster about the lower range of trend A.

The most widely used estimate of the undepleted upper mantle is that of pyrolite-1 (Ringwood 1966), composed of three parts "synthetic" alpine peridotite and one part Hawaiian tholeiite. Pyrolite-1 is thought to be a reasonable approximation of the upper mantle composition in areas of continental alkali basalt volcanism (Frey & Prinz 1978). Although the averaged compositions of the xenolith suites (Table 2) are significantly depleted in fusible components relative to the pyrolite model, the pyroxene lherzolite bulk compositions chosen in Table 6 closely approximate that of pyrolite (Table 6) in their contents of the major oxides. In addition, the concentrations of compatible minor elements

Table 6: UNDEPLETED MANTLE COMPOSITIONS

SAMPLE	JL 50009	CR 40010	FS 30012	FV 20046	NI 10069	1	2	3	4
SIO2	45.76	44.68	45.67	44.26	43.96	44.85	45.20	42.86	44.71
TIO2	0.14	0.11	0.18	0.10	0.15	0.14	0.71	0.33	0.16
AL2O3	3.94	3.88	4.60	3.71	4.01	4.03	3.54	6.99	2.46
CR2O3	0.44	0.46	0.36	0.37	0.44	0.41	0.48	0.18	0.42
MGO	37.38	39.12	36.07	40.27	39.41	38.44	37.50	35.07	41.00
FEO	7.46	7.72	7.75	8.41	8.13	7.89	8.04	7.22	8.15
MNO	0.12	0.15	0.16	0.18	0.10	0.14	0.14	0.14	0.18
NIO	0.17	0.22	0.17	0.20	-	0.19	0.20	0.20	0.26
CAO	4.17	3.42	4.61	2.35	3.46	3.60	3.08	4.37	2.42
NA2O	0.41	0.24	0.42	0.15	0.34	0.31	0.57	0.45	0.29
TOTAL	99.99	100.00	99.99	100.00	100.00	100.00	99.46	97.81	100.05
MOLAR PROPORTIONS BASED ON 100 CATIONS									
SI	38.68	37.58	38.78	37.14	36.90	37.80	38.44	37.07	37.41
TI	0.09	0.07	0.11	0.06	0.09	0.09	0.45	0.21	0.10
AL	3.92	3.85	4.60	3.67	3.97	4.00	3.55	7.12	2.43
CR	0.29	0.31	0.24	0.25	0.29	0.27	0.32	0.12	0.28
MG	47.09	49.04	45.65	50.36	49.31	48.29	47.53	45.21	51.14
FE	5.27	5.43	5.50	5.90	5.71	5.56	5.72	5.22	5.70
MN	0.09	0.11	0.12	0.13	0.07	0.10	0.10	0.10	0.13
NI	0.12	0.15	0.12	0.13	-	0.13	0.14	0.14	0.17
CA	3.78	3.08	4.19	2.11	3.11	3.25	2.81	4.05	2.17
NA	0.67	0.39	0.69	0.24	0.55	0.51	0.94	0.75	0.47
OXYGENS	140.54	139.53	140.97	139.04	138.85	139.77	140.36	140.53	138.63
MG/MG+FE	0.899	0.900	0.892	0.895	0.896	0.897	0.893	0.896	0.900
AL/AL+SI	0.092	0.093	0.106	0.090	0.097	0.096	0.085	0.161	0.061

1: Average of 5 Cordilleran undepleted samples

2: Ringwood (1966) Pyrolite-1, 3 parts dunite + 1 part Hawaiian tholeiite

3: Carter (1970) model based on spinel lherzolite from Kilbourne Hole, N.M.

4: Maaloe & Aoki (1977) model based on continental spinel lherzolite, with estimated TiO_2 and Na_2O weight percentages

Cr, Mn and Ni are very similar in the pyroxene lherzolite bulk compositions and pyrolite (Table 6). The average bulk composition of the five pyroxene lherzolite samples appears to be slightly higher in Al_2O_3 and CaO compared to pyrolite; however, the concentrations of these oxides approximate that of pyrolite for several of the five samples.

In contrast, pyrolite has a significantly greater concentration of Na_2O and TiO_2 than any of the Cordilleran pyroxene lherzolite samples. The Na_2O contents of pyrolite are only approached by JL9 and the hydrous Nunivak Island lherzolite samples, whereas the TiO_2 content of pyrolite is almost five times greater than the most Ti-rich bulk composition (0.15 wt. %; NI69) calculated for the xenolith samples. Kuno (1969) suggested that the Hawaiian tholeiite composition used by Ringwood (1966) was atypically high in its alkali and titania contents compared to common olivine tholeiites. Frey & Prinz (1978) have shown that pyrolite-1 is enriched in incompatible elements relative to the source region for the most mid-ocean-ridge basalts.

Carter (1970) estimated the vapor-free composition of the undepleted upper mantle based on a study of spinel lherzolite and wehrlite xenoliths from Kilbourne Hole, New Mexico. Carter's (1970) data show that samples in which the forsterite content of olivine is between 86 and 88% are rare. Because of the differences between testures, modes and compositions of samples on either side of this range, Carter (1970) suggested that both partial fusion and partial crystallization

play a dominant role in the genesis of ultramafic xenoliths and that the compositional interval between their expected products represents the undepleted composition of the upper mantle. The differences between Carter's model and the pyrolite model (Ringwood 1966) occur mainly for those oxides that show a preference for incorporation in the liquid phase; for example, TiO_2, Na_2O and K_2O. Carter (1970) noted that some of the difference between these models for the fusible components may result because of their immediate incorporation into the liquid phase with very low degrees of partial melting. With respect to the Cordilleran average, the Carter (1970) model is lower in the content of the compatible elements Mg, Fe and Cr. Carter's estimation does not fall along the Cordilleran partial melting path (trend A in Fig. 16B) in Mg-Fe space but lies within the field of pyroxene lherzolite-3 samples with cumulate affinities. This suggests that a better estimate from Carter's data might arise if some pristine mantle compositions were assumed to be included in the lherzolite population at Kilbourne Hole.

Maaloe & Aoki (1977) estimated the composition of the upper mantle based on a comparison of whole-rock compositions of spinel lherzolite and garnet lherzolite xenoliths. They showed that the chemical composition of continental and oceanic spinel lherzolites are very similar with the exception of CaO, Na_2O and TiO_2. Maaloe & Aoki (1977) assumed that the primitive mantle should have a magnesia content slightly lower than that of the average spinel lherzolite;

they proposed a value of 41.0 wt. % MgO. The remaining primitive oxide-contents were estimated for continental spinel lherzolite of this magnesia content, with the exception of Na_2O and TiO_2, which are estimated to approximate the higher values of oceanic spinel lherzolite. The model of Maaloe & Aoki (1977) suggests a slightly Mg-rich and Al-poor mantle compared to the average undepleted Cordilleran composition. Although the fusible element contents are closely comparable between these two estimates, Maaloe & Aoki's (1977) model composition lies between that of the lherzolite and pyroxene lherzolite xenolith groups in terms of Mg and Fe, and suggests that their mantle is slightly depleted relative to the pristine Cordillera.

The distribution of Cordilleran and Nunivak Island samples support Carter's (1970) assumption that products of both partial melting and fractional crystallization are present in the xenolith suites and that the compositions that most closely approximate the undepleted upper mantle should be intermediate between these. Although trend A (Fig. 16B) does not intersect the composition of pyrolite, an extension of it would include an upper mantle composition that might be appropriate as an alternate Cordilleran primitive mantle. Both the calculated Cordilleran mantle and pyrolite are Mg-poor compared to the harzburgite and lherzolite xenolith groups. In addition, the curvature suggested by trend A implies that the Cordilleran model may be slightly Fe-rich (approximately 6.0 mole % Fe) or possibly more Mg-rich

compared to pyrolite.

If the approach of Maaloe & Aoki (1977) of assuming an appropriate Mg content is adopted, the Cordilleran primitive mantle would have an Mg mole % approximating that of pyrolite. In addition these Cordilleran and pyrolite-1 models appear comparable (Fig. 17) for elements that display regular variations in concentration, such as Ca, Al and Ni. If the metasomatized Nunivak Island samples and those Cordilleran samples consistent with a cumulate model of origin are excluded, estimates for the primitive Cordilleran upper mantle contents of fusible elements can be made. Based on the distribution of Na and Ti for the range of xenolith samples (Fig. 17), the Cordilleran primitive mantle appears to have values of about 0.50 cation % Na and 0.08 cation % Ti. These concentrations are considerably Na- and Ti-poor compared to that of pyrolite-1. However, the pyrolite-1 model suggests distinctly Cr-poor compositions compared to the metasomatized Nunivak Island samples; it may provide a reasonable estimate of the Cr values of the primitive Cordilleran mantle.

THE CORDILLERAN LITHOSPHERE TODAY

It is possible that the partial melting episode(s) that resulted in the xenolith compositions may have occurred long ago. Although a cognate origin would imply that the evolution of the xenolith compositions occurred in a comparatively recent geologic timeframe, little evidence can be drawn from the majority of samples to support this model except that

they have been entrained in basaltic hosts of late Tertiary to Recent ages. This association requires that the xenolith samples reflect the comparatively recent compositions and physical conditions of the lithosphere, regardless of the petrogenetic model adopted. Estimates of physical equilibrium parameters for the xenoliths can be used with the variation in xenolith textures to illustrate the nature of the contemporary Cordilleran and Alaskan lithosphere and the degree of its heterogeneity throughout this region.

The pyroxene geothermometer of Wells (1977) yields calculated temperatures that are rather uniform. The equilibrium temperatures of the harzburgite, lherzolite and pyroxene lherzolite samples define a narrow range (60 to 110°C) in each suite. Most are several hundred degrees too low to reflect equilibrium with an extracted melt. One can conclude from this that the majority of xenolith samples reflect subsolidus re-equilibration following their depletion by partial melting. The only consistent departure from this range of calculated temperatures is for the group 4 peridotite samples, which have been shown to be distinctly higher than those calculated for the predominant xenolith groups 1, 2 and 3.

There is little evidence for the systematic variation in temperature expected from partial melting, except in the CR suite. In this suite the calculated results (Fig. 15) suggest that temperatures increase between xenolith groups over a narrow range in the sequence pyroxene lherzolite to lherzolite

to harzburgite. Although in the four remaining suites, a heterogeneous distribution of calculated temperatures between the xenolith groups is apparent, a consistent decrease in equilibration temperatures can be seen between the Cordilleran xenolith suites in the sequence JL = CR > FS > PV (Table 5).

At present, quantitative estimates of the equilibrium pressure conditions for the xenolith samples are much less reliable than those of temperature. Nevertheless, several compositional parameters, such as the distribution of Al^{iv} vs. Al^{vi} and the proportion of the jadeite component, suggest that the Cordilleran xenoliths have sampled a range of depths that decrease in the sequence JL > FS > PV > CR. Both of these fusible components are shown to be correlated (Fig. 11) by coupled solid-solution in the form $NaAlSi_2O_6$, and their variation in this sequence could be derived entirely from differing degrees of depletion with partial melting (Francis, pers. comm. 1982). However, if both the distribution of Al^{iv} vs. Al^{vi} and the proportion of jadeite are strictly related to partial melting, their average value for each suite should be correlated to the average degree of depletion as reflected in their average modal composition (Table 2). The degree of depletion increases in a somewhat different sequence, than that proposed to represent the sampled depth at each locality, i.e., PV > JL > FS = CR > NI.

The variation in pressure-dependent aluminous phases in the xenolith suites also suggests that the depths sampled by

the xenoliths decreases in the sequence JL > FS > PV > CR. Although not specifically considered in this study, the fact that plagioclase lherzolite and granulite (Table 1) samples are predominantly restricted to the PV, CR and NI suites supports their comparatively low pressures of equilibrium (8 to 9 kbar). A maximum pressure range in the xenolith suites is indicated by the reaction of garnet to form two pyroxenes and spinel, possible evidence for which lies in the occurrence of "holly leaf" spinel textures observed in some samples. Samples containing this texture are virtually restricted to the JL and FS suites and altogether absent in the PV suite. This sequence varies slightly from the results obtained using Ranalli's (1980) Cordilleran geotherm. (Fig. 15). However, the latter application is largely dependent on the distribution of calculated pyroxene equilibration temperatures.

In the Cordilleran suites, there is a gradational variation in the ratio of porphyroclasts to neoblasts from coarse equant (CE) to granuloblastic-textured (GE) xenoliths, with intermediate porphyroclastic (POR) or mosaic-porphyroclastic-textured (MP) xenoliths dominating the population. Mercier & Nicolas (1976) suggested that this type of textural spectrum represents recrystallization with deformation increasing from CE to POR to GE textures. If the textural variations are a result of partial melting, then the polarity expected is opposite to that observed in the Cordilleran suites, i.e., GE (pyroxene lherzolite) recrystallizing to POR (lherzolite)

and then GE (harzburgite) compositions, because an increased degree of recrystallization would be associated with an increased degree of depletion. Interestingly, Basu (1977) described a similar suite of spinel lherzolites from San Quintin, Baja California, in which the sequence expected from both partial melting and metamorphic recrystallization agree, i.e., CE (pyroxene lherzolite) to POR (lherzolite) to GE (harzburgite) compositions.

The ultramafic xenolith textures may reflect postmagmatic recrystallization in response to deformation. Recent studies by Ave'Lallement et al. (1980) suggest that only the relatively coarse original (paleoblast) grain size is clearly a function of depth. Application of a refined single pyroxene thermobarometry technique (Ave'Lallement et al. 1980) and careful determination of grain sizes for xenoliths in basalts show a general increase in paleoblast grain-size and the decrease of differential stresses with depth. The identical textural character of granuloblastic ultramafic and some granulite xenoliths from several of the Cordilleran suites suggests the increasing importance of crustal deformation processes extending below the depths of plagioclase stability (26 km), such that granuloblastic textures grade into porphyroclastic and coarse equant textures with increasing depth.

The correlations observed between chemistry and texture might be explained by a model in which different groups of xenoliths represent partial melting residues from different depths. Maaloe & Aoki (1977) did not consider the composi-

tional difference between spinel and garnet lherzolite as evidence for a systematic chemical variation in the mantle with depth. However, the garnet lherzolite from beneath the African continent does appear to deviate in composition from garnet lherzolites elsewhere, as well as from continental and oceanic spinel lherzolites. Maaloe & Aoki (1977) suggested that the African garnet lherzolites could be considered residual compositions from a spinel lherzolite, and might represent a primitive homogeneity. Carswell (1980) has reviewed various lherzolite xenolith studies that indicate the existence of lateral and vertical variations in the composition of the uppermost mantle. He suggested that there may be an overall chemical zonation to the upper mantle above the asthenosphere with the level of depletion in fusible components decreasing with depth. With respect to the Cordilleran xenolith suites, this would imply that the most depleted samples of the harzburgite group represent the deepest mantle compositions; these would be overlain by less depleted mantle residuals.

If degree of partial melting is significantly variable over small distances, then textural variations may merely reflect its operations. If this is the case, a likely analogue for the mantle source-region of the xenolith suites would be that of a high-grade migmatitic terrane with gneissic banding of leucosome and melanosome. In such rocks partial melting results in the segregation of felsic melt into bands that alternate with layers of mafic residue in a

lit-par-lit arrangement. In regions of shear stress or high thermal gradients, the melt component could become relatively mobile compared to the residue, resulting in a complex mixing or "marbling" of these units. Whereas direct equivalents to the leucosome-melanosome relationship in a banded gneiss are now known in a few composite xenoliths only, a suite of xenoliths with contrasting compositions and textures could have been derived from juxtaposed layers within the mantle. Rhodes & Dawson (1975) have described lherzolite xenoliths that show significant variations in the level of deformation over distances of only cm, indicating that deformation may be very localized. The variability in the extent of partial melting over small areas that such a model implies would not only explain many of the exceptions to the generally systematic variation of xenolith composition with texture (Fig. 3), but also the surprising homogeneity of the calculated subsolidus equilibrium temperatures between the xenolith groups.

Variations in the composition of the lithospheric upper mantle are clearly reflected in the range and relative proportions of the individual groups of xenoliths at each locality. Each xenolith suite contains a variable proportion of compositionally "fertile", pyroxene lherzolite xenoliths. These samples have been interpreted to approximate a common undepleted upper-mantle composition. Although both the CR and PV xenolith suites appear to have sampled approximately equivalent pressure ranges, their distinctly different populations (Fig. 2) suggest that the CR mantle has been much

more extensively depleted in fusible components, which in turn reflects considerably higher degrees of partial melting at this locality.

Francis (1978) showed there is a distinct gap in the Nunivak Island suite in terms of the gradational variation in grain size and in the ratio of porphyroclasts vs. neoblasts between xenoliths with coarse equant to tabular textures and those with granuloblastic textures. This gap occurs almost exactly in the position associated with pyroxene lherzolite compositions in the Cordilleran xenolith suites. The NI suite is comparable to the CR suite in that it probably reflects comparatively high degrees of partial melting, resulting in a very minor proportion of pyroxene lherzolite compositions in the extensively depleted lithosphere beneath this locality. The five xenolith suites can therefore be divided into two lithological associations: 1) The JL, FS and PV suites of xenoliths with a limited proportion of harzburgite and a large proportion of lherzolite and pyroxene lherzolite samples (Fig. 2); 2) The CR and NI suites with a much larger proportion of harzburgite, a lesser proportion of still predominant lherzolite and relatively few pyroxene lherzolite samples.

TECTONIC IMPLICATIONS OF THE XENOLITH SAMPLES

The results of many studies suggest that large regions of partial-melt residuum must be present within the earth's upper mantle in addition to less depleted and comparatively

pristine material. Some feel this partial melting occurs within the low velocity zone (LVZ) in the mantle. However, considerable controversy exists as to the variations in upper mantle compositions beneath differing tectonic environments. Carter (1970) maintained that the earth's upper mantle beneath the continents may be composed mainly of residuum material. Ringwood (1975) has also proposed that the uppermost mantle has a dominantly refractory, residual composition. In contrast, Green & Lieberman (1976) presented a model of chemical zonation within the oceanic mantle which predicts that the deeper part of the Low Velocity Zone (LVZ) is depleted in incompatible elements and overlain by an enriched layer, owing to continuous upward migration of a small fraction (< 2%) of melt of olivine melilitite composition. Ave'Lallement et al. (1980) suggested that continental extension zones most closely approximate the "average" oceanic mantle.

Differences in the lithologic association between the Cordilleran and Nunivak Island xenolith suites can be correlated with the regional geological character of the lithosphere at each locality. The JL suite, erupted only 25 km from the most westerly exposed member of the Rocky Mountain thrust belt, has probably sampled the upper mantle beneath a comparatively continental-type crust. A similar conclusion must hold for the FS and PV xenolith suites, which occur within the Omineca Belt, approximately along the Cordilleran strike with the JL suite. All three of these

suites are characterized by a relatively high proportion of pyroxene lherzolite samples. In contrast, the more depleted CR suite, erupted in the Intermontane Belt many kilometers west of any exposed continental basement rocks, may have sampled a lithospheric upper mantle beneath crust that is transitional in character between that of a craton and that of a continental margin. Thus, the contrast between the JL, FS and PV xenolith suites and the CR and NI xenolith suites suggest that the continental lithospheric upper mantle beneath the Omineca Belt is relatively undepleted compared to that beneath the Intermontane Belt further to the west or that beneath Nunivak Island.

Yoder (1978) reviewed two melting models that have reversed sequences of melt composition as a function of depth. In the "hot-subducting-plate" process a invariant-like liquid is constrained to one horizon, whereas in the "diapiric" process, that liquid is spread over a vertical distance of at least 35 km. If these sources are tapped from the top then, in the hot-subducting-plate model, the magma representing the smaller degree of melting will be intruded or extruded first, whereas in the diapiric model the magma representing the greater degree of melting will be first.

Considerable geophysical data are available for southern British Columbia. Blackwell (1969) defined a high heat-flow lineament of up to 90 mW/m2 striking northwest along the northern Rocky Mountains of the United States. He suggested that this thermal anomaly results from localized convection

cells in the deeper mantle. Jessop & Judge (1971) have shown that the thermal anomaly extends into Canada with heat flow of 80 mW/m2 along a line west of and parallel to the Rocky Mountain Trench. Using global heat-flow measurements, Pollack & Chapman (1977) have shown that lithospheric thicknesses show no special transitions at continent-ocean boundaries. The sharp gradients generally occur within the continents themselves and may be correlated with regions of high heat-flow, such as the Cordilleran thermal anomaly zone.

Wickens (1977) presented the results of seismic wave profiles in southern British Columbia. These show a shallow LVZ of 40 to 50 km thickness, capped with a 15 to 20 km crustal lid under the south-central Intermontane Belt. To the east and north the cap is thicker at depths from 20 to 40 km, underlain by a low-seismic-velocity zone from 50 to 70 km thick. The character of the upper-mantle LVZ to the northwest is similar to the mantle structures in the east, suggesting a shift of the deep structure to the west relative to the surficial tectonic trend. Wickens (1977) suggested that these variations could result if a subducting plate was descending beneath the eastern edge of the Coast Crystalline Belt and continued under the Intermontane Belt. The slope implied by the top of the LVZ is about 20 degrees from the horizontal, dipping to the northeast. As this region is relatively aseismic, a plate remnant, if it exists, must be dormant, with only the thermal trace above the much deeper plate being detected (Wickens 1977).

Application of the possible melting models to the Cordilleran and Nunivak Island xenolith localities can be illustrated by their volcanic associations. The JL, FS and PV suites are found in alkali basalt cinder cones that were erupted either on or nearby flat-lying tholeiitic basalt shields of Tertiary age. This, in addition to the lack of geophysical evidence for a subducting plate beneath the Omineca Belt, is consistent with a diapiric model for these three sites. Although the Nunivak Island volcanic rocks are much more voluminous, these consist of tholeiitic basalts, overlain by the xenolith-bearing alkaline basalts. Thus, a diapiric model may be suggested for the NI suite as well. In contrast, the CR suite is associated with the cyclical Mount Edziza volcanic complex, each series of which began with the eruption of primitive alkaline basalt of almost constant composition. This may support either a subducting plate or another model requiring a uniform heat-source that results in the accumulation of a large volume of liquid in a subcrustal reservoir.

Maaloe (1982) has shown that the compositions derived from partial melting will depend on the permeability of the upper mantle source. For the extreme, batch melting involves an increase in degree of partial melting to a permeability threshold followed by magma segregation, whereas fractional melting occurs only if the mantle is permeable at very low degrees of partial melting. Maaloe (1982) proposed that an intermediate type of partial melting, called critical melting,

occurs where the ascending mantle first undergoes batch melting to a certain degree of partial melting that represents the permeability threshold. Beyond this threshold, the magma generated is continuously squeezed out of the residuum and accumulates as horizontal layers of liquid dispersed throughout the melting region.

Although the limited variety of volcanic rocks at the JL, FS, PV and NI localities does not readily support a critical melting model, it may be applied to the CR suite. The large volume of volcanic rocks contained in the Mount Edziza Complex might imply some component of batch melting. This is also supported by the comparative homogeneity of the alkaline basalts that begin each cycle of the Mount Edziza Complex. Accumulation of melt in a large magma chamber may have occurred. In the CR xenolith suite, the products of this accumulation may be reflected by the group 4 samples. In addition, the pyroxene-rich portions of composite samples may represent recrystallized melt as predicted by Maaloe (1982).

Nicholls et al. (1982) suggested that in southern British Columbia the higher temperature ($>1000^{\circ}C$) portions of the mantle were sampled by magmas rising from a topographic high in the low velocity zone. They showed that the primary melts of nephelinite, basanite and alkali olivine basalt composition, from localities throughout British Columbia could be generated by between 4 and 17 % partial melting of pyrolite. Nicholls et al. (1982) propcsed that, although these calculated ranges of partial melting seem appropriate, the range

in residual compositions is too restricted for the xenolith compositions to represent the source material for these basalts. However, a more complete sampling of the Cordilleran xenolith localities does, in fact, correspond to what Nicholls et al. (1982) predicted for mantle residuum. The three Cordilleran xenolith suites, JL, FS and PV, which are characterized by a relatively larger proportion of "fertile" or pyroxene-rich xenolith, occur at isolated cinder cones, with only minor associated basalt flows. In contrast, both the CR and NI suites, with relatively "depleted" xenolith populations are associated with long, voluminous volcanic histories. This suggests the possibility that some correlation exists between the volume of volcanic rocks erupted at each locality and the average degree of depletion due to partial melting in the underlying mantle.

9. CONCLUSIONS

Ultramafic xenoliths are found with alkaline basalt host rocks within the Omineca and Intermontane Belts in the Canadian Cordillera and their equivalents in Alaska. The volcanic centers of the five xenolith suites considered here range from isolated eruptions that produced small cinder cones at Jacques Lake, Fort Selkirk and Prindle Volcano to voluminous centers characterized by either the eruption of a wide range of compositions as at Castle Rock to a bimodal suite of extensive tholeiitic basalt and lesser alkaline basalts as at Nunivak Island. Spinel lherzolite is the predominant lithology among the xenolith suites, with variable but subordinate proportions of harzburgite, olivine websterite, websterite and granulite lithologies.

A regular modal variation is seen in each suite between harzburgite, lherzolite and pyroxene lherzolite groups. The JL and PV suites have a larger proportion of pyroxene-rich xenoliths than do the CR and NI suites, whereas the FS suite is intermediate between these end-members. Cordilleran xenoliths display a continuous textural variation between coarse-grained samples in which the ratio of porphyroclasts to neoblasts is high, to fine-grained lithologies with a much lower ratio. The xenolith mineralogy is dominated by olivine and orthopyroxene, which tend to form porphyroclasts, whereas clinopyroxene is typically smaller in grain size. Spinel displays a variety of habits depending on the xenolith

texture.

All phases are essentially compositionally homogeneous. Olivine and orthopyroxene span a narrow range of major-element compositions. Clinopyroxene shows a wider range in major-element composition, from those rich in the fusible elements Al, Ti and Na of the pyroxene lherzolite samples, concentrations progressively decrease through those of the lherzolite group to those of the harzburgite group which are poor in such elements. Similar minor-element variations are also evident in orthopyroxene, although to a lesser extent. Spinel has a comparatively wide range in major element contents.

Pyroxene geothermometry suggests that most samples have undergone subsolidus re-equilibration, at about 960°C for the JL, CR and NI suites. The temperatures for the FS and PV suites are somewhat lower, suggesting a decrease in the temperature range sampled along the strike from southeast to northwest in the Cordillera. Little evidence is present for any correlation between the fusible element contents of the samples and their temperatures, except perhaps for the CR suite. Group 4 samples on the other hand have temperatures that approximate magmatic conditions. The xenolith samples appear to represent the range of the spinel stability field, with lower pressures characterized by the presence of abundant plagioclase lherzolites and fine-grained textures in the PV and CR suites, and higher pressures for the JL suite suggested by the occurrence of "holly-leaf" spinel

textures, coarse-grained textures and high Na contents.

The Nunivak Island suite is characterized by higher modal proportions of olivine- and orthopyroxene-rich lithologies, a comparative absence of pyroxene-rich lithologies and the presence of abundant amphibole, mica and fine-grained zones. Although the range of major-element contents for all four phases are similar to that in the Cordilleran samples, the minor-element contents support the addition of a metasomatic component, rich in some fusible elements. The NI suite is distinguished by the abundant evidence of metasomatically added hydrous phases compared to the four Cordilleran suites which are practically anhydrous.

Whereas the concentrations of Ca and Al reflect the modal proportion of pyroxene, the concentrations of Na, Ti and Cr are not strictly related to the pyroxene modes in the xenolith samples. The continuous depletion of both Na and Ti in the transition from pyroxene lherzolite to lherzolite is followed by comparatively smaller degrees of depletion in the transition from lherzolite to harzburgite, despite the continued decrease in modal clinopyroxene. A similar distribution is seen for the compatible element Cr, the harzburgite bulk compositions are the most Cr-poor, despite the concentration of Cr in the group 1 mineral compositions. This progressive depletion of the fusible elements, in the sequence pyroxene lherzolite to lherzolite to harzburgite, reflects an increase in the degree of melting these xenoliths represent. The transition from lherzolite to harzburgite

occurs at about 6 modal % clinopyroxene and marks the degree of depletion associated with the effective disappearance of clinopyroxene.

The harzburgite, lherzolite and pyroxene lherzolite xenolith groups from the five suites define a curved trend in Mg-Fe space which approximates an isotherm in the residual field of pyrolite. The NI samples follow the same trend, despite the metasomatism that they have experienced. The distribution of samples along this trend shows a common process in which the degree of partial melting increases from $<15\%$ in the pyroxene lherzolite group through the lherzolite group to $>25\%$ in the harzburgite group.

The principal differences between the xenolith suites lie in the average degree of depletion which characterizes each suite. The close similarity in the compositions of the pyroxene lherzolite samples and that of pyrolite-1 suggests that this xenolith group may approximate anhydrous undepleted upper mantle that is present in some proportion beneath each of the sample localities. The xenoliths of the lherzolite and harzburgite groups can be related by increasing degrees of partial melting of parental compositions that are approximately equivalent to the pyroxene lherzolite group. Thus, these three sample groups represent mantle compositions that are comparatively fertile, depleted and barren, respectively.

Variations in the composition of the lithospheric upper mantle are clearly reflected in the range and relative proportions of the individual groups of xenoliths at each

locality. The PV, FS and JL suites, characterized by a high proportion of pyroxene lherzolite samples, sampled the relatively undepleted upper mantle beneath a comparatively continental-type crust. The distinctly different populations at PV and CR suggest that the CR mantle has been more extensively depleted in fusible elements, which in turn reflects considerably higher degrees of partial melting at this locality. The absence of hydrous phases suggests that the levels of the Cordilleran upper mantle sampled are anhydrous over a large area. The NI suite is comparable to the CR suite in that it reflects comparatively high degrees of partial melting, resulting in a very minor proportion of pyroxene lherzolite compositions in the extensively depleted lithosphere beneath this locality.

The results of this study suggest several avenues for further work. Although the majority of xenolith suites throughout this region appear to be comparable to the anhydrous Cordilleran samples, a similar suite to that of NI may be present at Alligator Lake, Yukon (C. Bacon, pers. comm. 1982) and also perhaps at the Mud Hills of southwestern Alaska, not far from NI. These localities should be the principal targets of any further field-oriented studies. In addition, the relationship between the lherzolite and granulite samples in those suites in which the latter are well represented could essentially provide a stratigraphic section of the upper lithosphere at these localities. Finally, there appears to be some relationship between the average degree

of depletion of the xenolith suites and the volume of volcanic products erupted at each suite. Such a relationship conflicts with most prevailing models of ultramafic xenolith paragenesis, and should therefore be evaluated.

REFERENCES CITED

Albee, A. L. and L. Ray (1970) Correction factors for electron probe and microanalysis of silicates, carbonates, phosphates and sulphates. Anal. Chem., v. 42, p. 1408-1414.

Atwater, T. (1970) Implications of plate tectonics for the Cenozoic tectonic evolution of western North America. Geol. Soc. Amer., Bull., v. 81, p. 3513-3536.

Ave'Lallement, H. G., J. C. C. Mercier, N. L. Carter and J. V. Ross (1980) Rheology of the upper mantle: Inferences from peridotite xenoliths. Tectonophysics, v. 70, p. 85-113.

Basu, A. R. (1975) Petrogenesis of the ultramafic xenoliths from San Quintin volcanic field, Baja California. Ph.D. thesis, Univ. Calif., Davis. 227 pp.

Basu, A. R. (1977) Textures, microstructures and deformation of ultramafic xenoliths from San Quintin, Baja California. Tectonophysics, v. 43, p. 213-246.

Bell, P. M. and B. T. C. Davis (1965) Temperature - Composition section for jadeite - diopside. Carnegie Inst. Wash. Yearbook, v. 64, p. 120-123.

Bell, P. M. and B. T. C. Davis (1967) Investigation of a solvus in the system jadeite - diopside. Carnegie Inst. Wash. Yearbook, v. 65, p. 239-241.

Bence, A. E. and A. L. Albee (1968) Empirical correction factors for the electron microanalysis of silicates and oxides. Jour. Geology, v. 76, p. 382-403.

Bevier, M. L., R. L. Armstrong and J. G. Souther (1979) Miocene peralkaline volcanism in west-central British Columbia - Its temporal and plate-tectonics setting. Geology, v. 7, p. 389-392.

Blackwell, D. D. (1969) Heat-flow determinations in the northwestern United States. Jour. Geophys. Res., v. 74, p. 992-1007.

Boettcher, A. L. and J. R. O'Neil (1980) Stable isotope, chemical, and petrographic studies of high-pressure amphiboles and micas: evidence for metasomatism in the mantle source region of alkali basalts and kimberlites. Am. Jour. Sci., v. 280-A, p. 594-621.

Bostock, H. S. (1936) Carmacks district, Yukon. Geol. Survey Canada, Memoir 189, 67 pp.

Brearley, M. T., T. Fujii and C. M. Scarfe (1982) The petrology and geochemistry of ultramafic nodules from Summit Lake, near Prince George, British Columbia. Geol. Assoc. Canada - Mineral. Assoc. Canada, Program Abstr., v. 7, p. 40.

Brown, G. M., R. H. Pinsent and P. Coisy (1980) The petrology of spinel - peridotite xenoliths from the Massif Central, France. Amer. Jour. Sci., v. 280-A, p. 471-498.

Burns, R. G. (1973) The partitioning of trace transition elements in crystal structures: a provocative review with application to mantle geochemistry. Geochim. Cosmochim. Acta, v. 37, p. 2395-2403.

Cameron, M. and J. J. Papike (1981) Structural and chemical variations in pyroxenes. Amer. Mineral., v. 66, p. 1-50.

Campbell, R. B. (1961) Geology of Quesnel Lake (west half), British Columbia. Geol. Survey Canada, Map 3-1961.

Caner, B. (1970) Electrical conductivity structure in western Canada and petrological interpretation. Jour. Geomagnetism and Geoelectricity, v. 22, p. 113-129.

Carswell, D. A. (1980) Mantle derived lherzolite nodules associated with kimberlite, carbonatite and basalt magmatism: A review. Lithos, v. 13, p. 121-138.

Carter, J. L. (1970) Mineralogy and chemistry of the Earth's upper mantle based on the partial fusion - partial crystallization model. Geol. Soc. Amer. Bull., v. 81, p. 2021-2034.

Carter, N. L. and H. G. Ave'Lallemant (1970) High-temperature flow of dunite and peridotite. Geol. Soc. Amer. Bull., v. 81, p. 2181-2202.

Churkin, M., Jr., C. Carter and J. H. Trexler, Jr. (1980) Collision-deformed Paleozoic continental margin of Alaska - Foundation for microplate accretion. Geol. Soc. Amer. Bull., Part 1, v. 91, p. 648-654.

Danckwerth, P. A. and R. C. Newton (1978) Experimental determination of the spinel peridotite to garnet peridotite reaction in the system MgO-Al_2O_3-SiO_2 in the range 900 - 1100°C and Al_2O_3 isopleths of enstatite in the spinel field. Contrib. Mineral. Petrol., v. 66, p. 189-201.

Davis, B. T. C. and F. R. Boyd (1966) The join $Mg_2Si_2O_6$-$CaMgSi_2O_6$ at 30 kilobars pressure and its application to pyroxenes from kimberlites. Jour. Geophys. Res., v. 71, p. 3567-3576.

Deer, W. A., R. A. Howie and J. Zussman (1978) Rock-Forming Minerals, Vol. 2A, second edition, Single-Chain Silicates. New York: John Wiley.

Fiesinger, D. W. and J. Nicholls (1977) Petrography and Petrology of Quaternary Volcanic Rocks, Quesnel Lake Region, East-Central British Columbia. In: Baragar, W. R. A., L. C. Coleman and J. M. Hall (eds.), Volcanic Regimes in Canada. Geol. Assoc. Canada Spec., Paper 16: p. 25-38.

Foster, H. L. (1970) Reconnaissance geologic map of the Tanacross quadrangle, Alaska. U. S. Geol. Survey, Misc. Geologic Investigations Map I-593.

Foster, H. L., R. B. Forbes and D. M. Ragan (1966) Granulite and peridotite inclusions from Prindle Volcano, Yukon-Tanana Upland, Alaska. U. S. Geol. Survey Prof. Paper 550-B, p. B115-B119.

Francis, D. M. (1974) Xenoliths and the nature of the upper mantle and lower crust. Ph.D. thesis, Mass. Inst. Tech., 236 pp.

Francis, D. M. (1976a) The origin of amphibole in lherzolite xenoliths from Nunivak Island, Alaska. Jour. Petrol., v. 17, p. 357-378.

Francis, D. M. (1976b) Corona bearing pyroxene granulite xenoliths and the lower crust beneath Nunivak Island, Alaska. Can. Mineralogist, v. 14, p. 291-198.

Francis, D. M. (1976c) Amphibole pyroxenite xenoliths: cumulate or replacement phenomena from the upper mantle, Nunivak Island, Alaska. Contrib. Mineral. Petrol., v. 58, p. 51-61.

Francis, D. M. (1978) The implications of the compositional dependence of texture in spinel lherzolite xenoliths. Jour. Geology, v. 86, p. 473-485.

Frey, F. A. and D. H. Green (1974) The mineralogy, geochemistry and origin of lherzolite inclusions in Victorian basanites. Geochim. Cosmochim. Acta, v. 38, p. 1023-1059.

Frey, F. A. and M. Prinz (1978) Ultramafic inclusions from San Carlos, Arizona: Petrologic and geochemical data bearing on their petrogenesis. Earth Planet. Sci. Letters, v. 38, p. 129-176.

Fujii, T. and C. M. Scarfe (1981) Petrology of ultramafic nodules from Boss Mountain, central British Columbia. Geol. Assoc. Canada - Mineral. Assoc. Canada Joint Annual Meeting, Calgary. Abs., p. A-20.

Fujii, T. and C. M. Scarfe (1982) Equilibrium experiments on natural peridotite and basalt: A recalibration of the olivine-spinel geothermometer. Trans. Amer. Geophys. Union, Abs., v. 63, p. 471.

Fujii, T., C. M. Scarfe and T. S. Hamilton (1981) Geochemistry of ultramafic nodules from southern British Columbia: Evidence for banding in the upper mantle. Geol. Assoc. Canada - Mineral. Assoc. Canada Joint Annual Meeting, Calgary. Abs., p. A-20.

Ganguly, J. and S. Ghose (1979) Aluminous orthopyroxene: order-disorder, thermodynamic properties and petrologic implications. Contrib. Mineral. Petrol., v. 69, p. 375-385.

Green, D. H. and R. C. Lieberman (1976) Phase equilibria and elastic properties of a pyrolite model for the oceanic upper mantle. Tectonophysics, v. 32, p. 61-92.

Hamilton, T. S. and C. M. Scarfe (1982) Lava viscosities and nodule transport at Level Mountain, Northern British Columbia. Geol. Assoc. Canada - Mineral. Assoc. Canada Joint Annual Meeting, Winnipeg. Abs., p. 54.

Hanson, G. N. and C. H. Langmuir (1978) Modelling of major elements in mantle-melt systems using trace element approaches. Geochim. et Cosmochim. Acta, v. 42, p. 725-741.

Harte, B. (1977) Rock nomenclature with particular relation to deformation and recrystallization textures in olivine-bearing xenoliths. Jour. Geology, v. 85, p. 279-288.

Hervig, R. L. and J. V. Smith (1980) Sodium thermometer for pyroxenes in garnet and spinel lherzolites. Jour. Geol., v. 88, p. 337-342.

Herzberg, C. T. (1978) Pyroxene geothermometry and geobarometry: Experimental and thermodynamic evaluation of some subsolidus phase relations involving pyroxenes in the system CaO-MgO-Al_2O_3-SiO_2. Geochim. Cosmochim. Acta, v. 42, p. 945-957.

Hoare, J. M., W. H. Condon, A. Cox and G. B. Dalrymple (1968) Geology, paleomagnetism and potassium-argon ages of basalts from Nunivak Island, Alaska. Geol. Soc. Amer. Memoir 116, p. 377-412.

Irving, A. J. (1980) Petrology and geochemistry of composite ultramafic xenoliths in alkalic basalt and implications for magmatic processes within the mantle. Amer. Jour. Sci., v. 280-A, p. 389-426.

Jackson, E. D. (1969) Chemical variation in coexisting chromite and olivine in the chromitite zones of the Stillwater complex. Econ. Geol. Mon., v. 4, p. 41-71.

Jacques, A. L. and D. H. Green (1980) Anhydrous melting of peridotite at 0-15 Kb pressure and the genesis of tholeiitic basalts. Contrib. Mineral. Petrol., v. 73, p. 287-310.

Jenkins, D. M. and R. C. Newton (1970) Experimental determination of the spinel peridotite to garnet peridotite inversion at 900°C and 1000°C in the system CaO-MgO-Al_2O_3-SiO_2, and at 900°C with natural garnet and olivine. Contrib. Mineral. Petrol., v. 68, p. 407-419.

Jessop, A. M. and A. S. Judge (1971) Five measurements of heat flow in southern Canada. Can. Jour. Earth Sci., v. 8, p. 711-716.

Kuno, H. (1969) Mafic and ultramafic nodules in basaltic rocks of Hawaii. Geol. Soc. Amer., Memoir 115, p. 189-234.

Kushiro, I. (1969) The system forsterite-diopside-silica with and without water at high pressures. Amer. Jour. Sci., v. 267A, p. 269-294.

Langmuir, C. H. and G. N. Hanson (1980) An evaluation of major element heterogeneity in the mantle sources of basalts. Phil. Trans. R. Soc. Lond. A, v. 297, p. 383-407.

Lindsley, D. H. and S. A. Dixon (1976) Diopside-enstatite equilibria at 850 to 1400°C, 5 to 35 kb. Amer. Jour. Sci., v. 276, p. 1285-1301.

Littlejohn, A. L. and H. J. Greenwood (1974) Lherzolite nodules in basalts from British Columbia, Canada. Can. Jour. Earth Sci., v. 11, p. 1288-1308.

Maaloe, S. (1982) Geochemical aspects of permeability controlled partial melting and fractional crystallization. Geochim. Cosmochim. Acta, v. 46, p. 43-57.

Maaloe, S. and K. I. Aoki (1977) The major element composition of the upper mantle estimated from the composition of lherzolites. Contrib. Mineral. Petrol., v. 63, p. 161-173.

Mark, R. K. (1971) Strontium isotopic study of basalts from Nunivak Island, Alaska. Ph.D. thesis, Stanford University, 50 pp.

Menzies, M. A. and V. R. Murthy (1980) Nd and Sr isotope geochemistry of hydrous mantle nodules and their host alkali basalts: implications for local heterogeneities in metasomatically veined mantle. Earth Planet. Sci. Lett., v. 46, p. 323-334.

Mercier, J. and A. Nicolas (1976) Textures and fabrics of upper mantle peridotites as illustrated by xenoliths from basalts. J. Petrol., v. 16, p. 454-487.

Mertie, J. B., Jr. (1931) A geologic reconnaissance of the Dennison Fork district, Alaska. U. S. Geol. Survey Bull. 827, 44 pp.

Mertie, J. B., Jr. (1937) The Yukon-Tanana region, Alaska. U. S. Geol. Survey Bull. 872, 276 pp.

Mori, T. and D. H. Green (1975) Pyroxenes in the system $MgSi_2O_6$-$CaMgSi_2O_6$ at high pressure. Earth Planet. Sci. Lett., v. 26, p. 277-286.

Mysen, B. O. and A. L. Boettcher (1975) Melting of a hydrous mantle: I. Phase relations of natural peridotite at high pressures and temperatures with controlled activities of water, carbon dioxide and hydrogen. Jour. Petrol., v. 16, p. 520-548.

Mysen, B. O. and I. Kushiro (1977) Compositional variations of coexisting phases with degree of melting of peridotite in the upper mantle. Amer. Mineral., v. 62, p. 843-855.

Nicholls, J., M. Z. Stout and D. W. Fiesinger (1982) Petrologic variations in quaternary volcanic rocks, British Columbia, and the nature of the underlying upper mantle. Contrib. Mineral. Petrol., v. 79, p. 201-218.

Obata, M. (1976) The solubility of Al_2O_3 in orthopyroxenes in spinel and plagioclase peridotites and spinel pyroxenite. Amer. Mineral., v. 61, p. 804-816.

O'Hara, M. J. (1967) Mineral paragenesis in ultrabasic rocks. In: Ultramafic and related rocks (P. J. Wyllie, ed.) p. 393-402. New York: John Wiley.

O'Neill, H. St. C. (1981) The transition between spinel lherzolite and garnet lherzolite, and its use as a geobarometer. Contrib. Mineral. Petrol., v. 77, p. 185-194.

Pollack, H. N. and D. S. Chapman (1977) On the regional variation of heat flow, geotherms, and lithospheric thickness. Tectonophys., v. 38, p. 279-296.

Presnall, D. C. (1969) The geometrical analysis of partial fusion. Amer. Jour. Sci., v. 267, p. 1178-1194.

Presnall, D. C., J. R. Dixon, T. H. O'Donnell and S. A. Dixon (1979) Generation of mid ocean ridge tholeiites. Jour. Petrol., v. 20, p. 3-35.

Ranalli, G. (1980) Rheological properties of the upper mantle in Canada from olivine microrheology. Can. Jour. Earth Sci., v. 17, p. 1499-1505.

Rao, R. U. M. and A. M. Jessop (1975) A comparison of the thermal character of shields. Can. Jour. Earth Sci., v. 12, p. 347-360.

Reid, A. M. and J. B. Dawson (1972) Olivine-garnet reaction in peridotites from Tanzania. Lithos, v. 5, p. 115-124.

Rhodes, J. M. and J. B. Dawson (1975) Major and trace element chemistry of peridotite inclusions from the Lashaine Volcano, Tanzania. Phys. Chem. Earth, v. 9, p. 545-557.

Ringwood, A. E. (1966) The chemical composition and origin of the earth. In: Hurley, P. M. (ed.) Advances in Earth Science, Mass. Inst. Tech. Press, Cambridge, p. 287-356.

Ringwood, A. E. (1975) Composition and petrology of the earth's mantle. McGraw-Hill, Inc., New York, 618 pp.

Roden, M. F. (1982) Geochemistry of the earth's mantle, Nunivak Island, Alaska and other areas: Evidence from xenolith studies. Ph.D. thesis, Mass. Inst. Tech., 408 pp.

Roeder, P. L., I. H. Campbell and H. E. Jamieson (1979) A re-evaluation of the olivine-spinel geothermometer. Contrib. Mineral. Petrol., v. 68, p. 325-334.

Scarfe, C. M., B. O. Mysen and C. S. Rai (1979) Invariant melting behavior of mantle material: partial melting of two lherzolite nodules. Yearb. Carnegie Inst. Wash., v. 78, p. 498-501.

Scarfe, C. M., T. Fujii and M. Brearley (1982) Heterogeneities in the upper mantle beneath south and central British Columbia. EOS, (abs.) v. 18, p. 463.

Sinclair, P. D., D. J. Templeman-Kluit and L. G. Medaris, Jr. (1978) Lherzolite nodules from a Pleistocene cinder cone in central Yukon. Can. Jour. Earth Sci., v. 15, p. 220-226.

Smith, D. (1977) The origin and interpretation of pyroxene-spinel clusters in peridotite. Jour. Geol., v. 85, p. 476-482.

Souther, J. G. (1971) Telegraph Creek Map Area, British Columbia. Geol. Survey Canada Paper 71-44, 38 pp.

Souther, J. G. (1977) Volcanism and tectonic environments in the Canadian Cordillera - a second look. In Baragar, W. R. A., L. C. Coleman and J. M. Hall eds., Volcanic regimes in Canada. Geol. Soc. Canada Spec. Paper 16, p. 3-24.

Souther, J. G. and D. T. A. Symons (1974) Stratigraphy and paleomagnetism of the Mount Edziza volcanic complex, northwestern British Columbia. Geol. Survey Canada, Paper 73-32.

Stephens, W. E. and J. B. Dawson (1977) Statistical comparison between pyroxenes from kimberlites and their associated xenoliths. Jour. Geol., v. 85, p. 433-449.

Stosch, H. G. (1981) Sc, Cr, Co and Ni partitioning between minerals from spinel peridotite xenoliths. Contrib. Mineral. Petrol., v. 78, p. 166-174.

Streckeisen, A. (1976) To each plutonic rock its proper name. Earth Sci. Rev., v. 12, p. 1-33.

Takahashi, E. (1978) Petrologic model of the crust and upper mantle of the Japanese island arcs. Bull. Volcanol., v. 41-4, p. 529-547.

Templeman-Kluit, D. J. (1979) Transported cataclastite, ophiolite and granodiorite in Yukon: evidence of arc-continent collision. Geol. Survey Canada, Paper 79-14, 27 pp.

Templeman-Kluit, D. J. (1980) Evolution of physiography and drainage in southern Yukon. Can. Jour. Earth Sci., v. 17, p. 1189-1203.

Tipper, H. W., R. B. Campbell, G. C. Taylor and D. F. Stott (1974) Parsnip River, British Columbia. Geol. Survey Canada, Map 1424A.

Tipper, H. W., G. J. Woodsworth and H. Gabrielse (1981) Tectonic Assemblage Map of the Canadian Cordillera and adjacent parts of the United States of America. Geol. Survey Canada Map 1505A.

Wagner, L. R. and G. M. Brown (1966) Layered Igneous Rocks, W. H. Freeman, San Francisco, 588 pp.

Wass, S. Y. (1979) Geochemistry and origin of xenolith-bearing alkali basaltic rocks from the Southern Highlands, N.S.W., Australia. Amer. Jour. Sci., v. 280-A, p. 639-666.

Wass, S. Y. (1980) Mantle metasomatism-precursor to continental alkaline volcanism. Geochim. Cosmochim. Acta, v. 44, p. 1811-1823.

Wells, P. R. A. (1977) Pyroxene geothermometry in simple and complex systems. Contrib. Mineral. Petrol., v. 62, p. 129-139.

Wickens, A. J. (1977) The upper mantle of southern British Columbia. Can. Jour. Earth Sci., v. 14, p. 1100-1115.

Wood, B. J. (1976) Mixing properties of tschermakitic clinopyroxenes. Amer. Mineral., v. 61, p. 599-602.

Wood, B. J. and S. Banno (1973) Garnet-orthopyroxene and orthopyroxene-clinopyroxene relationships in simple and complex systems. Contrib. Mineral. Petrol., v. 42, p. 109-124.

Yoder, H. S., Jr. (1976) Generation of Basaltic Magma. National Acad. Sci., Wash., D.C., 265 pp.

Yoder, H. S., Jr. (1978) Basic Magma Generation and Aggregation. Bull. Volcan., v. 41, p. 301-316.

APPENDIX 1: MODAL PROPORTIONS OF ULTRAMAFIC XENOLITHS

SAMPLE NUMBER	ROCK TYPE	CLASS	OLV	OPX	CPX	SP	AMPH	MICA	FINE GR ZONES	POINTS COUNTED
JACQUES LAKE, BRITISH COLUMBIA										
50001*	Harz	4-PCR	56.6*	36.4*	4.0*	0.3*	-	-	2.8	1508
50002	Sp Lherz	2-MP	70.6	16.5	9.8	1.8	-	-	1.2	2526
50003	Sp Lherz	3-P/MP	59.1	21.5	18.0	0.5	-	-	0.9	1467
50004	Gabbro									
50005*	Sp Lherz	2-PCR	64.1*	24.1*	10.4*	1.5*	-	-	tr.	2263
50006*	Olv Webst	3-P/MP	34.2*	38.6*	21.1*	6.2*	-	-	-	2097
50007	Olv Webst	3-P/MP	39.8	47.1	10.2	3.0	-	-	tr	1761
50008	Sp Lherz	2-MP	62.0	23.9*	12.0*	2.0*	-	-	-	2650
50009*	Sp Lherz	3-P/MP	50.4*	26.9*	20.6*	2.0*	-	-	-	3015
50010	Sp Lherz	2-P/MP	60.3	25.2	13.4	1.0	-	-	-	1276
50011*	Sp Lherz	2-P/MP	67.0*	22.2*	8.0*	1.6*	-	-	1.2	2257
50012	Sp Lherz	2-C/P	60.3	30.3	8.0	1.4	-	-	-	2244
50013	Sp Lherz	3-MP	53.7	31.0	12.9	2.0	-	-	0.3	2341
50014	Sp Lherz	2-P/MP	60.5	28.2	7.4	1.9	-	-	1.9	3898
50015*	Harz	1-CR	87.9*	10.3*	1.4*	0.3*	-	-	-	4010
50016	Sp Lherz	2-C/P	66.7	21.3	10.7	1.1	-	-	tr	4034
50017	Sp Lherz	3-MP	54.8	33.5	9.6	2.1	-	-	-	2784
50018	Webst	4-PCR	8.6	45.9	42.2	3.0	-	-	0.3	4175
50019	Sp Lherz	4-P/MP	71.1	15.5*	11.9*	1.4*	-	-	0.2	4240
50020	Olv Webst	3-P/MP	40.5	33.0	22.1	4.4	-	-	-	3041
JL average mode			56.5	28.1	13.4	2.0				
CASTLE ROCK, BRITISH COLUMBIA										
40001	Sp Lherz	4-P/MP	68.0	16.8	11.7*	1.2*	-	-	2.3	2850
40002	Harz	2-MP	69.6	24.8	3.6	1.8	-	-	0.3	2589
40003*	Harz	1-C/P	82.8*	13.9*	2.3*	0.9*	-	-	tr	2404
40004	Composite, Spinel lherzolite and Ti-augite websterite									
40005	Harz	2-C/P	70.5	27.7	1.9	-	-	-	-	1819
40006	Sp Lherz	3-MP	58.4	25.2	14.4	2.1	-	-	-	3463
40007	Sp Lherz	2-P/MP	63.0	22.2	12.7	2.1	-	-	tr	2545
40008	Sp Lherz	2-MP	61.4	26.3	10.2	1.9	-	-	0.2	2400
40009	Sp Lherz	2-MP	62.6	27.3	8.2	1.9	-	-	-	2553
40010*	Sp Lherz	3-MP/G	55.2*	24.9*	15.7*	3.1*	-	-	1.1	1492
40011	Sp Lherz	2-P/MP	60.5	23.1	14.6	1.8	-	-	-	2091
40012	Harz	2-P/MP	69.3	24.1	4.7	1.2	-	-	0.7	2538
40013	Sp Lherz	2-MP/G	69.5	22.1	5.9	1.4	-	-	1.1	3248
40014	Sp Lherz	2-MP	63.0	20.8	14.5	1.4	-	-	0.4	2629
40015*	Harz	1-PCR	76.1*	18.3*	4.4*	1.1*	-	-	tr	2225
40016	Harzburgite, inhomogeneous									
40017*	Harz	2-GR	66.5*	27.8*	5.1*	0.6*	-	-	tr	2054
40018	Sp Lherz	2-MP/G	65.3	26.3	7.0*	1.5*	-	-	tr	1576

SAMPLE NUMBER	ROCK TYPE	CLASS	OLV	OPX	CPX	SP	AMPH	MICA	FINE GR ZONES	POINTS COUNTED
CASTLE ROCK, BRITISH COLUMBIA										
40019	Sp Lherz	1-C/P	83.2	10.7	5.6	0.5	-	-	-	2437
40020	Sp Lherz	2-MP	60.5	28.2	9.4*	1.9*	-	-	tr	2480
40021	Spinel Lherzolite, pyroxene-rich banding									
40022	Composite, Spinel Lherzolite and Websterite									
40023	Harz	1-POR	81.0	17.2	1.3	0.4	-	-	-	2271
40024	Sp Lherz	2-MP	67.2	21.9	8.7	2.1	-	-	-	2290
40025	Sp Lherz	2-MP	60.9	31.5	7.1	0.5	-	-	-	1613
40026	Sp Lherz	2-P/MP	67.7	18.9	12.7	0.8	-	-	-	2055
40027	Sp Lherz	3-POR	59.0	26.4	11.8	2.9	-	-	-	2399
40028	Sp Lherz	3-P/MP	58.7	28.1	11.9	1.4	-	-	-	2951
40029	Sp Lherz	2-P/MP	67.2	21.2	9.6	2.0	-	-	tr	3867
40030*	Sp Lherz	4-P/MP	67.0*	18.9*	13.4*	0.8*	-	-	-	2762
40031	Sp Lherz	2	68.7	23.0	6.4	1.2	-	-	0.7	1850
40032	Sp Lherz	2-MP	64.6	23.3	10.0	2.0	-	-	tr	2848
40033	Sp Lherz	3-MP	59.9	30.4	7.6	1.4	-	-	0.7	2484
40034	Harz	2-CP	71.8	25.2	1.6	1.2	-	-	0.2	2639
40035	Sp Lherz	2-P/MP	65.9	24.0	8.2	1.6	-	-	0.3	2168
40036	Sp Lherz	2-MP	60.1	28.5	8.7	1.8	-	-	0.9	2541
40037*	Sp Lherz	4-C/P	57.0*	28.2*	13.2*	1.6*	-	-	-	2916
40038	Sp Lherz	2	64.1	26.0	7.7	2.2	-	-	-	2463
40039	Composite, Spinel Lherzolite and Websterite									
40040	Sp Lherz	2-P/MP	61.9	29.6	6.8	1.4	-	-	0.3	2784
40041	Sp Lherz	2-P/MP	64.5	22.7	11.6	1.1	-	-	tr	2730
40042	Sp Lherz	2-P/MP	63.2	26.4	8.7	1.5	-	-	0.2	2652
40043	Harz	2-P/MP	67.7	26.5	5.1	0.6	-	-	-	2511
40044*	Harz	1-C/P	85.9*	9.6*	4.0*	0.3*	-	-	tr	2938
40045	Sp Lherz	2-MP	60.5	25.5	11.4	2.6	-	-	-	2700
40046	Harz	1-MP	75.8	18.5	4.1*	1.3*	-	-	0.2	2414
40047	Cpxenite	4	3.4	19.5	76.9	0.1	-	-	0.1	2341
40048	Webst	4	27.1	18.6	45.9	7.5	-	tr.	0.9	2373
40049	Webst	4	18.1	39.7	42.2	-	-	-	-	2719
40050	Harz	1-POR	79.0	18.6	1.3	1.1	-	-	-	2254
40051	Harz	2-MP	68.6	25.6	4.4	1.3	-	-	0.1	2715
40052	Sp Lherz	2-MP	73.8	16.0	7.6	0.9	-	-	1.6	2551
40053	Sp Lherz	2-MP	62.4	23.3	13.4	0.7	-	-	tr	2457
40054	Sp Lherz	2-MP	62.6	24.7*	10.5*	1.8*	-	-	0.4	2388
40055	Harz	4-POR	72.0*	24.5	2.9*	0.4*	-	-	0.1	2725
40056	Harz	1-C/P	77.8	20.2	1.1	0.5	-	-	0.3	2419
40057	Harz	2-POR	71.4	24.9	2.8	0.8	-	-	-	2258
40058	Spinel Lherzolite, inhomogeneous									
40059	Sp Lherz	2-MP	61.8	21.8	14.0	2.4	-	-	-	2514
40060	Sp Lherz	3-MP	59.7	30.9	7.6*	1.6*	-	-	0.1	2319
40061*	Sp Lherz	2-P/MP	75.8*	16.6*	5.8*	1.7*	-	-	-	2459
40062	Spinel Lherzolite, inhomogeneous									
40063	Sp Lherz	2-MP	62.6	25.4	9.3	2.7	-	-	-	2562
40064	Spinel Lherzolite, pyroxene + spinel banding									

SAMPLE NUMBER	ROCK TYPE	CLASS	OLV	OPX	CPX	SP	AMPH	MICA	FINE GR ZONES	POINTS COUNTED
CASTLE ROCK, BRITISH COLUMBIA										
40065	Sp Lherz	2-P/MP	60.5	25.9	11.0	2.7	-	-	-	1879
40066	Harzburgite, inhomogeneous									
40067	Sp Lherz	3-PCR	57.2	27.1	13.5	2.1	-	-	-	2770
40068	Sp Lherz	3-MP	58.0	27.7	12.3	1.9	-	-	tr	2589
40069	Plagioclase Lherzolite									
40070	Gabbro									
CR average mode			64.2	23.7	10.6	1.5				
FORT SELKIRK, YUKON										
30001	Harz	2-CE	71.0	23.3	2.6	2.4	-	-	0.8	3565
30002	Sp Lherz	2-P/MP	70.0	10.8	16.4	2.4	-	-	0.8	2019
30003	Sp Lherz	2-PCR	66.4	21.2*	9.2*	3.0*	-	-	0.2	3213
30004	Sp Lherz	3-PCR	56.2	30.3	12.0	1.2	-	-	0.2	2848
30005	Sp Lherz	3-PCR	59.8	30.9	7.0	2.3	-	-	tr	2940
30006*	Sp Lherz	2-C/P	65.4*	26.3*	6.8*	1.4*	-	-	0.2	2524
30007	Sp Lherz	2-PCR	60.7	23.1	11.0	3.1	-	-	2.1	2798
30008*	Sp Lherz	1-CE	79.8*	14.3*	5.5*	0.3*	-	-	tr	1464
30009	Harz	2-CE	73.4	20.1	5.0	0.1	-	-	1.3	2159
30010	Sp Lherz	3-MP	49.8	22.0	25.5	2.0	-	-	0.8	3273
30011	Harz	2-PCR	68.8	26.2	3.5	1.4	-	-	-	3327
30012*	Sp Lherz	3-PCR	47.0*	27.7*	22.7*	2.3*	-	-	0.2	2651
30013	Sp Lherz	2-P/MP	63.9	24.9	8.9	2.4	-	-	tr	2971
30014	Sp Lherz	2-P/MP	62.8	25.3	9.6	2.3	-	-	-	2690
30015	Sp Lherz	3-MP	56.5	26.3	12.2*	2.9*	-	-	2.0	4115
30016	Sp Lherz	2-P/MP	63.3	21.6	12.8	2.1	-	-	-	2441
30017	Sp Lherz	3-PCR	58.3	29.9	9.3	2.2	-	-	0.3	4684
30018	Sp Lherz	2-PCR	63.4	26.2	6.9	3.4	-	-	0.2	3223
30019	Sp Lherz	2-PCR	65.2	22.4	10.2	2.1	-	-	0.1	2934
30020*	Sp Lherz	2-C/P	74.3*	14.2*	9.6*	1.2*	-	-	0.7	2964
30021	Spinel Lherzolite, inhomogeneous									
30022*	Olv Websterite	3-PCR	39.3*	28.8*	25.3*	5.1*	-	-	1.5	5189
30023	Spinel Lherzolite, abundant fine grained melt zones									
30024	Spinel Lherzolite, extensive secondary alteration									
30025	Sp Lherz	1-CE	78.9	14.0	5.5	0.8	-	-	0.8	2785
30026	Sp Lherz	3-PCR	57.5	25.9	15.0	1.5	-	-	0.1	4150
30027	Sp Lherz	2-PCR	62.1	19.5	17.3	1.0	-	-	tr	4148
30028	Sp Lherz	3-C/P	57.4	34.4*	6.1*	2.0*	-	-	tr	3500
30029	Spinel Lherzolite, small, coarse grained sample									
30030	Sp Lherz	2-C/P	70.3	19.7	7.2	1.9	-	-	0.9	3079
30031	Sp Lherz	3-PCR	58.3	32.5	7.7	1.3	-	-	0.2	3271
30032	Sp Lherz	1-C/P	75.5	17.3	5.8	1.0	-	-	0.3	3149
30033	Sp Lherz	3-PCR	49.5	35.1	13.5	1.5	-	-	0.5	3851
30034	Sp Lherz	3-PCR	58.0	25.7	13.7	2.5	-	-	0.2	3537

SAMPLE NUMBER	ROCK TYPE	CLASS	OLV	OPX	CPX	SP	AMPH	MICA	FINE GR ZONES	POINTS COUNTED
FORT SELKIRK, YUKON										
30035	Sp Lherz	2-C/P	68.4	20.7	8.9	0.8	-	-	1.2	4027
FS average mode			63.3	24.0	10.8	1.9				
PRINDLE VOLCANO, ALASKA										
20001	Harz	1-MP/G	77.5	20.5	1.1	0.8	-	-	-	2390
20002	Webst	4	14.7	41.8	43.1	-	-	-	0.4	1410
20003	Harz	2-MP/G	70.9	24.3	3.6	1.3	-	-	-	2247
20004	Sp Lherz	3-MP	45.1	32.2	12.7*	3.0*	-	-	6.9	1491
20005	Sp Lherz	3-MP	58.0	23.9	15.3	2.8	-	-	-	1516
20006	Sp Lherz	3-P/MP	56.4	33.0	9.1	1.5	-	-	-	1444
20007	Opxenite	4	7.9	74.5	14.1	2.9	-	-	0.6	1450
20008	Sp Lherz	3-GE	43.5	40.2*	12.9*	3.4*	-	-	-	1663
20009	Webst	4	6.6	36.2	40.3	9.1	-	-	7.8	1565
20010	Sp Lherz	2-MP	60.3	24.7	10.5	2.1	-	-	2.4	1356
20011	Composite, Diopside Websterite and Spinel Lherzolite									
20012	Mafic Granulite									
20013	Plagioclase Lherzolite									
20014	Intermediate Granulite									
20015*	Sp Lherz	2-PGR	60.0*	27.9*	10.9*	1.1*	-	-	-	1453
20016	Sp Lherz	3-P/MP	59.4	29.7	8.6	2.1	-	-	0.2	1168
20017	Sp Lherz	3-MP	46.7	36.0	13.5	3.8	-	-	-	1479
20018	Sp Lherz	3-MP/G	53.1	30.6	14.2*	2.2*	-	-	-	1581
20019	Sp Lherz	3-P/MP	58.2	22.7	16.1	2.5	-	-	0.6	2196
20020	Composite, Spinel Lherzolite and Olivine Websterite									
20021	Webst	4-C/P	29.9	10.7	53.3	tr.	-	-	5.9	2609
20022	Harz	1-GE	76.8	20.6	2.1	0.5*	-	-	-	1407
20023	Lherz	3-C/P	46.5	29.9	23.6	-	-	-	-	1759
20024	Plagioclase Lherzolite									
20025	Plagioclase Lherzolite									
20026	Cpxenite	4	11.2	4.0	84.3	0.4	-	-	-	1853
20027	Composite, Spinel Lherzolite and Ti-augite Websterite									
20028	Sp. Lherzolite, inhomogeneous									
20029	Sp Lherz	2-MP	62.8*	25.2	9.6*	1.7*	-	-	0.7	2865
20030	Composite, Spinel Lherzolite and Diopside Websterite									
20031	Webst	4	10.4	47.0	26.8	13.4	-	-	2.4	2402
20032	Harzburgite, inhomogeneous									
20033	Plagioclase Lherzolite									
20034	Sp Lherz	2-GE	61.0	28.2	8.6	2.2	-	-	-	1946
20035	Webst	3-GE	31.9	47.4	15.1	2.9	-	-	2.8	2171
20036	Sp Lherz	2-MP	60.5	25.7	10.7	2.3	-	-	0.8	2144
20037	Sp Lherz	2-P/MP	61.0	25.1	12.0	1.9	-	-	-	2443
20038*	Harz	1-P/MP	79.8*	16.7*	2.8*	0.4*	-	-	0.3	1921
20039*	Sp Lherz	4-C/P	82.0*	6.7*	5.9*	5.2*	-	-	0.1	2845

SAMPLE NUMBER	ROCK TYPE	CLASS	OLV	OPX	CPX	SP	AMPH	MICA	FINE GR ZONES	POINTS COUNTED
PRINDLE VOLCANO, ALASKA										
20040	Sp Lherz	2-P/MP	60.5	28.8	8.2	2.5	-	-	-	2644
20041	Sp Lherz	3-MP	59.6	27.3	9.4	3.2	-	-	0.5	2372
20042	Cpxenite	4	21.7	13.5	61.4	2.3	-	-	1.1	1713
20043	Spinel Lherzolite, inhomogeneous									
20044	Sp Lherz	2-P/MP	60.6	25.2	12.2	1.8	-	-	0.2	2314
20045	Sp Lherz	2-P/MP	60.6	28.0	8.8	2.6	-	-	-	2378
20046*	Sp Lherz	3-P/MP	57.6*	28.3*	10.4*	3.1*	-	-	0.6	2228
20047	Sp Lherz	1-P/MP	78.5	15.2	5.5	0.8	-	-	-	2233
20048	Composite, Spinel Lherzolite and Ti-augite hetsterite									
20049	Sp Lherz	3-P/MP	52.8	26.6	17.0	3.2	-	-	0.5	2342
PV average mode			51.5	28.2	17.7	2.6				
NUNIVAK ISLAND, ALASKA										
10001*	Websterite	1-POR	26.9	28.8	38.2	0.9	-	-	5.2*	6399
10002*	Sp Lherz	2-POR	72.2	13.2	6.3	0.7	-	-	7.5*	2788
10003	Sp Lherz	2-P/MP	69.1	21.1	5.8	1.1	-	-	2.9	3669
10004*	Sp Lherz	2-P/MP	70.7	18.6	8.4	2.1	-	-	0.2	2415
10005	Sp Lherz	2-POR	67.8	23.8	6.2	1.2	-	-	1.0	4943
10006*	Amph Harz	2-C/P	74.5	16.2	4.1	0.3	0.3*	tr*	4.7*	2338
10007*	Harz	1-POR	80.9	14.4	3.0	1.1	-	-	0.5	3238
10008*	Harz	2-POR	74.1	20.2	3.6	1.7	-	-	0.4	4060
10009	Harz	1-POR	82.0	10.0	3.6	1.3	-	-	3.1	3456
10010*	Harz	1-POR	83.3	11.1	0.7	0.6	-	-	4.3*	2138
10013*	Amph Lherz	2-POR	62.8	9.9	3.9	1.2	1.7*	0.1*	20.4*	3870
10016*	Amph Lherz	2-POR	66.6	15.6	4.9	1.1	4.2*	0.1*	7.5	3477
10021	Cpxenite	4	18.5	26.7	53.9	0.3	-	-	0.6	3500
10022	Sp Lherz	2-POR	66.4	16.0	12.8	4.9	-	-	-	3786
10023	Sp Lherz	2-P/MP	71.1	21.9	5.8	1.2	-	-	-	3046
10024	Sp Lherz	2-POR	60.5	31.4	7.0	1.2	-	-	-	4093
10025	Sp Lherz	2-POR	70.3	22.0	6.7	1.0	-	-	-	3640
10026	Sp Lherz	2-MP/G	62.7	22.5	11.3	3.3	-	-	0.2	4026
10027	Sp Lherz	2-C/P	64.0	23.2	7.0	1.0	-	-	3.9	4214
10028	Harz	2-POR	72.4	21.8	5.0	0.8	-	-	-	4099
10055	Harz	2-C/P	71.4	9.2	1.7	0.3	-	-	17.4	4177
10067	Amph Lherz	3-MP/G	59.0	17.5	7.7	0.2	8.5	-	7.3	3213
10068*	Sp Lherz	3-MP/G	58.2*	32.8*	7.1*	1.9*	-	-	-	3162
10069*	Sp Lherz	3-MP/G	56.8*	23.4*	17.0*	2.8*	-	-	-	2488
10070	Sp Lherz	3-GE	57.3	27.2	12.6	2.9	-	-	-	2604
10071	Sp Lherz	1-POR	78.4	10.0	7.2	0.9	-	1.2	2.4	4171
10075	Sp Lherz	2-POR	74.5	13.0	7.9	1.0	0.4	0.2	2.8	1686
10211	Sp Lherz	3-MP/G	47.6	32.2	7.6	2.6	-	5.9	10.0	2092
15001	Harz	2-POR	71.5	18.1	3.6	0.4	-	-	0.6	4191
NI average mode			65.2	19.7	9.3	1.4	0.5	0.3	3.6	

Abbreviations used:
OLV= olivine; OPX= orthopyroxene; CPX= clinopyroxene; SP= spinel;
AMPH= amphibole; FINE GR ZONES= fine-grained melt zones;
HARZ= harzburgite; SP LHERZ= spinel lherzolite; WEBST= websterite;
CPXENITE= orthopyroxenite; CPXENITE= clinopyroxenite;
CLASS= xenolith group number & xenolith texture
tr= trace amounts (<0.1 modal %) present.
*= mineral or whole rock compositions available in Appendix 2 and 3.

APPENDIX 2: MINERAL COMPOSITIONS OF ULTRAMAFIC XENOLITHS

UMX OLIVINE

NUNIVAK ISLAND: COMPOSITIONS FROM FRANCIS (1974, 1975)
TOTAL FE AS FEO

SAMPLE	10007 NI	10006 NI	10010 NI	10008 NI	10001 NI	10002 NI	10016 NI
SIO2	40.88	40.90	40.55	40.48	40.39	40.75	40.83
TIO2	0.02	0.02	0.01	0.02	0.01	0.01	0.0
AL2O3	0.0	0.0	0.0	0.0	0.0	0.0	0.04
CR2O3	0.0	0.0	0.0	0.0	0.0	0.0	0.02
MGO	50.27	50.02	49.73	49.69	49.74	49.12	49.96
FEO	8.44	8.72	8.74	8.84	9.08	9.14	9.35
MNO	0.10	0.12	0.12	0.14	0.13	0.10	0.16
CAO	0.04	0.04	0.05	0.06	0.05	0.05	0.05
TOTAL	99.75	99.82	99.20	99.23	99.40	99.17	100.42

MOLAR PROPORTIONS BASED ON 3 CATIONS

SI	0.997	0.998	0.996	0.994	0.991	1.004	0.993
TI	0.000	0.000	0.000	0.000	0.000	0.000	0.0
AL	0.0	0.0	0.0	0.0	0.0	0.0	0.001
CR	0.0	0.0	0.0	0.0	0.0	0.0	0.000
MG	1.827	1.820	1.821	1.819	1.819	1.804	1.811
FE	0.172	0.178	0.180	0.182	0.186	0.188	0.190
MN	0.002	0.002	0.002	0.003	0.003	0.002	0.003
CA	0.001	0.001	0.001	0.002	0.001	0.001	0.001
OXYGENS	3.997	3.999	3.996	3.995	3.991	4.004	3.993
MG/(MG+FE)	0.914	0.911	0.910	0.909	0.907	0.905	0.905

UMX OLIVINE

NUNIVAK ISLAND: COMPOSITIONS FROM FRANCIS (1974, 1975)
TOTAL FE AS FEO

SAMPLE	10004 NI	10069 NI	10068 NI	10013 NI	20015 PV	20038 PV	20046 PV
SIO2	40.63	39.38	39.95	40.08	40.91	41.14	40.14
TIO2	0.01	0.0	0.0	0.0	-	-	-
AL2O3	0.0	0.03	0.02	0.02	-	-	-
CR2O3	0.0	0.03	0.03	0.03	0.0	0.0	0.0
MGO	49.35	49.84	48.61	49.37	50.52	50.39	49.50
FEO	9.46	10.11	10.29	10.91	8.58	8.75	10.20
MNO	0.12	0.07	0.17	0.17	0.13	0.14	0.15
NIO	-	-	-	-	0.36	0.36	0.33
CAO	0.08	0.10	0.06	0.07	0.04	0.03	0.04
TOTAL	99.65	99.56	99.13	100.65	100.54	100.81	100.36

MOLAR PROPORTIONS BASED ON 3 CATIONS

SI	0.997	0.966	0.988	0.977	0.991	0.995	0.980
TI	0.000	0.0	0.0	0.0	-	-	-
AL	0.0	0.001	0.001	0.001	-	-	-
CR	0.0	0.001	0.001	0.001	0.0	0.0	0.0
MG	1.804	1.822	1.792	1.794	1.824	1.817	1.801
FE	0.194	0.207	0.213	0.222	0.174	0.177	0.208
MN	0.002	0.001	0.004	0.004	0.003	0.003	0.003
NI	-	-	-	-	0.007	0.007	0.006
CA	0.002	0.003	0.002	0.002	0.001	0.001	0.001
OXYGENS	3.997	3.966	3.989	3.978	3.991	3.995	3.980
MG/(MG+FE)	0.903	0.898	0.894	0.890	0.913	0.911	0.896

UMX OLIVINE

TOTAL FE AS FEO

SAMPLE	20029 PV	20039 PV	30008 PV	30006 PV	30020 PV	30022 PV	30012 PV
SIO2	40.31	40.00	40.82	40.34	40.54	40.42	39.93
CR2O3	0.0	0.0	0.01	0.01	0.01	0.0	0.0
MGO	49.32	47.84	50.84	50.65	50.08	49.76	49.22
FEO	10.31	12.04	8.32	8.79	9.27	9.67	10.56
MNO	0.14	0.19	0.10	0.12	0.12	0.14	0.13
NIO	0.36	0.30	0.39	0.38	0.38	0.36	0.36
CAO	0.02	0.04	0.04	0.04	0.05	0.04	0.06
TOTAL	100.46	100.41	100.52	100.33	100.45	100.39	100.26

MOLAR PROPORTIONS BASED ON 3 CATIONS

SI	0.984	0.985	0.988	0.979	0.986	0.985	0.977
CR	0.0	0.0	0.000	0.000	0.000	0.0	0.0
MG	1.795	1.756	1.833	1.832	1.815	1.807	1.795
FE	0.211	0.248	0.168	0.178	0.188	0.197	0.216
MN	0.003	0.004	0.002	0.002	0.002	0.003	0.003
NI	0.007	0.006	0.008	0.007	0.007	0.007	0.007
CA	0.001	0.001	0.001	0.001	0.001	0.001	0.002
OXYGENS	3.984	3.985	3.988	3.979	3.986	3.985	3.977
MG/(MG+FE)	0.895	0.876	0.916	0.911	0.906	0.902	0.893

UNX CLIVINE

TOTAL FE AS FEO

SAMPLE	40044 CR	40015 CR	40003 CR	40030 CR	40017 CR	40001 CR	40010 CR
SIO2	40.54	40.88	40.98	40.55	40.77	40.62	40.35
CR2O3	0.01	0.02	0.0	0.02	0.0	0.0	0.0
MGO	50.96	50.68	50.44	50.54	50.41	49.91	49.64
FEO	8.29	8.51	8.52	8.64	8.78	9.55	9.79
MNO	0.11	0.13	0.13	0.16	0.10	0.15	0.13
NIO	0.38	0.39	0.40	0.36	0.41	0.40	0.38
CAO	0.06	0.10	0.07	0.13	0.05	0.11	0.05
TOTAL	100.35	100.71	100.54	100.40	100.52	100.74	100.34

MOLAR PROPORTIONS BASED ON 3 CATIONS

SI	0.982	0.988	0.993	0.984	0.989	0.986	0.984
CR	0.000	0.000	0.0	0.000	0.0	0.0	0.0
MG	1.839	1.826	1.822	1.827	1.822	1.806	1.805
FE	0.168	0.172	0.173	0.175	0.178	0.194	0.200
MN	0.002	0.003	0.003	0.003	0.002	0.003	0.003
NI	0.007	0.008	0.008	0.007	0.008	0.008	0.007
CA	0.002	0.003	0.002	0.003	0.001	0.003	0.001
OXYGENS	3.982	3.989	3.993	3.984	3.989	3.986	3.984
MG/(MG+FE)	0.916	0.914	0.913	0.912	0.911	0.903	0.900

UMX OLIVINE

TOTAL FE AS FEO

SAMPLE	40055 CR	40037 CR	50015 JL	50011 JL	50005 JL	50001 JL	50009 JL
SIO2	40.45	40.08	40.65	41.02	40.47	40.60	40.27
CR2O3	0.02	0.05	0.02	0.0	0.0	0.03	0.01
MGO	48.23	47.15	50.10	50.38	50.25	50.10	49.70
FEO	11.24	12.89	8.62	8.72	9.39	9.45	9.85
MNO	0.13	0.16	0.11	0.10	0.12	0.14	0.14
NIO	0.34	0.31	0.35	0.39	0.17	0.34	0.33
CAO	0.16	0.25	0.05	0.04	0.05	0.16	0.05
TOTAL	100.57	100.89	99.90	100.65	100.45	100.82	100.35

MOLAR PROPORTIONS BASED ON 3 CATIONS

SI	0.992	0.987	0.992	0.994	0.983	0.984	0.982
CR	0.000	0.001	0.000	0.0	0.0	0.001	0.000
MG	1.763	1.731	1.822	1.819	1.819	1.810	1.806
FE	0.231	0.265	0.176	0.177	0.191	0.192	0.201
MN	0.003	0.003	0.002	0.002	0.002	0.003	0.003
NI	0.007	0.006	0.007	0.008	0.003	0.007	0.006
CA	0.004	0.007	0.001	0.001	0.001	0.004	0.001
OXYGENS	3.992	3.987	3.992	3.994	3.983	3.984	3.982
MG/(MG+FE)	0.884	0.867	0.912	0.911	0.905	0.904	0.900

UMX OLIVINE

TOTAL FE AS FEO

SAMPLE	50006 JL
SIO2	40.39
CR2O3	0.01
MGO	49.62
FEO	10.30
MNO	0.15
NIO	0.35
CAO	0.04
TOTAL	100.86

MOLAR PROPORTIONS BASED ON 3 CATIONS

SI	0.962
CR	0.000
MG	1.798
FE	0.209
MN	0.003
NI	0.007
CA	0.001
OXYGENS	3.982
MG/(MG+FE)	0.896

UMX ORTHOPYROXENE

NUNIVAK ISLAND: COMPOSITIONS FROM FRANCIS (1974, 1975)
MOLE PROPORTION FE3+ CALCULATED FROM STOICHIOMETRY

SAMPLE	10007 NI	10006 NI	10010 NI	10008 NI	10016 NI	10001 NI	10002 NI
SIO2	57.13	56.32	56.69	56.49	57.07	55.77	56.44
TIO2	0.01	0.03	0.0	0.03	0.01	0.07	0.0
AL2O3	2.46	3.03	2.27	3.37	2.78	2.39	3.23
CR2O3	0.45	0.46	0.52	0.43	0.43	0.45	0.43
MGO	34.29	33.79	34.29	33.91	34.01	34.41	33.22
FEO	5.60	5.77	5.79	5.81	5.82	6.14	5.98
MNO	0.15	0.12	0.07	0.13	0.15	0.13	0.11
CAO	0.59	0.53	0.54	0.59	0.41	0.55	0.58
NA2O	0.07	0.03	0.20	0.04	0.08	0.04	0.26
TOTAL	100.75	100.08	100.37	100.80	100.76	99.95	100.25

MOLAR PROPORTIONS BASED ON 4 CATIONS

SI	1.952	1.939	1.942	1.931	1.952	1.920	1.941
AL4	0.048	0.061	0.058	0.070	0.048	0.080	0.059
TI	0.000	0.001	0.0	0.001	0.000	0.002	0.0
AL6	0.051	0.062	0.034	0.067	0.064	0.017	0.072
FE3+	0.0	0.0	0.023	0.0	0.0	0.050	0.0
CR	0.012	0.013	0.014	0.012	0.012	0.012	0.012
MG	1.746	1.734	1.751	1.727	1.733	1.766	1.703
FE2+	0.160	0.166	0.143	0.166	0.166	0.127	0.172
MN	0.004	0.003	0.002	0.004	0.004	0.004	0.003
CA	0.022	0.020	0.020	0.022	0.015	0.020	0.021
NA	0.005	0.002	0.013	0.003	0.005	0.003	0.017
OXYGENS	6.005	6.006	5.999	6.004	6.011	6.000	6.003
MG-NUMBER	0.916	0.913	0.925	0.912	0.912	0.933	0.908
CA/(CA+MG)	0.012	0.011	0.011	0.012	0.009	0.011	0.012

UMX ORTHOPYROXENE

NUNIVAK ISLAND: COMPOSITIONS FROM FRANCIS (1974, 1975)
MOLE PROPORTION FE3+ CALCULATED FROM STOICHIOMETRY

SAMPLE	10004 NI	10068 NI	10069 NI	10013 NI	20015 PV	20038 PV	20008 PV
SIO2	55.53	55.23	54.86	55.78	55.74	56.78	55.04
TIO2	0.04	0.14	0.17	0.04	0.05	0.0	0.11
AL2O3	3.76	4.57	4.93	3.27	3.06	1.72	3.75
CR2O3	0.41	0.26	0.33	0.41	0.50	0.34	0.28
MGO	33.03	33.45	32.83	32.92	34.70	34.61	33.63
FEO	6.11	6.40	6.35	6.78	5.47	5.82	6.65
MNO	0.14	0.13	0.16	0.17	0.26	0.16	0.38
CAO	0.61	0.64	0.86	0.60	0.50	0.44	0.43
NA2O	0.20	0.15	0.15	0.27	0.02	0.0	0.03
TOTAL	99.83	100.97	100.64	100.24	100.30	99.87	100.30

MOLAR PROPORTIONS BASED ON 4 CATIONS

SI	1.918	1.885	1.881	1.923	1.908	1.956	1.893
AL4	0.082	0.115	0.119	0.077	0.092	0.044	0.107
TI	0.001	0.004	0.004	0.001	0.001	0.0	0.003
AL6	0.071	0.068	0.080	0.056	0.031	0.025	0.045
FE3+	0.011	0.043	0.031	0.026	0.046	0.010	0.050
CR	0.011	0.007	0.009	0.011	0.014	0.009	0.008
MG	1.700	1.701	1.678	1.691	1.770	1.777	1.724
FE2+	0.165	0.140	0.151	0.169	0.110	0.158	0.141
MN	0.004	0.004	0.005	0.005	0.008	0.005	0.011
CA	0.023	0.023	0.032	0.022	0.018	0.016	0.016
NA	0.013	0.010	0.010	0.018	0.001	0.0	0.002
OXYGENS	5.999	6.000	6.000	6.000	6.000	6.000	6.000
MG-NUMBER	0.912	0.924	0.917	0.909	0.941	0.918	0.924
CA/(CA+MG)	0.013	0.014	0.018	0.013	0.010	0.009	0.009

UMX ORTHOPYROXENE

MOLE PROPORTION FE3+ CALCULATED FROM STOICHIOMETRY

SAMPLE	20046 PV	20039 PV	30008 FS	30006 FS	30003 FS	30020 FS	30022 FS
SIO2	55.09	54.52	56.43	55.62	55.00	54.66	54.50
TIO2	0.14	0.17	0.02	0.08	0.11	0.10	0.11
AL2O3	4.27	3.66	2.06	4.23	4.33	4.75	4.87
CR2O3	0.22	0.33	0.54	0.50	0.42	0.50	0.39
MGO	33.24	32.73	34.79	33.41	33.76	33.39	32.85
FEO	6.63	7.70	5.10	5.61	5.92	5.93	6.12
MNO	0.31	0.38	0.13	0.11	0.28	0.26	0.13
CAO	0.49	0.44	0.69	0.66	0.54	0.66	0.70
NA2O	0.03	0.01	0.02	0.04	0.05	0.08	0.05
TOTAL	100.42	99.94	99.78	100.26	100.41	100.33	99.72

MOLAR PROPORTIONS BASED ON 4 CATIONS

SI	1.894	1.892	1.941	1.911	1.885	1.876	1.885
AL4	0.106	0.108	0.059	0.089	0.115	0.124	0.115
TI	0.004	0.004	0.001	0.002	0.003	0.003	0.003
AL6	0.067	0.042	0.024	0.082	0.060	0.068	0.083
FE3+	0.027	0.049	0.021	0.0	0.041	0.042	0.019
CR	0.006	0.009	0.015	0.014	0.011	0.014	0.011
MG	1.704	1.693	1.783	1.711	1.725	1.708	1.693
FE2	0.163	0.175	0.126	0.161	0.129	0.126	0.158
MN	0.009	0.011	0.004	0.003	0.008	0.008	0.004
CA	0.018	0.016	0.025	0.024	0.020	0.024	0.026
NA	0.002	0.001	0.001	0.003	0.003	0.005	0.003
OXYGENS	5.999	6.000	6.000	6.004	5.999	6.000	5.999
MG-NUMBER	0.913	0.907	0.934	0.914	0.931	0.930	0.915
CA/(CA+MG)	0.010	0.010	0.014	0.014	0.011	0.014	0.015

UMX ORTHOPYROXENE

MOLE PROPORTION FE3+ CALCULATED FROM STOICHIOMETRY

SAMPLE	30028 FS	30012 FS	40044 CR	40015 CR	40003 CR	40017 CR	40030 CR
SIO2	55.66	54.51	56.73	56.05	56.08	56.21	55.17
TIO2	0.12	0.15	0.08	0.03	0.0	0.03	0.04
AL2O3	3.09	5.49	2.00	3.09	2.35	3.24	4.68
CR2O3	0.53	0.19	0.36	0.43	0.49	0.38	0.41
MGO	33.69	32.62	35.18	34.21	34.56	34.11	32.57
FEO	6.80	6.67	5.23	5.30	5.40	5.53	5.52
MNO	0.33	0.28	0.12	0.14	0.12	0.12	0.12
CAO	0.42	0.67	0.63	0.68	0.67	0.58	1.41
NA2O	0.02	0.08	0.02	0.02	0.0	0.02	0.11
TOTAL	100.66	100.66	100.35	99.95	99.67	100.22	100.03

MOLAR PROPORTIONS BASED ON 4 CATIONS

SI	1.911	1.871	1.939	1.927	1.932	1.929	1.902
AL4	0.089	0.129	0.061	0.073	0.068	0.071	0.098
TI	0.003	0.004	0.002	0.001	0.0	0.001	0.001
AL6	0.036	0.093	0.020	0.052	0.028	0.060	0.092
FE3+	0.033	0.029	0.030	0.009	0.027	0.001	0.0
CR	0.014	0.005	0.010	0.012	0.013	0.010	0.011
MG	1.724	1.669	1.792	1.753	1.775	1.744	1.674
FE2+	0.162	0.163	0.120	0.143	0.129	0.158	0.159
MN	0.010	0.008	0.003	0.004	0.004	0.003	0.004
CA	0.015	0.025	0.023	0.025	0.025	0.021	0.052
NA	0.001	0.005	0.001	0.001	0.0	0.001	0.007
OXYGENS	6.000	6.000	6.000	5.999	6.000	6.000	6.000
MG-NUMBER	0.914	0.911	0.937	0.925	0.932	0.917	0.913
CA/(CA+MG)	0.009	0.015	0.013	0.014	0.014	0.012	0.030

UMX ORTHOPYROXENE

MOLE PROPORTION FE3+ CALCULATED FROM STOICHIOMETRY

SAMPLE	40061 CR	40054 CR	40010 CR	40037 CR	50015 JL	50011 JL	50005 JL
SIO2	55.04	55.09	55.09	53.56	55.82	55.98	55.59
TIO2	0.08	0.09	0.12	0.24	0.07	0.04	0.08
AL2O3	3.93	4.09	4.28	5.94	2.81	3.30	4.41
CR2O3	0.37	0.36	0.22	0.60	0.61	0.56	0.44
MGO	33.65	33.56	33.55	30.11	33.72	34.19	32.70
FEO	6.09	6.22	6.17	7.96	5.43	5.61	5.95
MNO	0.29	0.28	0.29	0.12	0.13	0.18	0.14
CAO	0.69	0.62	0.56	1.45	0.76	0.63	0.73
NA2O	0.05	0.04	0.05	0.11	0.09	0.01	0.19
TOTAL	100.19	100.35	100.33	100.09	99.44	100.50	100.23

MOLAR PROPORTIONS BASED ON 4 CATIONS

SI	1.892	1.892	1.891	1.869	1.932	1.916	1.914
AL4	0.108	0.108	0.109	0.131	0.068	0.084	0.086
TI	0.002	0.002	0.003	0.006	0.002	0.001	0.002
AL6	0.051	0.058	0.065	0.113	0.047	0.050	0.093
FE3+	0.046	0.039	0.035	0.0	0.007	0.017	0.0
CR	0.010	0.010	0.006	0.017	0.017	0.015	0.012
MG	1.724	1.718	1.717	1.566	1.740	1.745	1.678
FE2+	0.130	0.140	0.142	0.232	0.150	0.143	0.171
MN	0.008	0.008	0.008	0.004	0.004	0.005	0.004
CA	0.025	0.023	0.021	0.054	0.028	0.023	0.027
NA	0.003	0.003	0.003	0.007	0.006	0.001	0.013
OXYGENS	6.000	6.000	5.999	6.002	6.000	5.999	6.005
MG-NUMBER	0.930	0.925	0.924	0.871	0.921	0.924	0.907
CA/(CA+MG)	0.015	0.013	0.012	0.033	0.016	0.013	0.016

UMX ORTHOPYROXENE

MOLE PROPORTION FE3+ CALCULATED FROM STOICHIOMETRY

SAMPLE	50008 JL	50019 JL	50001 JL	50009 JL	50006 JL
SIO2	55.12	54.46	54.06	54.74	54.55
TIO2	0.09	0.09	0.20	0.13	0.10
AL2O3	4.29	5.12	5.61	4.76	5.20
CR2O3	0.27	0.43	0.42	0.33	0.22
MGO	33.05	32.40	32.03	32.63	32.25
FEO	6.26	6.10	6.07	6.36	6.52
MNO	0.15	0.14	0.14	0.13	0.15
CAO	0.50	0.96	1.24	0.67	0.62
NA2O	0.04	0.18	0.14	0.08	0.08
TOTAL	99.77	99.88	99.90	99.83	99.69

MOLAR PROPORTIONS BASED ON 4 CATIONS

SI	1.906	1.881	1.869	1.893	1.891
AL4	0.094	0.119	0.131	0.107	0.109
TI	0.002	0.002	0.005	0.003	0.003
AL6	0.081	0.090	0.098	0.087	0.103
FE3+	0.004	0.025	0.021	0.009	0.0
CR	0.007	0.012	0.011	0.009	0.006
MG	1.703	1.668	1.651	1.682	1.666
FE2+	0.177	0.152	0.154	0.175	0.189
MN	0.004	0.004	0.004	0.004	0.004
CA	0.019	0.036	0.046	0.025	0.023
NA	0.003	0.012	0.009	0.005	0.005
OXYGENS	6.000	6.000	6.000	6.000	6.000
MG-NUMBER	0.906	0.917	0.914	0.906	0.898
CA/(CA+MG)	0.011	0.021	0.027	0.015	0.014

UMX CLINOPYROXENE

NUNIVAK ISLAND: COMPOSITIONS FROM FRANCIS (1974, 1975)
MOLE PROPORTION FE3+ CALCULATED FROM STOICIOMETRY

SAMPLE	10010 NI	10007 NI	10001 NI	10008 NI	10016 NI	10004 NI	10002 NI
SIO2	51.95	53.40	53.35	52.46	54.83	53.56	54.82
TIO2	0.03	0.06	0.13	0.10	0.02	0.20	0.07
AL2O3	5.62	2.71	2.92	3.25	3.27	4.22	4.45
CR2O3	2.44	0.91	0.87	0.68	0.78	0.66	0.90
MGO	16.47	17.07	17.52	17.40	16.22	17.14	16.55
FEO	2.05	2.35	2.45	2.47	2.42	2.66	2.83
MNO	0.08	0.10	0.08	0.05	0.13	0.07	0.07
CAO	19.79	21.70	22.08	23.01	19.89	20.90	18.77
NA2O	1.36	0.81	0.87	0.48	2.12	1.14	2.57
TOTAL	99.79	99.12	100.28	99.90	99.69	100.55	101.03

MOLAR PROPORTIONS BASED ON 4 CATIONS

SI	1.877	1.947	1.920	1.898	1.975	1.919	1.940
AL4	0.123	0.053	0.080	0.102	0.025	0.081	0.060
TI	0.001	0.002	0.004	0.003	0.001	0.005	0.002
AL6	0.116	0.064	0.044	0.037	0.114	0.097	0.126
FE3+	0.030	0.017	0.066	0.073	0.036	0.034	0.081
CR	0.070	0.026	0.025	0.019	0.022	0.019	0.025
MG	0.887	0.928	0.940	0.939	0.871	0.915	0.873
FE2+	0.032	0.055	0.008	0.002	0.037	0.046	0.002
MN	0.002	0.003	0.002	0.002	0.004	0.002	0.002
CA	0.766	0.848	0.851	0.892	0.768	0.802	0.712
NA	0.095	0.057	0.061	0.034	0.148	0.079	0.176
OXYGENS	6.000	6.000	5.999	6.000	6.000	6.000	5.999
MG-NUMBER	0.965	0.944	0.992	0.998	0.960	0.952	0.997
CA/(CA+MG)	0.463	0.477	0.475	0.487	0.469	0.467	0.449

UMX CLINOPYROXENE

NUNIVAK ISLAND: COMPOSITIONS FROM FRANCIS (1974, 1975)
MOLE PROPORTION FE3+ CALCULATED FROM STOICHIOMETRY

SAMPLE	10006 NI	10068 NI	10013 NI	10069 NI	20038 PV	20015 PV	20029 PV
SIO2	55.72	52.05	53.81	51.57	53.27	53.37	52.47
TIO2	0.02	0.62	0.01	0.63	0.02	0.15	0.48
AL203	4.19	6.88	4.77	7.18	2.34	4.31	5.42
CR203	0.82	0.64	0.96	0.63	0.90	0.92	0.67
MGO	15.88	15.47	16.04	16.15	16.65	16.47	15.66
FEO	2.88	2.85	3.24	3.36	2.21	2.21	2.54
MNO	0.11	0.12	0.10	0.11	0.07	0.08	0.09
CAO	17.65	19.84	18.82	18.91	22.67	21.73	21.59
NA2O	2.80	1.80	2.44	1.83	0.78	0.99	1.03
TOTAL	100.08	100.27	100.19	100.37	98.91	100.23	99.95

MOLAR PROPORTIONS BASED ON 4 CATIONS

SI	1.993	1.869	1.925	1.845	1.950	1.924	1.901
AL4	0.007	0.131	0.075	0.155	0.050	0.076	0.099
TI	0.001	0.017	0.000	0.017	0.001	0.004	0.013
AL6	0.169	0.160	0.126	0.148	0.051	0.107	0.132
FE3+	0.008	0.045	0.090	0.082	0.028	0.004	0.0
CR	0.023	0.018	0.027	0.018	0.026	0.026	0.019
MG	0.847	0.828	0.855	0.861	0.908	0.885	0.846
FE2+	0.078	0.040	0.007	0.019	0.040	0.063	0.077
MN	0.003	0.004	0.003	0.003	0.002	0.002	0.003
CA	0.676	0.763	0.721	0.725	0.889	0.839	0.838
NA	0.194	0.125	0.169	0.127	0.055	0.069	0.072
OXYGENS	6.000	5.999	6.000	6.000	6.000	6.000	6.003
MG-NUMBER	0.915	0.954	0.992	0.979	0.958	0.934	0.917
CA/(CA+MG)	0.444	0.480	0.458	0.457	0.495	0.487	0.498

UMX CLINOPYROXENE

MOLE PROPORTION FE3+ CALCULATED FROM STOICHIOMETRY

SAMPLE	20018 PV	20004 PV	20008 PV	20046 PV	20039 PV	30008 FS	30006 FS
SIO2	52.42	52.19	51.89	51.85	51.17	53.97	52.69
TIO2	0.38	0.55	0.50	0.63	0.96	0.02	0.31
AL203	5.47	6.37	5.70	6.38	6.32	2.54	5.75
CR203	0.61	0.63	0.62	0.60	0.74	1.26	1.05
MGO	15.56	15.34	15.11	15.18	14.87	17.25	15.75
FEO	2.68	2.75	2.73	2.82	3.23	2.03	2.33
MNO	0.07	0.09	0.09	0.07	0.13	0.07	0.07
CAO	21.35	21.09	21.29	20.82	21.15	21.98	20.93
NA20	1.25	1.40	1.26	1.41	1.30	0.70	1.41
TOTAL	99.79	100.41	99.19	99.76	99.87	99.82	100.29

MOLAR PROPORTIONS BASED ON 4 CATIONS

SI	1.899	1.878	1.894	1.879	1.859	1.956	1.896
AL4	0.101	0.122	0.106	0.121	0.141	0.044	0.104
TI	0.010	0.015	0.014	0.017	0.026	0.001	0.008
AL6	0.132	0.148	0.139	0.151	0.130	0.065	0.140
FE3+	0.018	0.024	0.011	0.018	0.029	0.0	0.016
CR	0.017	0.018	0.018	0.017	0.021	0.036	0.030
MG	0.840	0.823	0.822	0.820	0.805	0.932	0.845
FE2+	0.063	0.059	0.072	0.068	0.070	0.062	0.054
MN	0.002	0.003	0.003	0.002	0.004	0.002	0.002
CA	0.829	0.813	0.832	0.808	0.823	0.854	0.807
NA	0.088	0.098	0.089	0.099	0.092	0.045	0.098
OXYGENS	6.000	6.000	5.999	5.999	6.000	6.005	6.000
MG-NUMBER	0.930	0.933	0.920	0.924	0.920	0.938	0.940
CA/(CA+MG)	0.497	0.497	0.503	0.496	0.506	0.478	0.489

UNX CLINOPYROXENE

MOLE PROPORTION FE3+ CALCULATED FROM STOICHIOMETRY

SAMPLE	30015 FS	30020 FS	30022 FS	30003 FS	30028 FS	30012 FS	40003 CR
SIO2	51.95	52.49	52.41	52.44	52.32	51.68	53.88
TIO2	0.48	0.34	0.43	0.44	0.52	0.62	0.02
AL2O3	6.06	6.33	6.37	6.66	5.35	7.52	2.46
CR2O3	0.83	0.91	0.83	1.00	1.17	0.65	0.89
MGO	15.15	15.31	15.19	14.81	15.49	14.99	17.76
FEO	2.46	2.63	2.61	2.59	2.75	3.04	2.11
MNO	0.07	0.06	0.09	0.09	0.11	0.09	0.08
CAO	21.27	20.01	20.43	20.44	21.42	19.24	22.39
NA2O	1.38	1.42	1.49	1.67	1.08	1.78	0.21
TOTAL	99.65	99.50	99.85	100.14	100.21	99.61	99.80

MOLAR PROPORTIONS BASED ON 4 CATIONS

SI	1.864	1.905	1.896	1.892	1.895	1.870	1.956
AL4	0.116	0.095	0.104	0.108	0.106	0.130	0.044
TI	0.013	0.009	0.012	0.012	0.014	0.017	0.001
AL6	0.143	0.176	0.168	0.175	0.123	0.191	0.061
FE3+	0.019	0.0	0.0	0.0	0.0	0.012	0.0
CR	0.024	0.026	0.024	0.029	0.033	0.019	0.026
MG	0.819	0.828	0.819	0.796	0.836	0.808	0.961
FE2+	0.056	0.080	0.079	0.078	0.083	0.080	0.064
MN	0.002	0.002	0.003	0.003	0.003	0.003	0.002
CA	0.827	0.778	0.792	0.790	0.831	0.746	0.871
NA	0.097	0.100	0.105	0.117	0.076	0.125	0.015
OXYGENS	6.000	6.013	6.003	6.001	6.002	6.000	6.014
MG-NUMBER	0.937	0.912	0.912	0.911	0.909	0.910	0.938
CA/(CA+MG)	0.502	0.484	0.492	0.498	0.498	0.480	0.475

UNX CLINOPYROXENE

MOLE PROPORTION FE3+ CALCULATED FROM STOICHIOMETRY

SAMPLE	40044 CR	40015 CR	40017 CR	40020 CR	40046 CR	40060 CR	40018 CR
SIO2	54.11	53.65	54.21	52.15	52.37	53.00	52.72
TIO2	0.14	0.08	0.01	0.30	0.14	0.07	0.10
AL2O3	3.04	3.75	3.73	4.11	5.05	4.77	5.02
CR2O3	0.84	1.12	0.91	0.61	0.80	0.68	0.68
MGO	17.32	16.90	16.66	16.96	16.17	16.67	16.34
FEO	2.14	2.18	2.17	2.32	2.23	2.37	2.38
MNO	0.10	0.08	0.05	0.08	0.09	0.08	0.09
CAO	21.79	21.47	21.60	22.41	21.81	21.45	21.28
NA2O	0.88	0.65	0.63	0.42	1.00	0.88	0.98
TOTAL	100.36	99.88	99.97	99.36	99.66	99.97	99.59

MOLAR PROPORTIONS BASED ON 4 CATIONS

SI	1.946	1.945	1.964	1.900	1.897	1.913	1.914
AL4	0.054	0.055	0.036	0.100	0.103	0.087	0.089
TI	0.004	0.002	0.000	0.008	0.004	0.002	0.003
AL6	0.075	0.105	0.124	0.076	0.113	0.116	0.125
FE3+	0.008	0.0	0.0	0.020	0.030	0.009	0.008
CR	0.024	0.032	0.026	0.018	0.023	0.019	0.019
MG	0.929	0.913	0.900	0.921	0.873	0.897	0.883
FE2+	0.056	0.066	0.066	0.051	0.038	0.063	0.064
MN	0.003	0.002	0.002	0.002	0.003	0.002	0.003
CA	0.840	0.834	0.839	0.875	0.847	0.830	0.826
NA	0.061	0.046	0.044	0.030	0.070	0.062	0.069
OXYGENS	6.000	6.020	6.035	6.000	6.000	6.000	6.000
MG-NUMBER	0.943	0.933	0.932	0.948	0.958	0.934	0.933
CA/(CA+MG)	0.475	0.477	0.482	0.487	0.492	0.481	0.484

UNX CLINOPYROXENE

MOLE PROPORTION FE3+ CALCULATED FROM STOICHIOMETRY

SAMPLE	40061 CR	40030 CR	40010 CR	40054 CR	40055 CR	40001 CR	40037 CR
SIO2	52.13	52.47	52.23	53.23	52.94	51.85	50.76
TIO2	0.31	0.16	0.49	0.32	0.14	0.41	0.52
AL2O3	5.35	5.66	6.21	5.56	4.92	7.24	7.16
CR2O3	0.74	0.89	0.71	0.75	0.96	0.79	0.83
MGO	16.20	17.39	15.03	15.36	18.28	16.97	17.33
FEO	2.67	2.89	2.62	2.70	3.83	3.63	5.01
MNO	0.06	0.11	0.07	0.09	0.13	0.11	0.13
CAO	21.38	19.27	20.33	20.89	17.95	16.91	16.86
NA2O	0.94	0.93	1.48	1.07	0.89	1.29	0.85
TOTAL	99.78	99.77	99.17	99.97	100.04	99.20	99.45

MOLAR PROPORTIONS BASED ON 4 CATIONS

SI	1.889	1.893	1.903	1.930	1.906	1.879	1.844
AL4	0.111	0.107	0.097	0.070	0.094	0.121	0.156
TI	0.008	0.004	0.013	0.009	0.004	0.011	0.014
AL6	0.117	0.134	0.170	0.168	0.114	0.189	0.151
FE3+	0.022	0.003	0.0	0.0	0.007	0.0	0.012
CR	0.021	0.025	0.020	0.022	0.027	0.023	0.024
MG	0.875	0.935	0.816	0.830	0.981	0.917	0.939
FE2+	0.059	0.084	0.080	0.082	0.108	0.110	0.140
MN	0.002	0.003	0.002	0.003	0.004	0.003	0.004
CA	0.830	0.745	0.794	0.812	0.692	0.657	0.656
NA	0.066	0.065	0.105	0.075	0.062	0.091	0.060
OXYGENS	6.000	5.999	6.008	6.031	5.999	6.011	6.000
MG-NUMBER	0.937	0.918	0.911	0.910	0.901	0.893	0.870
CA/(CA+MG)	0.487	0.443	0.493	0.494	0.414	0.417	0.412

UNX CLINOPYROXENE

MOLE PROPORTION FE3+ CALCULATED FROM STOICHIOMETRY

SAMPLE	50011 JL	50015 JL	50008 JL	50005 JL	50009 JL	50006 JL	50019 JL
SIO2	53.26	53.90	51.56	52.64	51.86	52.31	52.24
TIO2	0.09	0.22	0.47	0.29	0.50	0.48	0.38
AL2O3	4.38	4.41	7.15	6.32	7.23	7.71	6.97
CR2O3	0.89	1.74	0.76	0.98	0.78	0.53	0.81
MGO	16.72	16.06	14.85	15.44	15.29	14.88	16.12
FEO	2.23	2.43	2.61	2.76	2.83	2.85	3.19
MNO	0.09	0.08	0.07	0.09	0.09	0.09	0.10
CAO	21.73	19.72	19.74	19.62	19.20	18.90	19.08
NA2O	0.83	1.62	1.76	1.92	1.89	1.75	1.28
TOTAL	100.22	100.18	98.99	100.06	99.67	99.50	100.17

MOLAR PROPORTIONS BASED ON 4 CATIONS

SI	1.920	1.943	1.876	1.893	1.871	1.894	1.881
AL4	0.080	0.057	0.124	0.107	0.129	0.106	0.119
TI	0.002	0.006	0.013	0.008	0.014	0.013	0.010
AL6	0.106	0.131	0.183	0.161	0.179	0.223	0.177
FE3+	0.001	0.0	0.019	0.036	0.032	0.0	0.0
CR	0.025	0.050	0.022	0.028	0.022	0.015	0.023
MG	0.898	0.863	0.805	0.828	0.822	0.803	0.865
FE2+	0.066	0.073	0.061	0.047	0.053	0.086	0.096
MN	0.003	0.002	0.002	0.003	0.003	0.003	0.003
CA	0.839	0.762	0.770	0.756	0.742	0.733	0.736
NA	0.058	0.113	0.126	0.134	0.132	0.123	0.089
OXYGENS	6.000	6.011	6.000	6.000	6.000	6.018	6.006
MG-NUMBER	0.932	0.922	0.930	0.947	0.939	0.903	0.900
CA/(CA+MG)	0.483	0.469	0.489	0.477	0.474	0.477	0.460

UNX CLINOPYROXENE

MOLE PROPORTION FE3+ CALCULATED FROM STOICHIOMETRY

SAMPLE	50001 JL
SIO2	51.58
TIO2	0.52
AL2O3	7.37
CR2O3	0.81
MGO	17.42
FEO	3.72
MNO	0.09
CAO	17.33
NA2O	1.11
TOTAL	99.95

MOLAR PROPORTIONS BASED ON 4 CATIONS

SI	1.856
AL4	0.144
TI	0.014
AL6	0.168
FE3+	0.002
CR	0.023
MG	0.934
FE2+	0.110
MN	0.003
CA	0.668
NA	0.077
OXYGENS	6.000
MG-NUMBER	0.895
CA/(CA+MG)	0.417

UMX SPINEL

NUNIVAK ISLAND: COMPOSITIONS FROM FRANCIS (1974, 1975)
MOLE PROPORTION FE3+ CALCULATED FROM STOICHIOMETRY

SAMPLE	10007 NI	10002 NI	10013 NI	10010 NI	10016 NI	10006 NI	10008 NI
SIO2	0.0	0.60	0.37	0.0	1.00	0.0	0.0
TIO2	0.09	0.02	0.05	0.0	0.01	0.02	0.03
AL2O3	31.67	32.74	38.99	27.05	35.87	34.76	45.68
CR2O3	35.00	33.69	27.99	40.29	32.17	32.01	21.49
MGO	17.00	16.81	17.46	17.13	16.79	17.90	19.99
FEO	15.63	15.40	14.97	14.54	13.75	14.41	12.32
MNO	0.06	0.63	0.44	0.73	0.61	0.50	0.35
CAO	0.0	0.02	0.02	0.0	0.02	0.0	0.0
TOTAL	99.45	99.92	100.29	99.74	100.22	99.60	99.86

MOLAR PROPORTIONS BASED ON 24 CATIONS

SI	0.0	0.138	0.083	0.0	0.227	0.0	0.0
TI	0.016	0.003	0.008	0.0	0.002	0.003	0.005
AL	8.653	8.875	10.266	7.498	9.592	9.324	11.615
FE3+	0.911	0.715	0.613	1.010	0.182	0.911	0.713
CR	6.415	6.126	4.944	7.492	5.771	5.760	3.666
MG	5.874	5.763	5.814	6.005	5.678	6.073	6.428
FE2+	2.119	2.248	2.183	1.850	2.427	1.832	1.510
MN	0.012	0.123	0.083	0.145	0.117	0.096	0.064
CA	0.0	0.005	0.005	0.0	0.005	0.0	0.0
OXYGENS	32.006	31.993	32.002	32.000	32.001	32.001	32.001
MG-NUMBER	0.735	0.720	0.727	0.764	0.701	0.768	0.810
CR/(CR+AL)	0.426	0.408	0.325	0.500	0.376	0.382	0.240

UMX SPINEL

NUNIVAK ISLAND: COMPOSITIONS FROM FRANCIS (1974, 1975)
MOLE PROPORTION FE3+ CALCULATED FROM STOICHIOMETRY

SAMPLE	10004 NI	10068 NI	10069 NI	10001 NI	20038 PV	20022 PV	20039 PV
SIO2	0.0	0.06	0.10	0.39	0.09	0.15	0.04
TIO2	0.13	0.0	0.0	0.22	0.02	0.0	0.24
AL2O3	50.52	59.52	58.23	47.16	27.02	22.86	54.02
CR2O3	15.29	8.30	8.43	19.19	37.18	43.94	12.22
MGO	21.32	21.58	21.71	21.53	15.43	17.55	19.14
FEO	12.83	10.36	11.25	9.31	18.94	13.92	13.95
MNO	0.35	0.19	0.21	0.22	0.25	0.25	0.14
NIO	-	-	-	-	0.16	0.18	0.31
CAO	0.0	0.01	0.0	0.06	-	-	-
TOTAL	100.44	100.02	99.93	98.08	99.09	98.85	100.06

MOLAR PROPORTIONS BASED ON 24 CATIONS

SI	0.0	0.012	0.020	0.084	0.021	0.036	0.008
TI	0.020	0.0	0.0	0.036	0.004	0.0	0.038
AL	12.477	14.295	14.037	11.966	7.603	6.467	13.390
FE3+	0.963	0.343	0.559	0.546	1.333	1.122	0.510
CR	2.533	1.337	1.363	3.267	7.018	8.339	2.032
MG	6.659	6.555	6.619	6.909	5.491	6.279	6.000
FE2+	1.286	1.422	1.366	1.131	2.451	1.672	1.944
MN	0.062	0.033	0.036	0.040	0.051	0.051	0.025
NI	-	-	-	-	0.031	0.035	0.052
CA	0.0	0.002	0.0	0.014	-	-	-
OXYGENS	32.006	31.999	32.001	31.997	32.002	32.000	32.013
MG-NUMBER	0.838	0.822	0.830	0.859	0.691	0.790	0.755
CR/(CR+AL)	0.169	0.086	0.089	0.214	0.480	0.563	0.132

UMX SPINEL

MOLE PROPORTION FE3+ CALCULATED FROM STOICHIOMETRY

SAMPLE	20015 PV	20018 EV	20008 EV	20029 PV	20046 PV	20004 EV	30028 FS
SIO2	0.07	0.03	0.17	0.06	0.07	0.10	0.06
TIO2	0.09	0.06	0.10	0.07	0.09	0.08	0.28
AL2O3	45.23	58.54	58.70	57.30	59.39	59.92	43.66
CR2O3	23.32	9.38	8.80	10.80	8.16	8.17	23.21
MGO	19.16	20.17	20.53	20.27	20.97	21.36	17.25
FEO	11.96	11.83	11.21	10.88	10.98	9.45	15.56
MNO	0.16	0.14	0.12	0.11	0.11	0.10	0.19
NIO	0.27	0.41	0.41	0.36	0.41	0.43	0.35
TOTAL	100.26	100.56	100.04	99.85	100.18	99.61	100.56

MOLAR PROPORTIONS BASED ON 24 CATIONS

SI	0.015	0.006	0.035	0.012	0.014	0.020	0.013
TI	0.015	0.009	0.015	0.011	0.014	0.012	0.046
AL	11.547	14.166	14.217	13.987	14.304	14.436	11.305
FE3+	0.409	0.287	0.263	0.205	0.331	0.187	0.576
CR	3.994	1.523	1.430	1.769	1.318	1.320	4.031
MG	6.186	6.173	6.288	6.257	6.387	6.508	5.649
FE2+	1.758	1.744	1.663	1.679	1.545	1.429	2.283
MN	0.029	0.024	0.021	0.019	0.019	0.017	0.035
NI	0.047	0.068	0.068	0.060	0.067	0.071	0.062
OXYGENS	32.004	32.003	32.005	32.003	32.004	32.004	32.015
MG-NUMBER	0.779	0.780	0.791	0.788	0.805	0.820	0.712
CR/(CR+AL)	0.257	0.097	0.091	0.112	0.084	0.084	0.263

UMX SPINEL

MOLE PROPORTION FE3+ CALCULATED FROM STOICHIOMETRY

SAMPLE	30008 FS	30006 FS	30015 FS	30020 FS	30003 FS	30012 FS	30022 FS
SIO2	0.08	0.05	0.03	0.09	0.06	0.08	0.05
TIO2	0.05	0.11	0.06	0.12	0.10	0.14	0.09
AL203	28.75	51.52	57.23	55.48	56.23	59.92	57.66
CR203	41.78	16.71	10.45	12.18	11.49	7.28	10.24
MGO	16.48	20.12	20.37	20.50	20.66	21.60	20.88
FEO	13.35	11.21	11.31	10.60	10.64	11.10	10.57
MNO	0.21	0.13	0.10	0.11	0.09	0.10	0.12
NIO	0.11	0.34	0.33	0.34	0.41	0.40	0.39
TOTAL	100.81	100.19	99.88	99.42	99.68	100.62	100.00

MOLAR PROPORTIONS BASED ON 24 CATIONS

SI	0.019	0.011	0.006	0.019	0.012	0.016	0.010
TI	0.009	0.017	0.009	0.019	0.016	0.021	0.014
AL	7.893	12.804	13.960	13.648	13.760	14.309	13.994
FE3+	0.363	0.365	0.305	0.279	0.308	0.464	0.300
CR	7.695	2.786	1.710	2.010	1.886	1.166	1.667
MG	5.722	6.324	6.284	6.378	6.394	6.524	6.409
FE2+	2.238	1.612	1.653	1.571	1.540	1.418	1.521
MN	0.041	0.023	0.018	0.019	0.016	0.017	0.021
NI	0.021	0.058	0.055	0.057	0.068	0.065	0.065
OXYGENS	32.002	32.005	32.003	32.007	32.005	32.007	32.005
MG-NUMBER	0.719	0.797	0.792	0.802	0.806	0.822	0.808
CR/(CR+AL)	0.494	0.179	0.109	0.128	0.121	0.075	0.106

UMX SPINEL

MOLE PROPORTION FE3+ CALCULATED FROM STOICHIOMETRY

SAMPLE	40055 CR	40037 CR	40044 CR	40003 CR	40020 CR	40015 CR	40017 CR
SIO2	0.15	0.23	0.14	0.07	0.12	0.18	0.14
TIO2	0.25	0.36	0.29	0.02	0.18	0.03	0.01
AL2O3	33.99	49.58	29.09	33.98	48.00	43.25	48.23
CR2O3	32.25	15.46	40.02	35.77	19.81	25.70	20.27
MGO	17.41	18.96	16.87	17.41	20.15	19.25	19.56
FEO	15.09	15.17	13.12	12.83	11.86	11.16	10.62
MNO	0.20	0.13	0.21	0.19	0.13	0.13	0.16
NIO	0.23	0.32	0.18	0.19	0.30	0.30	0.31
TOTAL	99.57	100.23	99.92	100.46	100.55	100.00	99.30

MOLAR PROPORTIONS BASED ON 24 CATIONS

SI	0.034	0.049	0.033	0.016	0.026	0.039	0.030
TI	0.043	0.058	0.051	0.003	0.029	0.005	0.002
AL	9.172	12.467	8.010	9.118	12.037	11.134	12.242
FE3+	0.864	0.746	0.464	0.406	0.541	0.342	0.244
CR	5.838	2.611	7.393	6.439	3.333	4.438	3.452
MG	5.942	6.029	5.875	5.908	6.391	6.267	6.279
FE2+	2.026	1.960	2.100	2.037	1.570	1.697	1.609
MN	0.039	0.023	0.042	0.037	0.023	0.024	0.029
NI	0.042	0.055	0.034	0.035	0.051	0.053	0.054
OXYGENS	32.015	32.019	32.017	32.001	32.009	32.002	32.001
MG-NUMBER	0.746	0.755	0.737	0.744	0.803	0.787	0.790
CR/(CR+AL)	0.389	0.173	0.480	0.414	0.217	0.285	0.220

UMX SPINEL

MOLE PROPORTION FE3+ CALCULATED FROM STOICHIOMETRY

SAMPLE	40061 CR	40054 CR	40001 CR	40018 CR	40030 CR	40046 CR	40010 CR
SIO2	0.19	0.09	0.12	0.13	0.16	0.15	0.08
TIO2	0.12	0.11	0.15	0.04	0.09	0.04	0.10
AL2O3	54.53	57.12	56.67	55.34	51.22	54.01	58.46
CR2O3	12.85	10.77	10.51	13.03	17.10	14.36	9.46
MGO	20.94	21.07	21.33	20.88	20.87	20.93	21.08
FEO	10.90	10.44	10.55	10.33	10.24	9.91	10.00
MNO	0.12	0.13	0.09	0.11	0.13	0.14	0.09
NIO	0.37	0.36	0.37	0.35	0.37	0.35	0.34
TOTAL	100.02	100.09	99.79	100.21	100.18	99.89	99.61

MOLAR PROPORTIONS BASED ON 24 CATIONS

SI	0.040	0.019	0.025	0.027	0.034	0.031	0.016
TI	0.019	0.017	0.023	0.006	0.014	0.006	0.015
AL	13.362	13.863	13.780	13.515	12.687	13.276	14.174
FE3+	0.422	0.323	0.425	0.288	0.385	0.285	0.234
CR	2.112	1.754	1.714	2.135	2.842	2.368	1.539
MG	6.489	6.467	6.560	6.449	6.538	6.506	6.464
FE2+	1.474	1.475	1.396	1.502	1.415	1.444	1.486
MN	0.021	0.023	0.016	0.019	0.023	0.025	0.016
NI	0.062	0.060	0.061	0.058	0.063	0.059	0.056
OXYGENS	32.006	32.005	32.007	32.002	32.004	32.002	32.005
MG-NUMBER	0.815	0.814	0.824	0.811	0.822	0.818	0.813
CR/(CR+AL)	0.137	0.112	0.111	0.136	0.183	0.151	0.098

UMX SPINEL

MOLE PROPORTION FE3+ CALCULATED FROM STOICHIOMETRY

SAMPLE	40060 CR	50015 JL	50011 JL	50005 JL	50001 JL	50009 JL	50019 JL
SIO2	0.17	0.07	0.20	0.10	0.16	0.08	0.14
TIO2	0.04	0.24	0.08	0.13	0.38	0.12	0.16
AL2O3	55.21	33.04	42.57	51.62	54.82	58.15	55.08
CR2O3	13.03	35.08	25.61	15.63	11.53	9.38	11.80
MGO	21.31	17.02	18.86	20.28	20.90	20.96	21.17
FEO	9.80	14.10	12.33	12.03	11.39	10.65	10.76
MNO	0.09	0.23	0.17	0.15	0.13	0.13	0.10
NIO	0.38	0.24	0.23	0.38	0.36	0.40	0.41
TOTAL	100.01	100.02	100.05	100.32	99.67	99.87	99.62

MOLAR PROPORTIONS BASED ON 24 CATIONS

SI	0.035	0.016	0.044	0.021	0.033	0.016	0.029
TI	0.006	0.041	0.013	0.021	0.060	0.019	0.025
AL	13.475	8.945	11.003	12.795	13.455	14.054	13.492
FE3+	0.313	0.596	0.451	0.536	0.501	0.323	0.477
CR	2.133	6.371	4.441	2.599	1.898	1.525	1.939
MG	6.578	5.828	6.165	6.357	6.487	6.425	6.558
FE2+	1.384	2.113	1.811	1.580	1.483	1.509	1.393
MN	0.016	0.045	0.032	0.027	0.023	0.023	0.018
NI	0.060	0.044	0.041	0.064	0.060	0.066	0.069
OXYGENS	32.001	32.014	32.004	32.007	32.019	32.006	32.006
MG-NUMBER	0.826	0.734	0.773	0.801	0.814	0.810	0.825
CR/(CR+AL)	0.137	0.416	0.288	0.169	0.124	0.098	0.126

UMX SPINEL

MOLE PROPORTION FE3+ CALCULATED FROM STOICHIOMETRY

SAMPLE	50008 JL	50C06 JL
SIO2	0.06	0.05
TIO2	0.06	0.08
AL2O3	58.84	62.61
CR2O3	8.66	5.20
MGO	21.16	21.77
FEO	10.62	9.83
MNO	0.11	0.10
NIO	0.39	0.42
TOTAL	99.90	100.06

MOLAR PROPORTIONS BASED ON 24 CATIONS

SI	0.012	0.010
TI	0.009	0.012
AL	14.210	14.869
FE3+	0.350	0.268
CR	1.403	0.828
MG	6.463	6.539
FE2+	1.469	1.389
MN	0.019	0.017
NI	0.064	0.068
OXYGENS	32.003	32.005
MG-NUMBER	0.815	0.825
CR/(CR+AL)	0.090	0.053

UMX AMPHIBOLE

NUNIVAK ISLAND: COMPOSITIONS FROM FRANCIS (1974, 1975)
TOTAL FE AS FEO

SAMPLE	10013 NI	10006 NI	10016 NI
SIO2	44.52	46.80	46.62
TIO2	0.31	0.10	0.09
AL2O3	13.60	12.48	11.75
CR2O3	2.37	2.30	2.66
MGO	17.94	18.90	18.93
FEO	4.04	3.42	3.33
MNO	0.10	0.06	0.11
CAO	9.73	8.90	9.41
NA2O	3.79	4.83	4.44
K2O	1.27	0.93	0.72
TOTAL	97.67	98.72	98.06

MOLAR PROPORTIONS BASED ON 23 OXYGENS

SI	6.768	6.808	6.805
TI	0.004	0.001	0.001
AL	0.277	0.254	0.239
CR	0.032	0.031	0.036
MG	0.461	0.486	0.487
FE	0.058	0.049	0.048
MN	0.001	0.001	0.002
CA	0.180	0.165	0.174
NA	0.127	0.162	0.149
K	0.028	0.020	0.016
CATIONS	1.937	1.978	1.957
MG/(MG+FE)	0.888	0.908	0.910
CR/(CR+AL)	0.105	0.110	0.132

UNX MICA

NUNIVAK ISLAND: COMPOSITIONS FROM FRANCIS (1974, 1975)
TOTAL FE AS FEO

SAMPLE	10013 NI	10006 NI	10016 NI
SIO2	38.60	38.31	39.91
TIO2	0.45	0.14	0.20
AL2O3	17.54	16.72	17.75
CR2O3	2.02	2.48	2.17
MGO	22.96	23.53	23.76
FEO	4.00	3.75	3.43
MNO	0.05	0.05	0.05
NA2O	0.95	0.82	1.47
K2O	8.54	9.19	7.30
TOTAL	95.11	94.99	96.04

MOLAR PROPORTIONS BASED ON 22 OXYGENS

SI	0.664	0.659	0.688
TI	0.006	0.002	0.003
AL	0.356	0.339	0.361
CR	0.027	0.034	0.030
MG	0.589	0.603	0.610
FE	0.058	0.054	0.049
MN	0.001	0.001	0.001
NA	0.032	0.027	0.049
K	0.188	0.202	0.160
CATIONS	1.920	1.920	1.951
MG/(MG+FE)	0.911	0.918	0.925
CR/(CR+AL)	0.072	0.090	0.076

UMX GLASS

NUNIVAK ISLAND: COMPOSITIONS FROM FRANCIS (1974, 1975)
TOTAL FE AS FEO

SAMPLE	10006 NI	10010 NI	10002 NI	10013 NI	10001 NI
SIO2	59.05	58.99	55.61	51.61	52.90
TIO2	0.10	0.16	0.18	0.53	1.32
AL2O3	26.56	20.87	23.84	22.68	22.29
CR2O3	0.14	0.09	0.15	0.46	0.05
MGO	1.43	3.60	4.00	4.44	4.30
FEO	0.54	2.77	3.37	3.85	3.78
MNO	0.01	0.07	0.03	0.09	0.06
CAO	2.33	6.58	7.46	8.29	9.11
NA2O	7.98	4.57	3.45	4.39	3.94
K2O	2.32	2.10	1.42	3.23	2.00
TOTAL	100.46	99.80	99.51	99.57	99.75

MOLAR PROPORTIONS BASED ON 100 CATIONS

SI	51.77	53.57	50.90	46.69	48.19
TI	0.07	0.11	0.12	0.36	0.90
AL	27.44	22.34	25.72	24.18	23.93
CR	0.10	0.06	0.11	0.33	0.04
MG	1.87	4.87	5.46	5.99	5.84
FE	0.40	2.10	2.58	2.91	2.88
MN	0.01	0.05	0.02	0.07	0.05
CA	2.19	6.40	7.32	8.04	8.89
NA	13.57	8.05	6.12	7.70	8.96
K	2.59	2.43	1.66	3.73	2.32
OXYGENS	157.53	159.64	160.04	153.60	156.44
MG/(MG+FE)	0.825	0.698	0.679	0.673	0.670

APPENDIX 3: CALCULATED COMPOSITIONS OF ULTRAMAFIC XENOLITHS

ULTRAMAFIC XENOLITHS

ANALYSES NORMALIZED TO 100 WT.%
TOTAL FE AS FEO

SAMPLE	10010 NI	10007 NI	10002 NI	10006 NI	10016 NI	10013 NI	10008 NI
SIO2	42.76	43.19	44.21	44.33	44.15	43.07	43.61
TIO2	0.01	0.02	0.01	0.02	0.0	0.03	0.02
AL2O3	0.81	0.78	1.59	1.24	1.82	3.05	1.57
CR2O3	0.45	0.48	0.52	0.32	0.75	0.87	0.47
MGO	46.70	46.65	42.94	44.54	42.44	39.73	45.04
FEO	8.26	7.93	8.11	7.82	7.95	9.05	8.09
MNO	0.11	0.10	0.10	0.12	0.15	0.16	0.13
CAO	0.73	0.77	2.11	1.29	2.26	3.24	0.99
NA2O	0.10	0.03	0.34	0.27	0.40	0.61	0.02
K2O	0.01	0.0	0.02	0.01	0.04	0.16	0.0
TOTAL	99.94	99.95	99.95	99.96	99.96	99.97	99.94

MOLAR PROPORTIONS BASED ON 100 CATIONS

SI	35.14	35.51	36.74	36.63	36.74	36.15	36.05
TI	0.01	0.01	0.01	0.01	0.0	0.02	0.01
AL	0.78	0.76	1.56	1.21	1.79	3.02	1.53
CR	0.29	0.31	0.34	0.21	0.49	0.58	0.31
MG	57.21	57.16	53.19	54.86	52.64	49.70	55.50
FE	5.68	5.45	5.64	5.40	5.53	6.35	5.59
MN	0.08	0.07	0.07	0.08	0.11	0.11	0.09
CA	0.64	0.68	1.88	1.14	2.02	2.91	0.88
NA	0.16	0.05	0.55	0.43	0.65	0.99	0.03
K	0.01	0.0	0.02	0.01	0.04	0.17	0.0
OX	135.60	136.03	137.42	137.13	137.54	137.38	136.97
MG/MG+FE	0.910	0.913	0.904	0.910	0.905	0.887	0.908
AL/AL+SI	0.022	0.021	0.041	0.032	0.046	0.077	0.041

ULTRAMAFIC XENOLITHS

ANALYSES NORMALIZED TO 100 WT.%
TOTAL FE AS FEO

SAMPLE	10001 NI	10004 NI	10069 NI	10068 NI	20038 PV	20015 PV	20039 PV
SIO2	49.86	43.73	43.96	45.08	43.70	45.76	39.44
TIO2	0.09	0.03	0.15	0.08	0.0	0.03	0.08
AL2O3	2.58	2.11	4.01	3.11	0.46	1.81	3.42
CR2O3	0.68	0.45	0.44	0.30	0.23	0.49	0.70
MGO	31.50	43.13	39.41	40.91	46.34	41.84	43.21
FEO	5.49	8.35	8.13	8.51	8.06	7.02	11.28
MNO	0.10	0.12	0.10	0.15	0.14	0.16	0.19
NIO	-	-	-	-	0.28	0.21	0.26
CAO	9.24	1.92	3.46	1.64	0.73	2.52	1.31
NA2O	0.40	0.13	0.34	0.17	0.02	0.11	0.07
K2O	0.02	0.0	0.0	0.0	-	-	-
TOTAL	99.96	99.97	100.00	99.95	99.96	99.95	99.96

MOLAR PROPORTIONS BASED ON 100 CATIONS

SI	43.04	36.36	36.90	37.77	36.00	38.21	32.91
TI	0.06	0.02	0.09	0.05	0.0	0.02	0.05
AL	2.63	2.07	3.97	3.07	0.45	1.78	3.36
CR	0.46	0.30	0.29	0.20	0.15	0.32	0.46
MG	40.53	53.45	49.31	51.09	56.90	52.08	53.75
FE	3.96	5.81	5.71	5.96	5.55	4.90	7.87
MN	0.07	0.08	0.07	0.11	0.10	0.11	0.13
NI	-	-	-	-	0.19	0.14	0.17
CA	8.55	1.71	3.11	1.47	0.64	2.25	1.17
NA	0.67	0.21	0.55	0.28	0.03	0.18	0.11
K	0.02	0.0	0.0	0.0	-	-	-
OX	144.30	137.45	138.85	139.32	136.28	139.19	134.82
MG/MG+FE	0.911	0.902	0.896	0.895	0.911	0.914	0.872
AL/AL+SI	0.057	0.054	0.097	0.075	0.012	0.045	0.093

ULTRAMAFIC XENOLITHS

ANALYSES NORMALIZED TO 100 WT.%
TOTAL FE AS FEO

SAMPLE	20046 PV	30C08 FS	30C06 FS	30020 FS	30022 FS	30C12 FS	40044 CB
SIO2	44.23	43.50	44.45	43.09	45.56	45.64	42.36
TIO2	0.10	0.0	0.04	0.04	0.14	0.18	0.01
AL2O3	3.71	0.52	2.19	1.96	6.01	4.60	0.39
CR2O3	0.37	0.27	0.43	0.32	0.85	0.36	0.19
MGO	40.25	46.39	43.25	43.79	34.40	36.05	47.83
FEO	8.40	7.49	7.53	8.13	6.85	7.75	7.73
MNO	0.18	0.10	0.11	0.13	0.12	0.16	0.11
NIO	0.20	0.31	0.25	0.18	0.16	0.17	0.32
CAO	2.35	1.34	1.60	2.07	5.48	4.61	0.98
NA2O	0.15	0.04	0.10	0.14	0.39	0.42	0.03
TOTAL	99.94	99.96	99.95	99.85	99.96	99.94	99.95

MOLAR PROPORTIONS BASED ON 100 CATIONS

SI	37.13	35.78	36.93	35.76	38.85	38.77	34.67
TI	0.06	0.0	0.02	0.02	0.09	0.11	0.01
AL	3.67	0.50	2.14	1.92	6.04	4.61	0.38
CR	0.25	0.18	0.28	0.21	0.57	0.24	0.12
MG	50.37	56.87	53.56	54.17	43.72	45.64	58.34
FE	5.90	5.15	5.23	5.64	4.88	5.51	5.29
MN	0.13	0.07	0.08	0.09	0.09	0.12	0.08
NI	0.14	0.21	0.17	0.12	0.11	0.12	0.21
CA	2.11	1.18	1.42	1.84	5.01	4.20	0.86
NA	0.24	0.06	0.16	0.23	0.64	0.69	0.05
OX	139.03	136.09	138.09	136.74	141.92	140.56	134.90
MG/MG+FE	0.895	0.917	0.911	0.906	0.900	0.892	0.917
AL/AL+SI	0.090	0.014	0.055	0.051	0.135	0.106	0.011

ULTRAMAFIC XENOLITHS

ANALYSES NORMALIZED TO 100 WT.%
TOTAL FE AS FEO

SAMPLE	40003 CR	40015 CR	40017 CR	40030 CR	40037 CR	40061 CR	40010 CR
SIO2	42.85	43.56	45.33	44.48	44.47	42.75	44.64
TIO2	0.0	0.0	0.0	0.02	0.14	0.03	0.11
AL2O3	0.68	1.20	1.38	2.05	3.41	1.89	3.88
CR2O3	0.40	0.42	0.27	0.34	0.55	0.32	0.46
MGO	46.97	45.56	43.77	42.34	37.72	44.47	39.10
FEO	7.94	7.62	7.51	7.27	10.43	8.54	7.72
MNO	0.12	0.12	0.11	0.14	0.14	0.16	0.15
NIO	0.33	0.29	0.27	0.24	0.18	0.30	0.22
CAO	0.66	1.14	1.29	2.93	2.78	1.44	3.42
NA2O	0.0	0.03	0.03	0.14	0.14	0.06	0.24
TOTAL	99.95	99.94	99.96	99.95	99.96	99.96	99.94

MOLAR PROPORTIONS BASED ON 100 CATIONS

SI	35.21	35.94	37.64	37.04	37.85	35.41	37.57
TI	0.0	0.0	0.0	0.01	0.09	0.02	0.07
AL	0.66	1.17	1.35	2.01	3.42	1.85	3.85
CR	0.26	0.27	0.18	0.22	0.37	0.21	0.31
MG	57.53	56.03	54.17	52.55	47.85	54.91	49.04
FE	5.46	5.26	5.21	5.06	7.42	5.92	5.43
MN	0.08	0.08	0.08	0.10	0.10	0.11	0.11
NI	0.22	0.19	0.18	0.16	0.12	0.20	0.15
CA	0.58	1.01	1.15	2.61	2.54	1.28	3.08
NA	0.0	0.05	0.05	0.23	0.23	0.10	0.39
OX	135.67	136.64	138.38	138.06	139.72	136.41	139.52
MG/MG+FE	0.913	0.914	0.912	0.912	0.866	0.903	0.900
AL/AL+SI	0.018	0.031	0.035	0.052	0.083	0.050	0.093

ULTRAMAFIC XENOLITHS

ANALYSES NORMALIZED TO 100 WT.%
TOTAL FE AS FEO

SAMPLE	50015 JL	50011 JL	50005 JL	50001 JL	50009 JL	50006 JL
SIO2	42.34	44.47	44.61	45.78	45.74	45.86
TIO2	0.01	0.01	0.05	0.09	0.14	0.14
AL2O3	0.45	1.77	2.48	2.56	3.94	7.52
CR2O3	0.21	0.60	0.44	0.24	0.44	0.52
MGO	47.89	43.24	41.79	41.68	37.37	33.78
FEO	8.23	7.50	7.88	7.91	7.46	7.22
MNO	0.11	0.11	0.12	0.13	0.12	0.13
NIO	0.30	0.26	0.11	0.19	0.17	0.14
CAO	0.39	1.92	2.24	1.26	4.17	4.25
NA2O	0.03	0.06	0.24	0.09	0.41	0.40
TOTAL	99.96	99.94	99.96	99.93	99.96	99.96

MOLAR PROPORTIONS BASED ON 100 CATIONS

SI	34.67	36.99	37.22	38.28	38.67	39.14
TI	0.01	0.01	0.03	0.06	0.09	0.09
AL	0.43	1.73	2.44	2.52	3.93	7.56
CR	0.14	0.39	0.29	0.16	0.29	0.35
MG	58.45	53.60	51.97	51.95	47.09	42.97
FE	5.64	5.22	5.50	5.53	5.27	5.15
MN	0.08	0.08	0.08	0.09	0.09	0.09
NI	0.20	0.17	0.07	0.13	0.12	0.10
CA	0.34	1.71	2.00	1.13	3.78	3.89
NA	0.05	0.10	0.39	0.15	0.67	0.66
OX	134.94	138.01	138.42	139.61	140.53	142.85
MG/MG+FE	0.912	0.911	0.904	0.904	0.899	0.893
AL/AL+SI	0.012	0.045	0.061	0.062	0.092	0.162